AFGL-TR-77-0123

CLOUD COMPOSITION DETERMINATION BY SATELLITE SENSING USING
THE NIMBUS VI HIGH RESOLUTION INFRARED SOUNDER

Robert G. Feddes
Kuo-Nan Liou

University of Utah
Department of Meteorology
Salt Lake City, Utah 84112

DDC
RECEIVED
DEC 14 1977
F.
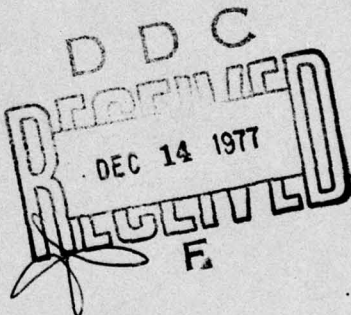
May 15, 1977

Scientific Report No. 3

Approved for public release; distribution unlimited.

AIR FORCE GEOPHYSICS LABORATORY
AIR FORCE SYSTEMS COMMAND
UNITED STATES AIR FORCE
HANSCOM AFB, MASSACHUSETTS 01731

REPORT DOCUMENTATION PAGE	READ INSTRUCTIONS BEFORE COMPLETING FORM

1. REPORT NUMBER	2. GOVT ACCESSION NO.	3. RECIPIENT'S CATALOG NUMBER
AFGL-TR-77-0123		

4. TITLE (and Subtitle)	5. TYPE OF REPORT & PERIOD COVERED
CLOUD COMPOSITION DETERMINATION BY SATELLITE SENSING USING THE NIMBUS VI HIGH RESOLUTION INFRARED SOUNDER	Scientific - Interim rept.
	Scientific
	6. PERFORMING ORG. REPORT NUMBER

7. AUTHOR(s)	8. CONTRACT OR GRANT NUMBER(s)
Robert G. Feddes Kuo-Nan Liou	F19628-75-C-0107

9. PERFORMING ORGANIZATION NAME AND ADDRESS	10. PROGRAM ELEMENT, PROJECT, TASK AREA & WORK UNIT NUMBERS
Department of Meteorology University of Utah Salt Lake City, Utah 84112	63311F 8628-12-02

11. CONTROLLING OFFICE NAME AND ADDRESS	12. REPORT DATE
Air Force Geophysics Laboratory Hanscom AFB, Massachusetts 01731 Contract Monitor - James T. Bunting/LYU	May 15, 1977
	13. NUMBER OF PAGES
	151 p.

14. MONITORING AGENCY NAME & ADDRESS(if different from Controlling Office)	15. SECURITY CLASS. (of this report)
	Unclassified
	15a. DECLASSIFICATION/DOWNGRADING SCHEDULE

16. DISTRIBUTION STATEMENT (of this Report)

Approved for public release, distribution unlimited.

17. DISTRIBUTION STATEMENT (of the abstract entered in Block 20, if different from Report)

18. SUPPLEMENTARY NOTES

19. KEY WORDS (Continue on reverse side if necessary and identify by block number)

Satellite Sensing	Infrared Radiation
Clouds	Cloud Radiation
Infrared Sounders	Atmospheric Radiation
Nimbus VI Satellite	

20. ABSTRACT (Continue on reverse side if necessary and identify by block number)

The emphasis in this study is to determine cloud compositions from satellites. The radiative transfer model of spectral infrared radiation in cloudy atmospheres is applied to the most complete set of radiance observations currently available from the Nimbus VI HIRS instrument. The radiative properties of clouds in the HIRS channels are investigated using the discrete-ordinate method for approximating the solution of the radiative transfer equation as it is applied to nonisothermal, inhomogeneous cloudy atmospheres. Analysis of the up-welling radiances from the model indicates that cirrus clouds decrease the

DD FORM 1473 EDITION OF 1 NOV 65 IS OBSOLETE
1 JAN 73

20. Abstract (continued)

upwelling radiance more than middle clouds and that multilayered middle and cirrus clouds are indistinguishable from thick cirrus clouds. Upwelling radiances in cirrus or middle cloud conditions for shortwave CO_2 channels are decreased by a greater percentage from their clear column values than are the long-wave CO_2 channel radiances.

A method for the estimate of cloud compositions from multispectral HIRS radiances, including both short-wave and long-wave CO_2 channels, is developed. Theoretical calculations of the upwelling radiance at satellite altitude for a number of thicknesses involving middle level and cirrus clouds are carried out. The resulting theoretical radiances are then parameterized and an empirical method to determine cloud type and ice and water content of the clouds is described. Satellite passes from five days over the Western United States are employed to test the empirical parameterizations of the theoretical results. Synoptic maps and discussions as well as NOAA 4 satellite mosaics are illustrated for the basic five days. Comparisons of the cloud type determinations with NOAA 4 mosaic are shown to agree reasonably well. Cloud ice and water content derived from the parameterizations of the HIRS data is compared with that obtained from the Air Force Three Dimensional Nephanalysis (3DNEPH) program. Examples of the application of this technique to global mapping of ice and water content are displayed. Extension of the parameterizations from an overcast field-of-view to a partly cloudy atmosphere is further described. Finally, we discuss the combination of the present technique with microwave and broad band radiometer parameterizations to increase the accuracy of cloud composition determinations.

PREFACE

The work presented in the Scientific Report No. 3 represents one phase of satellite sensing and radiative transfer research carried out in the Department of Meteorology, University of Utah under the sponsorship of AFGL.

iii

TABLE OF CONTENTS

LIST OF FIGURES

LIST OF FIGURES (Continued)

ix

LIST OF FIGURES (Continued)

CHAPTER 1

INTRODUCTION

The newest source of meteorological data in the last decade has come from meteorological satellites. Computer processing of this data has increased the application of satellite data to many long standing meteorological problems. Each year improved satellite instrumentation becomes available to further enhance the passive remote sensing of the environment. Along with this improved instrumentation are greater volumes of data and the requirement for more computer resources. Through these new and improved forms of data, accurate and reliable information can be attained in the inference of the atmospheric state. An important area that is only receiving attention recently is the interpretation of satellite radiance measurements to infer the structure and composition of clouds. This report describes recent developments on the inference of cloud compositions and structures from a satellite point of view, using some of the most recent data available, and the updated radiative transfer theory applicable to cloudy atmospheres.

The recovery of atmospheric parameters other than clouds has proven to be successful. Accurate atmospheric temperature profiles have been retrieved for clear areas (Chahine, 1970; Smith, 1970). The techniques have also been developed for the determination of the active atmospheric minor gases such as water vapor (see, e.g.,

Conrath, 1974) and ozone (Prabhakara, et al., 1970), and for the
estimation of the cloud top temperature and surface conditions in
a clear atmosphere. Furthermore, Chahine (1974) presented a numer-
ical procedure to derive vertical temperature profiles in cloudy
atmospheres from two overlapping fields of view. Taylor (1974)
describes an approach employing soundings at two different zenith
angles to determine temperature profiles in the presence of clouds.
However, there has been very little study focusing on the retrieval
of cloud properties.

Broad band radiometers such as those on the NOAA and ITOS
series of satellites have been used extensively to derive cloud
cover in the field-of-view of the satellite radiometer. Many of
these methods are completely statistical. These are represented
by publications such as Miller and Feddes (1971). With the addi-
tion of the broad band infrared channel on the NOAA series, analysis
was accomplished on both channels at the same time. A further use
of the broad band visible channel to infer cloud thickness from a
satistical point of view was done by Park et al., (1974) and Kaveney
et al., (1977) who correlated the low cloud thicknesses directly with
brightness observations.

The paper by Houghton and Hunt (1971) represents the first
attempt to explore the inference of cirrus clouds from passive remote
sensing. Liou (1974) described emmission and transmission properties
of cirrus clouds in the 10 μm region in conjunction with their remote
sensing potential. Bunting and Conover (1974) proposed a simple
means for estimation of vertical ice content for cirrus clouds by

assuming exponential attenuation of the infrared radiation. Additional research in cirrus clouds was done by Stoffel (1976) in whose work effects of the temperature gradient in the cirrus cloud were considered in the transfer process. Recently, Liou (1977) proposed a retrieval technique for recovering the thickness and ice content of cirrus clouds employing four spectral regions in the 10 μm window. Also, Liou, et al., (1977) developed a spectral radiative transfer model for NOAA 4 Vertical Temperature Profile Radiometer (VTPR) channels to study the effects of cirrus clouds on these upwelling radiances and to explore the feasibility of deriving cirrus cloud parameters from a combination of channels.

The purpose of the research described here is to analytically approach the important problem of the interaction of thermal infrared (or terrestrial) radiation with known compositions of cirrus and middle clouds. Significant improvements over past studies are incorporated in this solution of the problem, although certain aspects remain simple approximations to the real physics involved. Details of the approach will be found in later descriptions of the analysis. It can be stated, however, that the formulation of this radiation problem is based on the discrete-ordinate method originally proposed by Chandrasekhar (1950) and further developed by Liou (1973). The method is applied to isothermal layers of model cirrus and middle clouds. The clouds are assumed to be of infinite horizontal extent in a plane parallel atmosphere assumed to be in local thermodynamic equilibrium. The theoretical model is applied to selected High Resolution Infrared Sounder (HIRS) channels with

several combinations of middle and cirrus clouds. The theoretical results are parameterized and then used to infer cloud characteristics from actual HIRS data.

Chapter 2 contains a development of the theoretical considerations in the radiative transfer through clouds. The chapter includes a section on the radiative transfer in scattering atmospheres, the theoretical derivation of the boundary conditions of the transfer process, and the application of this theory to satellite channels. The second section of the chapter describes the application of the discrete-ordinate method and then presents a method used to obtain gaseous absorption coefficients for use in the scattering atmosphere.

Chapter 3 gives a brief description of the characteristics of the HIRS channels and the model atmosphere used in the study. The next section describes how the model developed in Chapter 2 was applied to the HIRS channels. The final section of this chapter discusses the sensitivity of the upwelling radiances to different theoretical cloud scenes.

Chapter 4 describes the parameterization of the theoretical results for cloudy atmospheres to infer cloud compositions. Two variables are inferred from this parameterization and they include the identification of cloud type (cirrus or middle clouds) and the ice and water content of these cloud types.

Chapter 5 is used to give a description of the HIRS data used for applying the theoretical results. The second section of the chapter gives a brief description of the Three Dimensional Neph-analysis (3DNEPH) routinely produced at the Air Force Global Weather

Central (AFGWC). The 3DNEPH was used to compare the ice or water content derived from the HIRS data.

Chapter 6 contains five separate sections. Section 1 and 2 address the selection criteria for the HIRS data to be used in the comparison and also contains a description of the parameterization of the 3DNEPH to obtain cloud thickness. Section 3 contains satellite pictures, synoptic maps and a synoptic discussion for the days that comparisons were made. Section 4 compares cloud type determination with the satellite photographs in the previous section and estimates of ice and water content derived from the HIRS data is compared to the 3DNEPH derived thicknesses. The final section of the chapter contains mapping of ice and water content over areas for two separate days and a discussion on the application of this technique to global mapping of these parameters.

Chapter 7 describes the use of the parameterizations from the overcast theory to a partly cloudy atmosphere. The first section of the chapter describes problems experienced in the recovery of the amount of cloudiness from the empirical relationships developed in Chapter 4. The second section in this chapter demonstrates the use of the overcast parameterizations to indicate equivalent liquid water or ice content in a partly cloudy atmosphere. The final section of the chapter uses some actual HIRS data to illustrate the application of this technique to a partly cloudy atmosphere.

Applications and limitations of the technique developed in the dissertation to routine satellite operations and further

recommendations with respect to the incorporation of microwave
sounders are carried out in the final chapter.

CHAPTER 2

THEORETICAL DEVELOPMENT OF INFRARED RADIATION
FOR SPECTRAL CHANNELS

A study of the effects of clouds on satellite upwelling radi-
ances requires a theoretical basis for these calculations. Section 1
of this chapter describes the fundamentals for the transfer of
spectral infrared radiation in scattering atmospheres. In addition,
the theoretical derivation of the boundary conditions in a non-
scattering atmosphere is shown. Finally the application of this
theory to the satellite instrument is described. Section 2
of this chapter describes the application of the discrete-ordinate
method for radiative transfer in non-isothermal and inhomogeneous
cloud layers. Lastly, the method used to derive equivalent absorp-
tion coefficients for use in cloud scattering calculations is
described.

2.1 Fundamentals for the Transfer of Spectral Infrared Radiation
in Scattering Atmospheres

The infrared radiation program begins by solving the transfer equa-
tion for a plane-parallel cloud layer consisting of cloud particles and absorbing
gases in local thermodynamic equilibrium. The basic equation describ-
ing the monochromatic infrared radiation field is given by

$$\mu \frac{dI_\nu(\tau,\mu)}{d\tau} = I_\nu(\tau,\mu) - \frac{\tilde{\omega}_\nu}{2} \int_{-1}^{+1} P_\nu(\mu,\mu') I_\nu(\tau,\mu') d\mu'$$

$$- (1-\tilde{\omega}_\nu) B_\nu[T(\tau)], \qquad (2.1)$$

$$\tilde{\omega}_\nu = \beta_{s,\nu}/(\beta_{s,\nu} + \beta_{a,\nu} + nk_\nu), \qquad (2.2)$$

$$B_\nu(T) = 2hc^2\nu^3/(e^{hc\nu/KT}-1), \qquad (2.3)$$

where I_ν represents the monochromatic radiance of wavenumber ν, μ the cosine of the emergent angle with respect to the zenith, τ the optical depth, P_ν the normalized axially symmetrical phase function, T the cloud temperature which is a function of height or optical depth, $\tilde{\omega}_\nu$ *the single scattering albedo*, $B_\nu(T)$ the Planck function, h and K the Planck's and Boltzmann's constants, respectively, c the velocity of light, $\beta_{s,\nu}$ and $\beta_{a,\nu}$ the volume scattering and absorption cross sections for cloud particles of wavenumber ν, n the number density of the absorbing gases within the cloud layer, and k_ν the absorption coefficient of the gases.

The normalized phase function may be expanded into Legendre polynomials consisting of a finite number of terms. Upon replacing the integration in Eq. (2.1) by summation according to the Gauss' quadrature formula, a set of first-order inhomogeneous differential equations are derived. By seeking the homogeneous and particular solutions of the differential equations as described by Chandrasekhar (1950), the complete solutions of the scattered radiance for a given discrete-stream j assuming an isothermal cloud temperature T_c may be written (Liou, 1975)

$$I_\nu(\tau,\mu_j) = \sum_m L_m \phi_m(\mu_j) e^{-k_m\tau} + B_\nu(T_c), \qquad (2.4)$$

where $\sum_m$ denotes summation over the 2n discrete streams employed, ϕ_m and k_m are the eigenfunction and eigenvalue of the differential equations, whose values depend upon the phase function and single-scattering albedo, and L_m are a set of constants of proportionality to be determined from the radiation boundary conditions above and below the cloud layer.

The upward and downward radiances arising from the molecular absorption and emission reaching the cloud bottom and top, respectively, can be obtained by solving the transfer equation for a non-scattering atmosphere in local thermodynamic equilibrium. They are given by

$$I_\nu^{\downarrow}(z_t,-\mu_i) = \int_{z_t}^{\infty} B_\nu[T(z)]d\,T_\nu(z,z_t;-\mu_i), \tag{2.5}$$

$$I_\nu^{\uparrow}(z_b,\mu_i) = B_\nu(T_s)T_\nu(z_b,0;\mu_i)$$

$$+ \int_0^{z_b} B_\nu[T(z)]d\,T_\nu(z_b,z;\mu_i), \tag{2.6}$$

$$T_\nu(z_2,z_1;\mu_i) = \exp\left[-\frac{1}{\mu_i}\int_{z_1}^{z_2} k_\nu(z)n(z)dz\right], \tag{2.7}$$

where T_s is the surface temperature, and z_t and z_b are cloud top and base heights, respectively.

Assume that variation of Planck function with respect to the wavenumber is much smaller than that of the transmission function T_ν. Thus, upon multiplying Eqs. (2.5) and (2.6) by the instrumental slit function $\phi(\nu)$ and performing the wavenumber integration over the spectral interval (ν_1,ν_2), we have

$$I_{\Delta\nu}{}^{\downarrow}(z_t,-\mu_i) = \int_{\nu_1}^{\nu_2} I_{\nu}{}^{\downarrow}(z_t,-\mu_i)\phi(\nu) \frac{d\nu}{\Delta\nu}$$

$$= \int_{z_t}^{\infty} B_{\Delta\nu}[T(z)]d\, T_{\Delta\nu}(z,z_t;-\mu_i), \tag{2.8}$$

$$I_{\Delta\nu}{}^{\uparrow}(z_b,\mu_i) = \int_{\nu_1}^{\nu_2} I_{\nu}{}^{\uparrow}(z_b,\mu_i)\phi(\nu) \frac{d\nu}{\Delta\nu}$$

$$= B_{\Delta\nu}(T_s)T_{\Delta\nu}(z_b,0;\mu_i)$$

$$+ \int_{0}^{z_b} B_{\Delta\nu}[T(z)]d\, T_{\Delta\nu}(z_b,z;\mu_i), \tag{2.9}$$

$$T_{\Delta\nu}(z_2,z_1;\mu_i) = \int_{\nu_1}^{\nu_2} \exp\left[-\frac{1}{\mu_i}\int_{z_1}^{z_2} k_{\nu}(z)n(z)dz\right]$$

$$\times \phi(\nu)\frac{d\nu}{\Delta\nu}. \tag{2.10}$$

How are we going to incorporate the spectral clear column radiances into the radiative transfer program for the scattering cloud layer?

The transmission function (or transmittance) must first be examined. For a given height z, the transmittances are normally available in the special form of Eq. (2.10)

$$T_{\Delta\nu}(z) = T_{\Delta\nu}(z,\infty;1) = \int_{\nu_1}^{\nu_2} \exp\left[-\int_{\infty}^{z} k_{\nu}(z)n(z)dz\right]$$

$$\times \phi(\nu)\frac{d\nu}{\Delta\nu}. \tag{2.11}$$

However, spectral radiative transfer for clouds require the clear column angular upward and downward radiances reaching the cloud base and top, respectively. To evaluate these radiances, the angular dependent transmittances from 0° to 90° zenith angles are needed. The calculations for these angular transmittances for HIRS channels will be described in Chapter 3.

Recalling Eqs. (2.1) and (2.2), it can be noticed that the gaseous absorption coefficient k_ν is needed to carry out the transfer of infrared radiation in cloud layers composed of absorbing gases. However, k_ν is known only through the absorption line parameters of gases and its values vary greatly with wavenumber in a small spectral interval. It is very difficult, if not impossible, to carry out line-by-line calculations including scattering contributions of cloud particles. Thus, the simplier approach for the gaseous absorption in a scattering layer would be to make use of the known transmittances which have been obtained to a good accuracy by means of line-by-line calculations for inhomogeneous atmospheres in conjunction with satellite sensing. Recognizing the definition of the vertical transmittance in Eq. (2.11), it may be approximated by

$$T_{\Delta\nu}(u) \simeq \int_{\nu_1}^{\nu_2} e^{-\overline{k}_\nu u} \frac{d\nu}{\Delta\nu} \simeq \sum_{j=1}^{M} w_j e^{-k_j u}, \qquad (2.12)$$

where the vertical path length

$$u = \int_{\infty}^{Z} \rho_v(z')dz',$$

k_j may be thought of as an equivalent absorption coefficient, w_j is the weight and M denotes the total number of finite terms in the fitting of the transmittances. A discussion on how to obtain the equivalent absorption coefficient is in the next section. Once k_j and w_j have been determined, we may consider the transfer of spectral infrared radiation as monochromatic in the sub-spectral interval j and carry out transfer calculations in a cloud layer M times with a new single scattering albedo $\tilde{\omega}_\nu^j$. Here, it is assumed that the phase

function and the absorption and scattering cross sections of ice crystals are independent of the wavenumber within a spectral interval. These assumptions are justified in view of the relatively slow varying refractive indices of ice and water in the infrared regions as evident in the next section.

The resulting M radiances calculated from the transfer program will be denoted as I_j. Hence, the transmitted and reflected spectral radiances at the cloud top and bottom, respectively, are now given by

$$I_{\Delta\nu}{}^{\uparrow}(z_t,\mu_i) = \sum_{j=1}^{M} I_j^{\uparrow}(z_t,\mu_i)$$

$$I_{\Delta\nu}{}^{\downarrow}(z_b,-\mu_i) = \sum_{j=1}^{M} I_j^{\downarrow}(z_b,-\mu_i)$$

(2.13)

The upward radiance at the satellite point of view in completely cloudy conditions can now be obtained by

$$I_{\Delta\nu}^{C}(\infty,\mu_i) = \int_{\nu_1}^{\nu_2} I_j^{\uparrow}(z_T;\mu_i)T_j(\infty,z_T;\mu_i)\phi(\nu)d\nu$$

$$+ \int_{z_T}^{\infty} B_{\Delta\nu}[T(z)]dT_{\Delta\nu}(\infty, z;\mu_i),$$

(2.14)

where T, denotes the sub-spectral transmittance associated with the sub-spectral radiance $I_j^{\uparrow}$. The second term on the right-hand side is for the clear atmosphere above the cloud layer and it is an exact expression. However, the first term requires further approximations. Since the spatial transmittances for satellite channels $T_{\Delta\nu}$ are available from the top of the cloud to the top of the atmosphere, upon utilizing the first equation in (2.13) the upwelling radiance at the top of the atmosphere may be approximated in the form

$$I_{\Delta\nu}{}^{C}(\infty,\mu_i) \simeq I_{\Delta\nu}{}^{\uparrow}(z_t,\mu_i)T_{\Delta\nu}(\infty,z_t;\mu_i)$$

$$+ \int_{z_t}^{\infty} B_{\Delta\nu}[T(z)]d\ T_{\Delta\nu}^{\cdot}(\infty,z;\mu_i). \tag{2.15}$$

Note here that the approximation also has a physical foundation. Since the variation of the radiative property of clouds over a small spectral interval is much smaller than that of the transmittance, we may take an averaged spectral radiance as defined by Eq. (2.13) and remove it from the wavenumber integration. The upward radiance at the satellite point of view in clear conditions is simply

$$I_{\Delta\nu}{}^{NC}(\infty,\mu_i) = B_{\Delta\nu}(T_s)T_{\Delta\nu}(\infty,0;\mu_i)$$

$$+ \int_{0}^{\infty} B_{\Delta\nu}[T(z)]d\ T_{\Delta\nu}(\infty,z;\mu_i). \tag{2.16}$$

Thus, if within the field-of-view of the satellite radiometer, there is η portion of cloudiness, the upward radiance at the top of a partly cloudy atmosphere is then given by

$$I_{\Delta\nu}{}^{PC}(\infty,\mu_i) = \eta I_{\Delta\nu}{}^{C}(\infty,\mu_i) + (1-\eta)I_{\Delta\nu}{}^{NC}(\infty,\mu_i). \tag{2.17}$$

At this point, we have completed our discussions on the theoretical foundation for calculating spectral infrared radiation in scattering cloudy atmospheres.

2.2 Discrete-ordinate method for radiative transfer in non-isothermal and inhomogeneous cloud layers

The solution of the infrared radiative transfer equation given by Eq. (2.4) is applicable only to isothermal and homogeneous cloud layers. The question of inhomogeneity of cloud compositions is a

difficult one. In the first place, there have not been many obser-
vations available. For the purpose of radiative transfer calcula-
tions, it seems that averaged property of cloud compositions may
be appropriate. However, the effect of the non-isothermal struc-
ture of clouds on their radiative properties is more critical. Phys-
ically, a cold cloud top would reduce the transmitted radiances. It is
conceivable therefore, that an overestimation of upward radiance is
likely to take place. Although our main concern is to determine the
cloud structure, the transfer program described below may be utilized
to investigate, if desirable, the inhomogeneous properties of clouds
as well.

In reference to Figure 2.1, the cloud layer is divided into
a number of sub-layers each of which is considered to be isothermal
and homogeneous. The optical depth is evaluated from the cloud top
to the bottom of the sub-layer. The index ℓ is used to denote the
number of the sub-layer. The solution of the radiative transfer equa-
tion given by Eq. (2.4) is applied to each sub-layer and sub-
spectral interval j to obtain (Σ_m denotes summation over discrete-
streams, (-n,n))

$$I_j^\ell(\tau,\mu_i) = \sum_m L_m^\ell \phi_m(\mu_i) e^{-k_m^\ell \tau} + B_j(T_c^\ell). \tag{2.18}$$

In order to determine the unknown coefficients L_m^ℓ, the radia-
tion continuity relationships are needed in addition to two radiation
boundary conditions specified in Eqs. (2.8) and (2.9). At the cloud
top the downward radiance has to be equal to that from the molecular
atmosphere above, so that
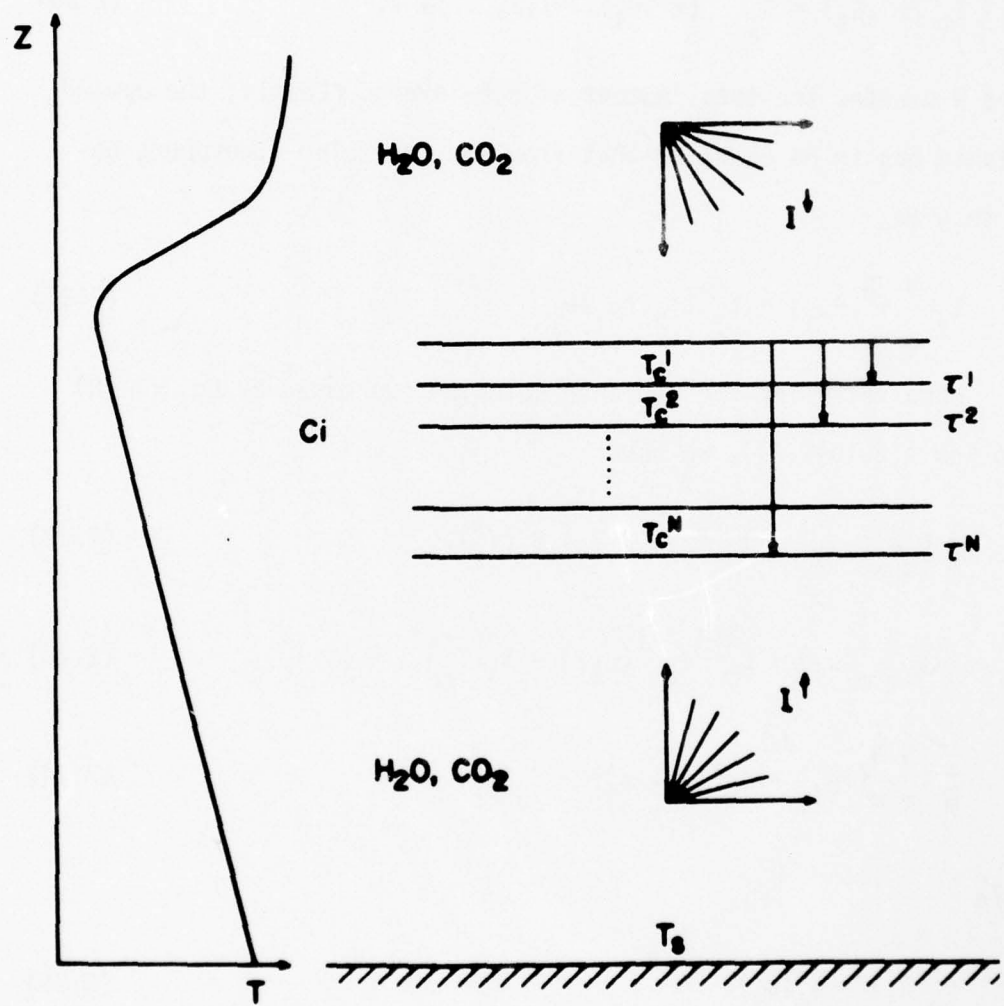
Figure 2.1 A model of the non-isothermal cloud. The temperature
within each pre-divided layer is assumed to be
isothermal.

$$I_j^1(0,-\mu_i) = I_{\Delta\nu}^{\downarrow}(z_t,-\mu_i)w_j \tag{2.19}$$

Between the layers, the radiances from all directions must be continuous. Thus,

$$I_j^{\ell}(\tau^{\ell},\mu_i) = I_j^{\ell+1}(\tau^{\ell},\mu_i), \ell=1,2,\ldots;N-1, \tag{2.20}$$

where N denotes the total number of sub-layers. Lastly, the upward radiance has to be equal to that from the molecular atmosphere below to give

$$I_j^N(\tau^N,+\mu_i) = I_j^{\uparrow}(z_b,+\mu_i)w_j \tag{2.21}$$

Upon inserting the radiance solution expressed by Eq. (2.18) into Eqs. (2.19-2.21), we have

$$\sum_m L_m^{\ell}\phi_m^{\ell}(-\mu_i) = I_j^{\downarrow}(z_t,-\mu_i) - B_j(T_c^{\ell}), \tag{2.22}$$

$$\sum_m [L_m^{\ell}\gamma_m^{\ell}(\mu_i) + L_m^{\ell+1}\delta_m^{\ell+1}(\mu_i)] \approx B_j(T_c^{\ell+1}) - B_j(T_c^{\ell}), \tag{2.23}$$

$$\sum_m L_m^N\gamma_m^N(+\mu_i) = I_j^{\uparrow}(z_b,+\mu_i) - B_j(T_c^N), \tag{2.24}$$

where

$$\gamma_m^{\ell}(\mu_i) = \phi_m^{\ell}(\mu_i)e^{-k_m^{\ell}\tau^{\ell}}, \tag{2.25}$$

$$\delta_m^{\ell+1}(\mu_i) = -\phi_m^{\ell}(\mu_i)e^{-k_m^{\ell+1}\tau^{\ell}}, \tag{2.26}$$

Eqs. (2.22-2.24) represent a system of 2n x N linear equations from which the L_m^{ℓ} coefficients may be determined using a matrix inversion

technique. Eqs. (2.20-2.22) may be rewritten in a compact matrix form

$$\underset{\sim}{\phi} \, \underset{\sim}{L} \; = \; \underset{\sim}{B}, \tag{2.27}$$

where the unknown coefficients of proportionality

$$\underset{\sim}{L} \; = \; \begin{bmatrix} L_{-n}^{\ell} \\ \vdots \\ L_{n}^{\ell} \\ L_{-n}^{2} \\ \vdots \\ L_{n}^{2} \\ \vdots \\ L_{-n}^{N} \\ \vdots \\ L_{n}^{N} \end{bmatrix} . \tag{2.28}$$

The matrix denoting the contribution due to cloud emission and upward and downward radiances reaching the cloud base and top, respectively, is

$$\underset{\sim}{B} \; = \; \begin{bmatrix} I_j^{\downarrow}(z_t, -\mu_n) - B_j(T_c^1) \\ \vdots \\ I_j^{\downarrow}(z_t, -\mu_1) - B_j(T_c^1) \\ B_j(T_c^2) - B_j(T_c^1) \\ B_j(T_c^2) - B_j(T_c^1) \\ \vdots \\ I_j^{\uparrow}(z_b, +\mu_1) - B_j(T_c^N) \\ \vdots \\ I_j^{\uparrow}(z_b, +\mu_n) - B_j(T_c^N) \end{bmatrix} \tag{2.30}$$

and the 2n x N by 2n x N matrix

$$
\underset{\sim}{\Phi} = \begin{bmatrix}
\phi_{-n}^{\ell}(-\mu_n) & \cdots & \phi_{n}^{\ell}(-\mu_n) & & & & & & \\
\vdots & & \vdots & & & & & & \\
\phi_{-n}^{\ell}(-\mu_1) & \cdots & \phi_{n}^{\ell}(-\mu_1) & & & & & & \\
\gamma_{-n}^{1}(-\mu_n) & \cdots & \gamma_{n}^{1}(-\mu_n)\delta_{-n}^{2}(-\mu_n) & \cdots & \delta_{n}^{2}(-\mu_n) & & & & \\
\vdots & & \vdots & & & & & & \\
\gamma_{-n}^{1}(\mu_n) & \cdots & \gamma_{n}^{1}(\mu_n)\delta_{-n}^{2}(\mu_n) & \cdots & \delta_{n}^{2}(\mu_n) & & & & \\
& & \vdots & & \vdots & \vdots & & & \vdots \\
& & & & & \gamma_{-n}^{N}(\mu_1) & \cdots & \gamma_{n}^{N}(\mu_1) & \\
& & & & & \vdots & & \vdots & \\
& & & & & \gamma_{-n}^{N}(\mu_n) & \cdots & \gamma_{n}^{N}(\mu_n) &
\end{bmatrix} \qquad (2.30)
$$

In Eq. (2.30), the blank spaces denote zero elements. A similar procedure has been employed by Liou (1975) for the transfer of solar radiation in inhomogeneous atmospheres. Once L_m^{ℓ} have been determined, they can be inserted into Eq. (2.18) to obtain the sub-spectral radiance distribution within each sub-layer. Eqs. (2.14) and (2.15) are then followed to evaluate the upward radiances at the cloud top and at the top of the atmosphere.

2.3 Derivation of Equivalent Absorption Coefficients

To derive a set of equivalent absorption coefficients for use in cloud scattering calculations, an exponential fit of the form denoted in Eq. (2.12) was applied to transmission curves of the HIRS channels. The fitting routine as described by Avrett and Hummer (1965) has been successfully applied to the broad band transmittances by Liou and Sasamori (1975). However, when applied to the curves in HIRS channels it proved unsuccessful.

The transmission curves for satellite channels take into account absorption by more than one gas simultaneously while each gas is distributed differently. The transmission curve also includes the instrument slit function. These curves cover the entire atmosphere from 0.01 mb to the surface, which introduces a significant pressure variation. All these factors lead to the non-exponential shape of the transmission curves $T_{\Delta \nu}(u)$ as functions of the major absorber.

Since the spectral transmittances are available above and below the cloud it was decided to fit the transmittances over the range of pathlength covered by the thickest clouds to be considered so as to incorporate the gaseous absorption in scattering cloud layers. This was done by selecting a base height of 700 mb and a maxium height of 250 mb; the variation in pressure in this range is not enough to produce significant deviation from exponential behavior and the water vapor concentration is small enough to be neglected in calculating the pathlength. The curve was generated by using a constant CO_2 concentration of 5.11×10^{-4} gm cm^{-2} mb^{-1}, and saturated conditions in water vapor channels. The transmission was read off the true curve at an altitude of 250 mb and considered as 1.0. The transmission at each subsequent level below this was considered as a fraction of what the value was at 250 mb. For CO_2 channels, the neglection of water vapor absorption above 700 mb could produce some small errors. As for water vapor channels, actual water vapor concentration profiles were used in the fitting program.

A simplified fitting routine was developed which guaranteed the required restriction on w_j and k_j (both have to be positive). The numerical scheme is based on the following iterative process. An initial $T_{\Delta\nu}(u_1)$ and w_1 are chosen (initially $w_1 = 1$) and k_1 is generated from (see Eq. (2.12))

$$K_1 = \frac{1}{u_1} \ln \frac{w_1}{T_{\Delta\nu}(u_1)} .$$

The curve $T'_{\Delta\nu}(u) = w_1 e^{-k_1 u}$ is then generated point by point; as each new point is generated it is compared with the true value $T_{\Delta\nu}(u)$ to make sure it meets the following conditions.

$$T'_{\Delta\nu}(u) < T_{\Delta\nu}(u),$$

$$\frac{dT'_{\Delta\nu}(u)}{du} < \frac{dT_{\Delta\nu}(u)}{du} .$$

The second condition requires only a rough approximation for the derivative. If either of these are not met, a new w_1 is generated, i.e. ($w_1 = w_1 \times$ constant) so that the new w_1 is slightly less than the old one, and the above is repeated. If no w_1 can be found, a new u_1 is selected (larger than the old point). When a good w_1 and k_1 are found, the above process is then repeated to produce an w_2 and k_2 using values of $T_{\Delta\nu}(u) - T'_{\Delta\nu}(u)$ instead of $T_{\Delta\nu}(u)$. The number of points needed to fit the curve then depends only on the size of the error tolerance used and on the range of u over which $T_{\Delta\nu}(u)$ is to be fitted. It was possible to fit the curve between 700 mb and 250 mb within a few percent. Application and verification of the fit in the cloud layers will be described in Chapter 3.

CHAPTER 3

SENSITIVITY OF HIRS CHANNEL RADIANCES

TO CLOUDY ATMOSPHERES

The launch of the Nimbus VI satellite made available data in
an expanded number of IR Channels and upwelling radiances in the
microwave portion of the spectrum simultaneously. These two
sources of data have been used by Smith and Woolf (1976) to
simultaneously recover temperature and water vapor profiles and
cloud parameters. This chapter describes results of the infra-
red transfer model for cloudy atmospheres in the channels of the
Nimbus VI HIRS instrument. Sensitivities of single and multi-
layered clouds on the satellite upwelling radiances are investi-
gated. Section 2 of this chapter describes the HIRS instrument
and the characteristics of the channels utilized in the analysis.
This section also describes the model atmosphere used to perform
the calculations. Section 3 describes how the transfer program
described in the previous chapter was used and the methods used to
generate the required input for the calculations. Section 4 is an
analysis of the sensitivity of the upwelling radiance to the combin-
ation of different cloud thicknesses.

3.1 Characteristics of HIRS Channels and Model Atmosphere

The Nimbus VI HIRS instrument is a third generation infrared
radiation sounder. This instrument is similar to the Infrared

Temperature Profile Radiometer (ITPR) on the Nimbus V Satellite. The instrument scans perpendicular to the satellite subtrack. There are 42 scan spots per scan line with a resolution of 23 km near nadir and 31 km at the extremes of the scan. The Nimbus VI satellite was successfully launched in June 1975 and the HIRS instrument has short periods during which all channels were operating successfully. A sample of good data was obtained from Dr. W. L. Smith (private communication) that covers a period of 20-30 August 1975 and a geographical coverage from 80°-150° W and 20° to 50° N. This data will be used for comparison in work subsequent to the sensitivity analysis described here.

The HIRS instrument senses infrared radiation in 17 channels. These include 7 channels in the 15 μm CO_2 band, 5 channels in the 4.3 μm CO_2 band, water vapor channels at 6.8 μm and 8.6 μm, respectiviely and 3 channels in windows at 11 μm, 3.68 μm and .69 μm.

In this analysis only those channels which peak below 100 mb would be substantially effected by clouds, therefore, this sensitivity analysis will include only those channels. The information compiled in Table 3.1 and Figure 3.1 are taken from Smith, et al. (1975). The table includes channel number, wavelength and wavenumber, principal absorbers and the approximate peaks of the weighting function. Figure 3.1 is a plot of the weighting functions for the channels in Table 3.1. The peaks in this figure indicates the approximate location in the troposphere from which its energy is derived.

Table 3.1 HIRS Channel Characteristics.

Channel	$\nu(cm^{-1})$	λ (μm)	Principal Absorbers	Level of Maximum (weighting function (mb))
1	668	15.0	CO_2	30
2	679	14.7	CO_2	60
3	690	14.4	CO_2	100
4	702	14.2	CO_2	250
5	716	14.0	CO_2	500
6	733	13.6	CO_2/H_2O	750
7	749	13.4	CO_2/H_2O	900
8	900	11.0	Window	Surface
9	1224	8.2	H_2O	900
10	1496	6.7	H_2O	400
11	2190	4.57	N_2O	950
12	2212	4.52	N_2O	850
13	2242	4.46	CO_2/N_2O	700
14	2275	4.40	CO_2/N_2O	600
15	2357	4.24	CO_2	5
16	2692	3.71	Window	Surface
17	14.443	0.69	Window	Surface
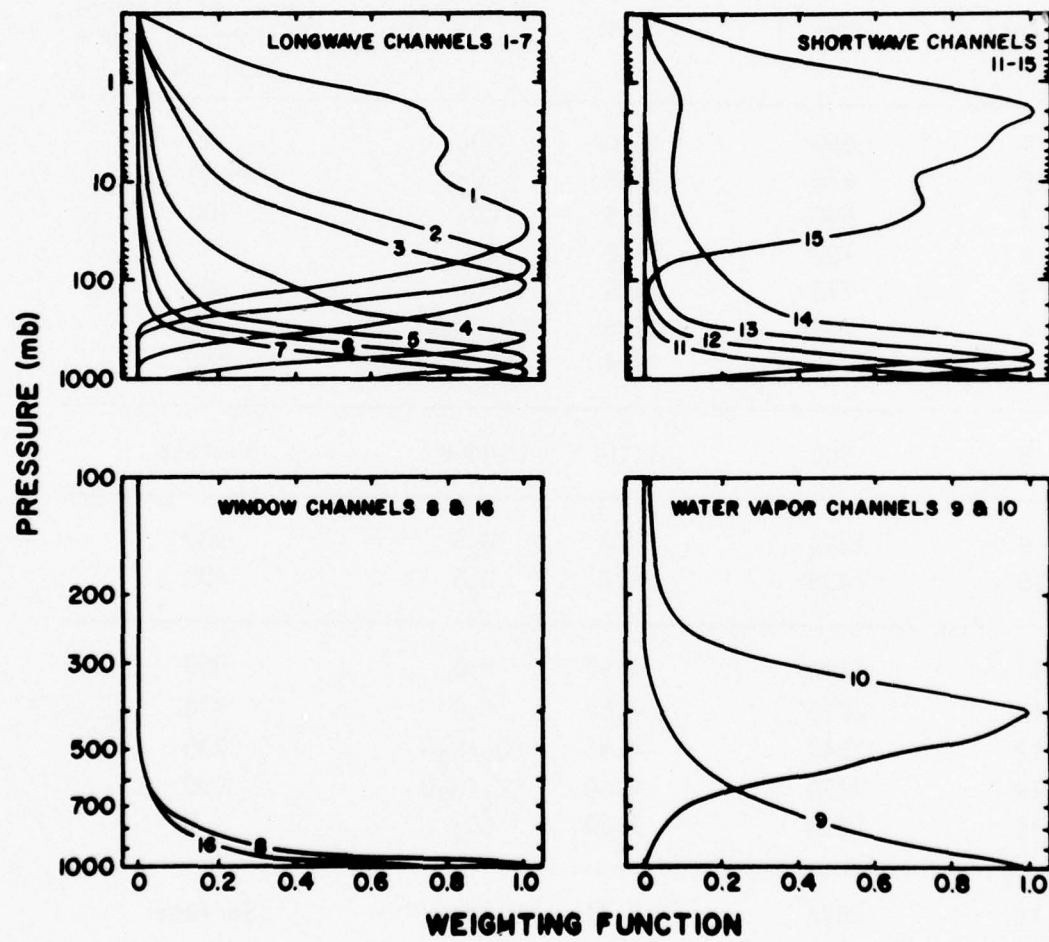
Figure 3.1 The weighting functions of the HIRS channels.

The model atmosphere used in this analysis was the mid-latitude summer atmosphere described by McClatchey (1972) and is portrayed in Figure 3.2. The left-hand side of this figure depicts the temperature, mixing ratio and pressure profiles as functions of the height. Due to the computational time and the actual HIRS data that was obtained (August) the sensitivity analysis would be carried out on only the mid-latitude summer atmosphere. This atmosphere is also significant since the present analysis will use mid-latitude summer data.

The model atmosphere was divided in such a way that it would coincide with the pressure levels used in the clear column radiance program (CCR) developed at NOAA/NESS, and supplied to us for our use. There are 40 pressure levels for the CCR program. The program utilizes predetermined transmission profiles which can be adjusted as a function of the atmospheric temperature profile used. It includes contributions from all the major gases listed in Table 3.1. To further utilize this predetermined vertical structure and facilitate the execution of the cloud transfer program, the base of the middle cloud was fixed at 700 mb and the top of the high cloud was fixed at 250 mb. The thicknesses of the high and middle clouds were allowed to vary from 1.26 to 4.12 km and from 0.35 to 2.68 km, respectively (the right-hand side of Figure 3.2). These values represent realistic thickness variations for high and middle clouds in the atmosphere. Thus, two distinct cloud layers with changing thicknesses are formed. The infrared transfer program described below is developed to include all the possible combinations of thickness variations.
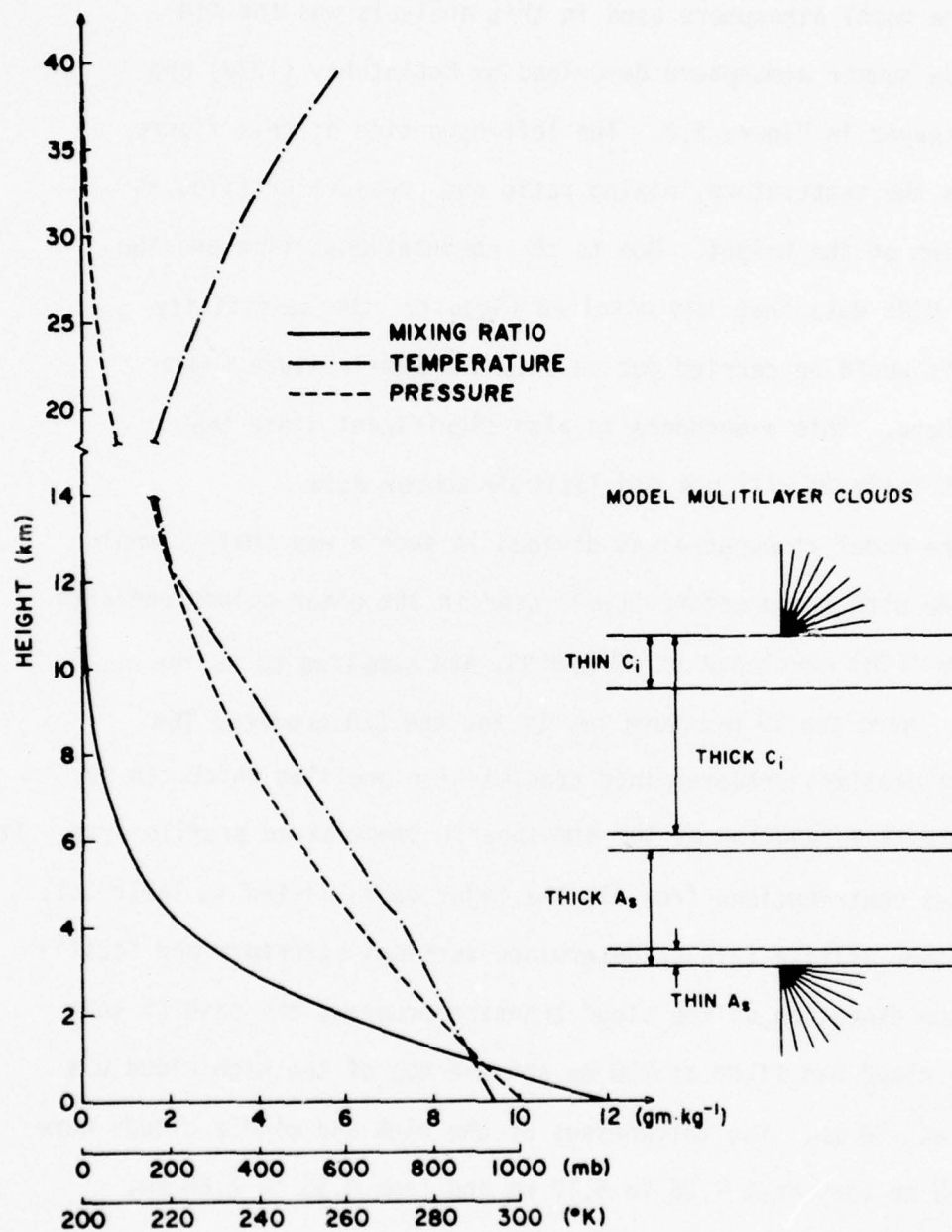
Figure 3.2 Midlatitude summer atmosphere from the surface to
40 km for temperature (°K), pressure (mb), and
mixing ratio (gkg⁻¹). The right-hand side shows
the atmospheric location for thick and thin cirrus
and middle cloud and the discrete angles used in the
discrete ordinate method for radiative transfer.

3.2   Description of the Infrared Transfer Program

The transfer program begins with the generation of the upper and lower boundary conditions. For this purpose the CCR program provided by Dr. W. L. Smith NOAA/NESS (personal communication) was used. It calculates CCR transmission values at all 40 pressure levels up to .1 mb over the range of scan angles of the HIRS instrument. This program was modified to calculate transmission values at the discrete-ordinate angles shown in the right-hand side of Figure 3.2 in conjunction with radiative transfer calculations involving clouds.

The upper boundary conditions were calculated directly by computing the CCR at each of the required discrete ordinate angles. Numerically integrating Eq. (2.5) for the upper boundary condition was then carried out by summing the contribution of each layer above 250 mb. The numerical value of the boundary condition increases with angle which is physically correct since the path lengths are longer at larger angles with respect to the satellite nadir angle, or the cloud top zenith angle.

Utilizing the same output for the lower boundary condition an adjustment had to be made in the transmission values below 700 mb. This was required since the transmission calculation from the satellite point of view are with respect to the top of the atmosphere and the satellite transmission function becomes very small below 700 mb especially for channels that peak high in the atmosphere. To adjust the satellite based transmission functions

relative to the base of the cloud the transmission function is
evaluated for the ith layer below the cloud by means of the rela-
tion $T_{\Delta\nu}^{ij} = 1 - |T_{\Delta\nu}^{i} - T_{\Delta\nu}^{j}|$ where $T_{\Delta\nu}^{ij}$ is the contribution from the
first layer below the cloud and j denotes the layer below the ith
layer. This procedure was repeated for all levels down to the
surface and thus a transmission function relative to the base was
produced. For channels that peak high in the troposphere (channels
4, 14 and 10) the transmission function was virtually zero below
700 mb. Therefore, it was assumed that there was no contribution
from layers between the surface and the cloud base and thus a
constant lower boundary condition at each discrete angle was
employed.

These transmission functions were then calculated for all
remaining channels utilized in the analysis for a satellite scan
angle of zero degrees. These vertical transmittances were then
calculated for the discrete ordinate angles using Eq. (2.12).

By performing numerical integration on Eq. (2.6) for the
lower boundary condition the upwelling radiance contribution reach-
ing the cloud base from the surface and the atmosphere below
is obtained.   It should be noted that the lower boundary conditions
are relative to a zenith angle of 90° which in effect increases the
values of the lower boundary conditions as 180° is approached.

The contribution of the absorbing gases within the cloud layer
in the transfer calculation were handled by an equation similar to
that used to fit the lower boundary condition. This fitting
utilized the approximation to the vertical transmittance given by

Eq. (2.12). It is identical to the one used for the lower bound-
ary condition except the angular dependence is no longer necessary
in the cloud layers. Note here that the amount of water vapor
within ice and water clouds is estimated from the saturation con-
dition over ice and water, respectively, whereas the amount of
carbon dioxide within the clouds is assumed to be the same as that
of the environment.

The single scattering parameters for altostratus cloud
were calculated using Mie type scattering computations
for the central wavenumber in each band. The cirrus cloud was
assumed to be entirely ice and the altostratus cloud was assumed
to be all water.

Calculation for the ice crystal parameters utilized a theoret-
ical model developed by Liou (1972) which used ice cylinders randomly
oriented in a horizontal plane. The major and minor axes of the
cylinder used are 200 and 60 μm, respectively with a concentration
of 0.05 cm^{-3}. Table 3.2 lists the optical properties of the ice
cylinders. The real and imaginary part of the index of refraction
are taken from the recent measurement by Schaaf and Williams (1973).
From Table 3.2 it is apparent that the real part of the index of
refraction increases with increasing wavenumber and the imaginary
part decreases with increasing wavenumber. The single scattering
albedo is largest in the window channels, (channels 16 and 8) and
the extinction cross section is greatest in the 15 μm band (chan-
nels 4-7).

Table 3.2 Optical Properties of Cirrus and Altostratus Clouds

Channel	ν (cm^{-1})	ICE				WATER			
		n_r	n_i	$\tilde{\omega}_0$	β_{ext} (km^{-1})	n_r	n_i	$\tilde{\omega}_0$	β_{ext} (km^{-1})
4	701.91								
5	716.83								
6	732.55	1.556	.305	.533	1.464	1.193	.356	.442	13.05
7	749.18								
14	2274.63								
13	2244.21	1.299	.0218	.527	1.391	1.333	.0128	.719	13.82
12	2211.97								
11	2191.02								
16	2691.20	1.392	.007	.625	1.360	1.372	.00356	.867	13.58
8	899.99	1.101	.280	.698	1.33	1.147	.105	.487	11.77
10	1508.29	1.316	.057	.51	1.326	1.332	.035	.619	14.69
9	1223.22	1.307	.04	.698	1.33	1.287	.035	.677	15.72

The single scattering parameters for the water cloud util-
ized a drop size distribution developed by Feddes and Smith (1974).
This distribution is a exponential fitting of the best published
measurements taken from cloud physics literature. Although this
fitting was done for ten cloud types only the altostratus cloud
distribution is used. In the calculation of the single scattering
parameters for altostratus clouds a liquid water content of
$0.15gm\ m^{-3}$ was used. Table 3.2 also contains the optical properties
of the water droplets. The real and imaginary parts of the index
of refraction for each band was taken from Hale and Querry (1973).
From Table 3.2 it can be seen that the real part of the index of
refraction generally increases with increasing wavenumber and the
imaginary part decreases. The single scattering albedo is the
largest corresponding to the largest wavenumber and the extinc-
tion cross section is the greatest in the water vapor bands (chan-
nels 9 and 10). Only one calculation was made for each of the CO_2
bands since the real and imaginary parts of the index of refraction
vary slowly.

Once the boundary conditions have been generated, the gaseous
absorption in the clouds has been fitted, and the optical proper-
ties of the ice and water have been calculated, the cloud transfer
program described in the previous chapter can now be utilized

To obtain the upwelling radiance at the top of the atmosphere
it is necessary to account for the contribution in the atmosphere
above the cloud. This step is accomplished by executing the CCR

program over a range of satellite scan angles larger than the extremes of the HIRS instrument scan (± 36.9°). Because only one atmosphere is utilized this calculation can be made once and for all. The transfer calculation assumes a plane parallel atmosphere. In this case the scan angle of the satellite is equal to the angle made by the satellite with the local zenith. When viewed from a satellite at scan angles greater than zero the resolution of the instrument decreases with increasing scan angle. This decrease in resolution is due to the increase in the distance between the satellite and the sampling point and the curvature of the earth. To account for this difference due to the curvature of the earth the CCR program uses the angle the earth's local zenith makes with the satellite which is derived from the satellite scan angle. In this way the contribution to the final upwelling radiance from above the cloud top accounts for the curvature of the earth and as a result the plane parallel assumption is minimized.

Prior to the calculation of the data used in the sensitivity analysis, two tests were made. One test was to check the accuracy of the exponential fitting of the gaseous absorption in the clouds and the second to check the accuracy of the cloud transfer program applicable to the HIRS channels.

To test the fitting of the gaseous absorption all three layers in the transfer calculation are assumed to be composed of gases only (Rayleigh layers). The resulting upwelling radiances from this calculation were compared to the upwelling radiances calculated with the clear column radiance program. A plot of this

comparison is given in Figure 3.3. An examination of the figure indicates that all the channels with the exception of channel 8 have higher upwelling radiances than the CCR results. The close comparison of these results would indicate that the exponential fit used for the gaseous absorption within the clouds is physically correct. The small differences noted in Figure 3 are removed by scaling all subsequent calculated upwelling radiances at the top of the atmosphere by the ratio of the CCR divided by the Rayleigh upwelling radiance.

The second test used to verify the modification of the program to the HIRS channels was accomplished by inserting a very thin cloud at 700 mb with a thickness of 0.01 km. Transfer calculations involving such a thin cloud were then carried out. Physically there should be a slight decrease of the upwelling radiance from the thin cloud when compared to the CCR. A plot of the thin cloud case is also shown in Figure 3.3. It should be noted that in all twelve channels the thin cloud case has less upwelling radiance than the CCR and that the radiance differences between the thin cloud case and CCR are insignificantly small. These comparisons reveal that the modification of the transfer program to the HIRS channels was successful.

To actually execute the transfer program, the optical properties for the clouds and the Rayleigh layer (consisting of gases only) become input as well as the atmospheric profile. Because of the computer storage and computer time limitations, only one temperature for cirrus and middle clouds was allowed in the transfer calculations. The cloud temperatures used in all calculations are the averaged temperatures corresponding to the thickest cloud layers obtained from the
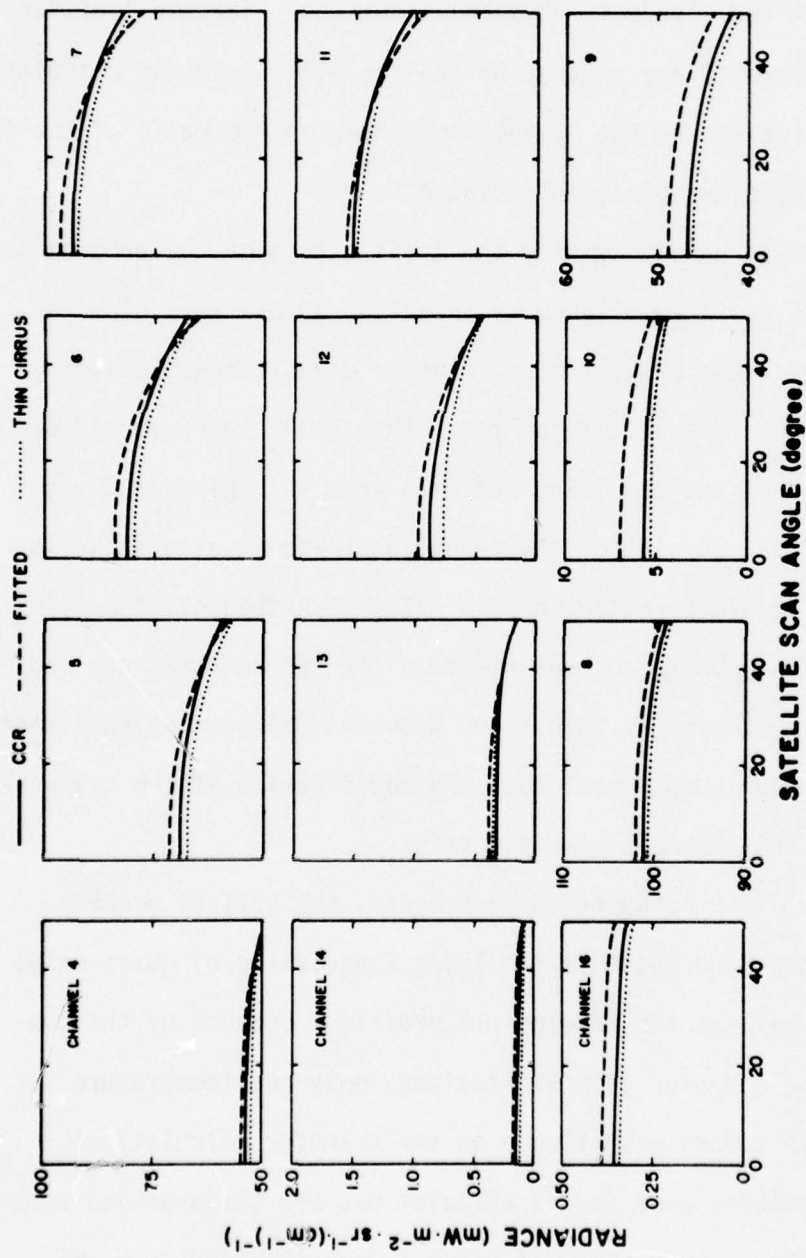
Figure 3.3 Comparison of the clear column radiance, CCR, evaluated from the satellite transmittance (solid lines) with those obtained from the exponential fitting of the transmittance (dashed lines) and with radiances calculated from the spectral radiative transfer program assuming a thin cloud with a thickness of 0.01 km (dotted lines).

atmospheric temperature profile. This was necessary to enable us to examine the change in upwelling radiance due strictly to the change in cloud mass. If more than one parameter was allowed to vary in subsequent calculations, the different temperatures would mask the change in upwelling radiance caused by the change in cloud mass. The only output from the transfer program utilized in subsequent analysis is the upwelling radiances at the discrete ordinate angles coming out of the top of the cloud. These values are then linearly interpolated to 51 angles corresponding to whole satellite scan angles and then attenuated to the top of the atmosphere utilizing the computations described earlier in this section.

3.3 Sensitivity Analysis

To conduct sensitivity analysis of the upwelling radiance at the top of the atmosphere a series of combinations of clouds were inserted into the transfer program. The resulting upwelling radiances at the top of the atmosphere were then plotted as a function of satellite scan angle. The results of these calculations are shown in Figures 3.4, 3.5 and 3.6. In each of the cases the lower boundary conditions were calculated by assuming that no low cloud was present thus the lower boundary condition is a summation of the contribution from the ground plus the contribution from each of the atmospheric layers below the cloud.

In each case the top of the cirrus cloud and the base of the altostratus cloud are held constant. To change the cloud

combinations the base of the cirrus cloud and the top of the middle cloud are varied. Since the model atmosphere has ten layers between 700 mb, the base of the middle cloud, and 250 mb, the top of the high cloud, the middle cloud could include up to four layers from 700 to 500 mb and the high cloud could include up to five layers from 475 mb to 250 mb. These ten layers were predetermined from those set in the CCR program. One layer between the two cloud decks must be clear so that three layers exist to insure proper execution of the transfer program. The four symbols used in Figures 3.4-3.6 have the following meaning. I_k^C indicates thick cirrus clouds (five atmospheric layer), I_n^C indicates thin cirrus (one atmospheric layer), I_k^A indicates thick middle clouds (four atmospheric layers), and I_n^A indicates thin middle cloud (one atmospheric layer).

The twelve channels of data are divided into the three figures in the following way. Figure 3.4 contains the four channels in the 15 μm CO_2 band. Plot 1a is for combinations of both high and middle cloud and plot 1b is for middle or high cloud alone. The same pattern is followed for each set of plots in Figure 3.4. The plots are arranged from right to left correspond to decreasing absorption by CO_2. The arrangement of Figure 3.5 is identical to Figure 3.4 for the four channels in the 4.3 μm CO_2 band. Figure 3.6 is similar to the previous figures with plots 3 and 4 corresponding to the water vapor bands (channels 10 and 9), respectively. Plots 1 and 2 of Figure 3.6 correspond to window channels, 16 and 8 respectively.
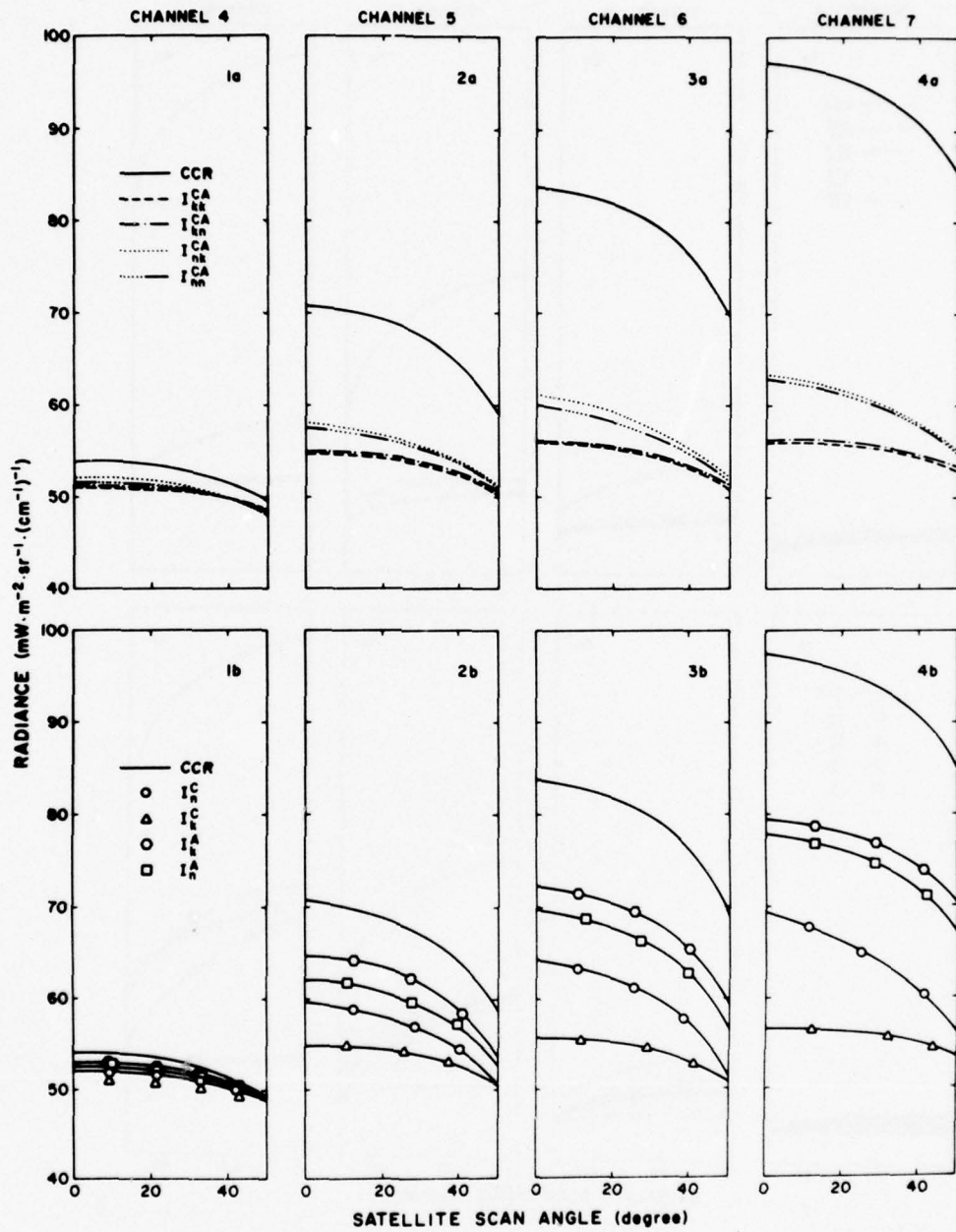
Figure 3.4 Comparison of the upwelling radiance for cloudy atmospheres with CCR in channels 4-7. Part a is for multilayer combinations of thick and thin cirrus and middle cloud. Part b is for single layers of thick and thin cirrus and middle cloud.
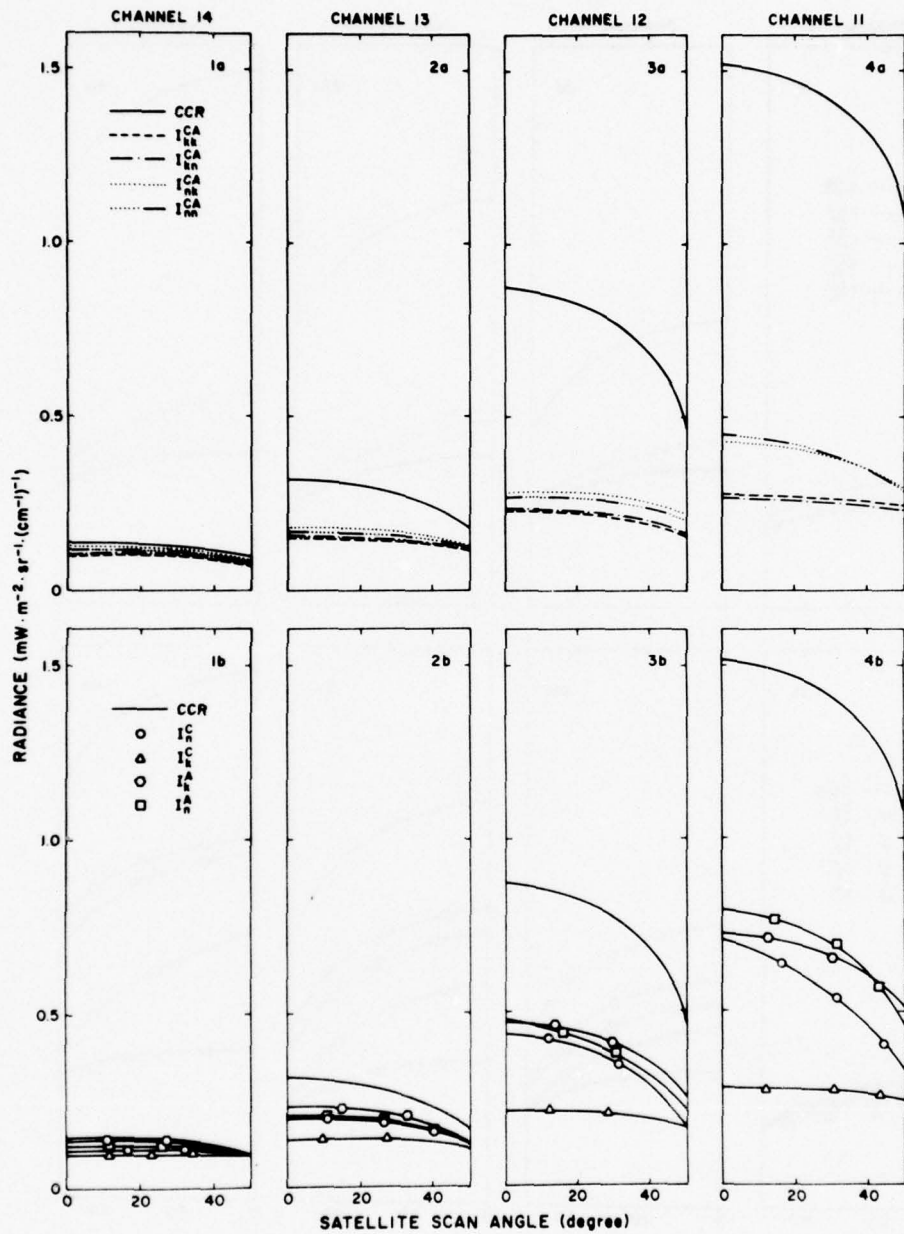
Figure 3.5 Comparison of the upwelling radiance for cloudy atmospheres with CCR in short wave CO_2 channels. Part a is for multilayer combinations of thick and thin cirrus and middle cloud. Part b is for single layers of thick and thin cirrus and middle cloud.
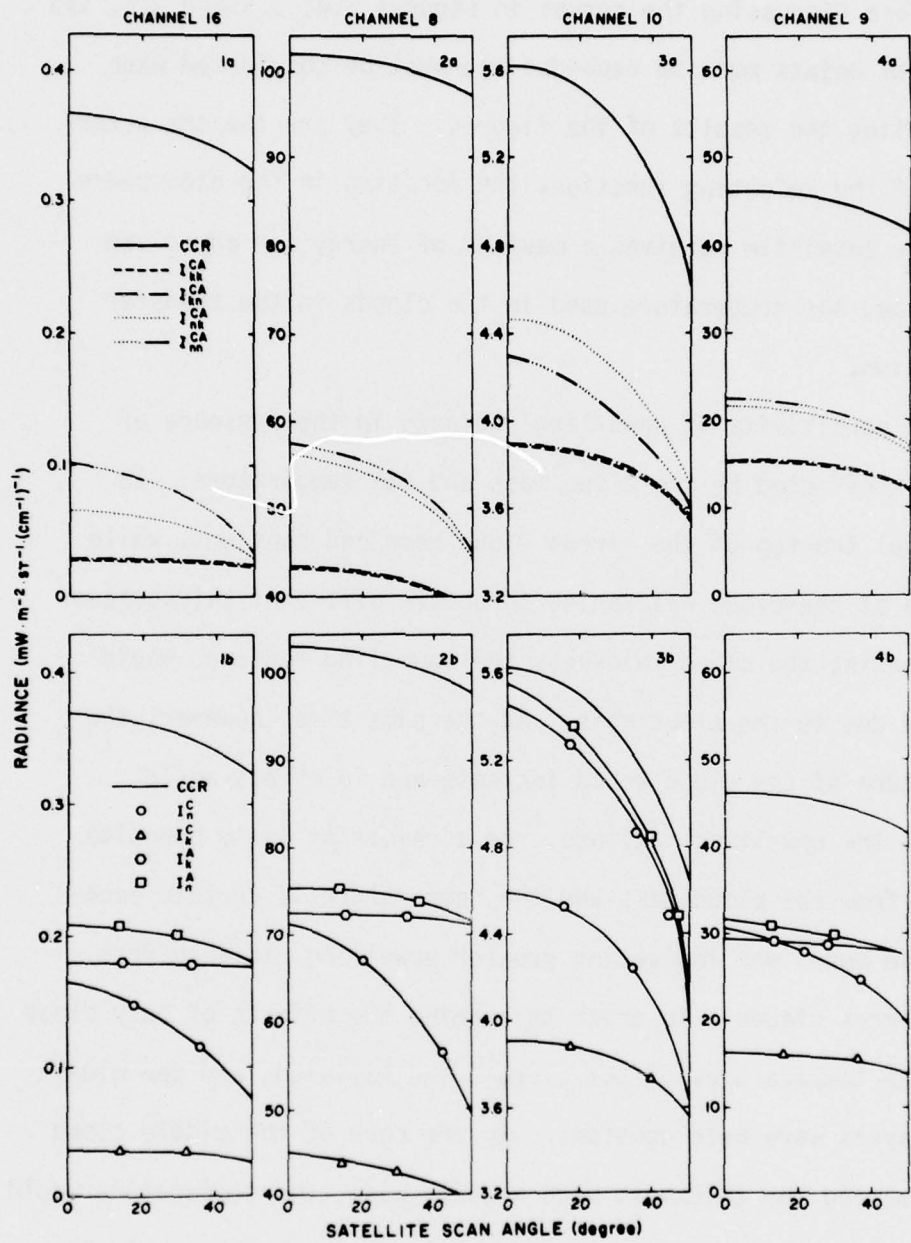
Figure 3.6 Comparison of the upwelling radiance for cloudy atmospheres with CCR in window and water vapor channels. Part a is for multilayer combinations of thick and thin cirrus and middle cloud. Part b is for single layers of thick and thin cirrus and middle cloud.

Before discussing the curves in Figures 3.4, 3.5 and 3.6, two additional points must be expanded and must be considered when interpreting the results of the figures. They are the characteristics of the weighting function, the location in the atmosphere where the satellite receives a maximum of energy for any given channel, and the temperature used in the clouds in the transfer calculation.

The sensitivity of upwelling radiance in the presence of clouds is effected by the cloud mass and its temperature. In this model the top of the cirrus cloud remained constant, while the base of the cloud was varied to obtain different thicknesses. By increasing the cloud thickness the upwelling radiance would decrease due to the cloud mass. At the same time, however, the temperature of the cloud would increase and in effect would increase the upwelling radiance. As a result of these opposite effects from the cloud mass and the temperature in certain occasions the model was indicating greater upwelling radiance from thick cirrus clouds. In order to examine the effects of only cloud mass, the temperatures of the cirrus, the Rayleigh, and the middle cloud layers were held constant. In the case of the middle cloud by increasing the thickness with a fixed base, the temperature would decrease and the two effects would compliment each other. In the figures I_k^C and I_n^C represent cirrus thicknesses of 4.12 km and 1.26 km respectively. The temperature for the cirrus cloud was taken to be the temperature of I_k^C from the model atmosphere and has

a value of 244.9°K. The temperature of the Rayleigh layer
was constant in all transfer calculations and was represented
by the temperature of the middle layer when both thick cirrus
and thick altostratus were present and has a value of 250.1°K.
In the figures I_k^A and I_n^A represent middle cloud thicknesses of
2.68 km and 0.35 km, respectively. The middle cloud temperature
was that of a thick cloud from the model atmosphere and is repre-
sented by a value of 270.17°K. The symbols I_{kk}^{CA} and I_{kn}^{CA} represent
multilayered combinations for thick cirrus with thick middle cloud
and thick cirrus with thin middle cloud, respectively. I_{nk}^{CA} repre-
sents thin cirrus with thick middle cloud and I_{nn}^{CA} is thin cirrus
with thin middle cloud.

The characteristic of the weighting function and the level
in the atmosphere where the most energy for a channel is present
must be considered in the interpretation of the figures. If the
maximum energy of a channel is located above the top of the cloud
being examined, the upwelling radiance in the channel will be
reduced from the cloud effects in addition to the gaseous absorp-
tion above the cloud.

As an example consider thin and thick middle cloud in channel
5. This channel obtains its maximum energy from near 500 mb which
is above the thin middle cloud and right at the top of the thick
middle cloud. In the thin cloud case the absorption above the
cloud has more effect than the cloud in the thick case. The result
is more attenuation of the upwelling radiance in the thin cloud case.

This problem does not exist for cirrus since the weighting functions all peak below or in the cirrus cloud.

Figures 1a and 1b of Figure 3.4 are for channel 4 of the HIRS instrument which is located at 701.91 cm^{-1} in the $15 \mu m$ CO_2 band. The weighting function for this channel peaks at 300 mb. 2a and 2b are for channel 5 located at 716.83 cm^{-1} and it has its maximum energy from 500 mb. Channel 6 located at 732.55 cm^{-1} with a maximum energy obtained near 720 mb is shown in plots 3a and 3b. The final plot of Figure 3.4 is for channel 7 which has a central wavenumber and maximum energy at 749.18 cm^{-1} and 920 mb, respectively.

Examination of part a of Figure 3.4 indicates the same general pattern with all four multicloud combinations. The greatest upwelling radiance is obtained from thin cirrus with thick middle cloud in all channels. Although the effects of attenuation above the middle cloud is highly masked by the cirrus cloud, the thin cirrus with thick middle cloud still has the greatest upwelling radiance. In the case of thick cirrus in part a, the change of middle cloud thickness has no effect on the upwelling radiance. In the presence of thick cirrus the transfer process is completely dominated by this thick cloud.

Part b of Figure 3.4 displays the same general pattern as part a. Single layer clouds show a greater variability in upwelling radiances. In all cases the thick middle cloud produces the greatest upwelling radiance as discussed earlier. The least radiation comes from the thick cirrus cloud. The locations of the cirrus

curves compared to the middle cloud curves is in part due to the cloud temperatures. The effect of the·weighting function can be seen by noting the decrease in difference of the upwelling radiance for middle cloud and an increase for cirrus cloud. As the peak of the weighting function moves closer to the ground the effect of this energy maximum becomes less important in the upwelling radiance. The decrease in slope of the curves as a function of scan angle for thick cloud cases is consistent with the fact that scattering becomes more isotropic as the cloud thickness increases.

The channels represented in Figure 3.5 are 14, 13, 12 and 11 which have central wavenumbers at 2274.6, 2244.2, 2211.97 and 2191.0 cm^{-1}, respectively. They are located in the 4.3μm CO_2 band and have their weighting functions peak at 600, 700, 850 and 950 mb. Figure 3.5 displays the same characteristics as Figure 3.4. This would be expected since they both have CO_2 as the major absorber. In part a of Figure 3.5 the presence of cirrus cloud again is dominant. There is only a slight change in the upwelling radiance when middle cloud thicknesses are changed with thin cirrus. Plot 4a of Figure 3.5 shows an interesting crossing pattern for thin cirrus. This is caused by the location of the level of maximum energy for the channel (950 mb). In all cases so far discussed, cirrus cloud is the dominant influence. In cases where channels peak higher than the middle base the thick middle cloud has a greater upwelling radiance than the thin middle cloud.

Since the temperature is held constant three factors are important in the results of Figure 3.5. They include the cirrus cloud thickness, the middle cloud thickness and the peak of the weighting function. In the case of Figure 3.5 where the crossing pattern is observed the thickness of the middle cloud has become more dominant than the attenuation above the middle cloud. This factor is useful in using the HIRS data to infer cloud parameters.

Figure 3.6 is a plot of two HIRS window channels and two water vapor channels. Plots 1 and 2 represent window channels 16 and 8 that have central wavenumbers at 2691.2 and 899.99, respectively. Since these are window channels they receive the maximum energy from the earth's surface. The plots 1a and 2a show the results in the presence of multilayered clouds. With the absence of major absorbing gases in the atmosphere, the problems cited in the CO_2 channels concerning absorption above the cloud is now minimal. This can be seen by noting the greater difference between thick and thin middle cloud in the presence of thin cirrus when compared to Figures 3.4 and 3.5. Plots 1b and 2b of Figure 3.6 also indicate the effects of clouds on upwelling radiance more readily than the CO_2 channels. As would be expected thin clouds have a greater upwelling radiance than thick clouds. Cirrus clouds attenuate more radiation than middle clouds when only one cloud deck is present. This last point can be attributed in part to the temperature of the two clouds.

Plots 3 and 4 of Figure 3.6 correspond to channels 10 and 9, respectively. Channel 10 peaks at 400 mb and has a central

wavenumber of 1508.29. Channel 9 peaks at 900 mb and has a

central wavenumber of 1223.22. Since the concentration of CO_2

in the atmosphere is independent of temperature, the crossing

patterns observed in Figures 4 and 5 will always be present. On

the other hand, however, the concentration of water vapor is a

function of temperature and the gaseous absorption above the cloud

will vary with temperature in channel 10. The gaseous absorption

in the clouds was fitted with the saturation conditions as noted

earlier. In the case of the Rayleigh layer the prevailing mois-

ture concentration of the model atmosphere was assumed. The cross-

ing pattern for thick and thin middle clouds are not present for

the water vapor channels. This can be attributed to the fact that

the thickness of the middle cloud has a greater effect on the final

upwelling radiance than the absorption above the cloud although

the real effects of the middle cloud are somewhat less due to the

gaseous absorption above the cloud. The same patterns are observed

in the water vapor channels as in all other channels analyzed. The

thick cirrus cloud dominates in plots 3a and 4a and has the same

upwelling radiance for thick cirrus in 3b and 4b of Figure 3.6.

CHAPTER 4

PARAMETERIZATION OF RADIANCE CALCULATIONS FROM
CLOUDY ATMOSPHERES

This chapter discusses the parameterizations accomplished
on the theoretically calculated upwelling radiances to recover
cloud type and moisture content. This parameterization was
accomplished in three steps. First, the cloudy and the clear
column radiances were ratioed; second, the radiances were fit
with an empirical function that would indicate cloud type; third,
the results of these cloud type parameterizations were fit with
another empirical function to recover ice or water content of the
cloud.

The sensitivity analysis discussed in the previous chapter
was accomplished for cloud combinations I_{nn}^{CA}, I_{kk}^{CA}, I_{n}^{C}, I_{K}^{C}, I_{n}^{A}, and
I_{K}^{A}. As discussed in the previous chapter, I_{nn}^{CA} and I_{nk}^{CA} displayed
much the same characteristics as I_{K}^{C} which would imply that multi-
layered cloud cases would have to be treated as thick cirrus.

Another important point to note from the sensitivity analyses
is the relatively small difference displayed by the thin and thick
middle cloud. This small difference is due to the attenuation
above the middle cloud. In the model, a constant tempera-
ture was used in the theoretical calculation to see if the change
in thickness had any influence on the upwelling radiance. This

difference although small, will prove to be important in sub-
sequent analyses. Physically, as the middle cloud thickness
increases, the cloud becomes opaque to radiation from below so
that, in effect, the satellite receives all of its energy from
the temperature at the cloud top.

4.1 Ratioing of Upwelling Radiances

As noted earlier, the theoretical model calculated upwell-
ing radiances for one atmosphere, one cloud temperature, one
cloud composition, and over the scan angles of the HIRS instru-
ment. In addition, the cloud top height for the cirrus and the
cloud base for the middle cloud were held constant. In the real
atmosphere, the temperature profile is always changing, the cloud
composition is variable, and the location of the clouds in the
vertical is never constant. A method that will minimize the
effects of the model assumptions when parameterizing the real
atmosphere is desirable.

The information available from each channel from the model
output is the clear column radiance and the cloudy radiances at
many scan angles. To minimize the computer requirements and
redundancy in analysis all the subsequent relationships were
derived for a scan angle of 0 degrees. These same relationships
could be developed for any scan angle or range of scan angles.

To minimize the model assumptions and to normalize the real
data to the model, the clear column radiances were divided into
the cloudy radiances for each channel. This ratio represents

the relative reduction of upwelling radiances due to the cloud effects in the atmosphere and the quantity is dimensionless. There are several advantages in working with these ratios. Physically, the ratio will reduce the effect of the change in atmospheric profile on the cloudy radiances. In addition, the degradation of the ratio coupled with the peaking of the weighting function gives an immediate indication of clouds at that level or above. Another advantage of the ratio technique is that in addition to normalization between different atmospheres, the effects of clouds on the ratio of each channel can be compared with other channels. In the subsequent analysis, channels 4-7 of 15 μm CO_2 band, 11-14 of the 4.3 μm CO_2 band, 8 at 11.11 μm in the window, 9 in the 8.2 μm water vapor band and 10 in the 6.3 μm water vapor band were utilized.

The theoretical model was executed for cirrus thicknesses of 1, 2, 3, and 4 km and middle cloud thicknesses of 0.3, 0.5, 0.7, 1.0, 2.0, and 3.0 km. These ratios are given in Table 4.1. Part a and part b of Table 4.1 are for cirrus and middle clouds, respectively. Examination of Table 4.1 shows that the transparent quality of cirrus is evident in the infrared spectrum. There is a successive decrease of upwelling radiances in all channels as the cloud thicknesses increase. The successive decrease of the ratios continues all the way to 4 km.

Between 3 and 4 km the decrease in ratio in each channel is only slight indicating that near 4 km the cirrus cloud used in the model is becoming opaque to the infrared radiation, and the cloud

TABLE 4.1 Ratios of Cloudy Radiances to Clear Column Radiances for 11 HIRS Channels for Several Thicknesses. Part a is for Cirrus Clouds Part b is for Middle Clouds.

Part a (Cirrus Clouds)

Channel	Thickness (km)			
	1.	2.	3.	4.
4	.970	.957	.952	.950
5	.866	.811	.789	.780
6	.799	.716	.683	.670
7	.748	.644	.603	.587
8	.743	.583	.499	.452
9	.718	.529	.426	.371
10	.960	.777	.717	.697
11	.538	.327	.237	.200
12	.563	.368	.286	.253
13	.679	.544	.488	.465
14	.858	.798	.774	.764

Part b (Middle Clouds)

Channel	Thickness (km)					
	.3	.5	.7	1.	2.	3.
4	.996	.990	.984	.979	.974	.972
5	.936	.921	.920	.900	.889	.879
6	.884	.867	.865	.847	.835	.835
7	.839	.820	.817	.804	.796	.796
8	.755	.720	.711	.708	.708	.708
9	.702	.653	.641	.637	.637	.637
10	.997	.971	.969	.968	.968	.968
11	.601	.519	.492	.466	.453	.453
12	.652	.572	.549	.510	.488	.488
13	.813	.748	.735	.668	.634	.634
14	.956	.919	.915	.863	.863	.863

temperature now becomes important in the transfer process. At
cloud thicknesses greater than 4 km, the upwelling radiance is
representative of the Planckian temperature of the cloud top.

Analysis of the middle cloud thickness indicates the cloud
mass becomes opaque between 2 and 3 km. This can be understood
in view of the greater particle concentration when compared to
the cirrus cloud. Again the cloud temperature used is represented
in the radiances at thicknesses of 2 km or greater.

A decrease of the lower boundary condition in the transfer
calculation is in effect inserting opaque low clouds into the lower
atmosphere. The effect on the upwelling radiance as seen from a
satellite would be to decrease the ratio. Another decreasing
effect would be the use of a colder middle cloud temperature. These
two cases for middle cloud alone are presented in Table 4.2 for
thick low clouds in Part a and a cloud temperature of 265° A in
Part b.

Comparison of Table 4.1b with Table 4.2a shows some interest-
ing effects on the ratios of the upwelling radiances. The decrease
in energy at the middle cloud base due to the presence of opaque
low clouds decreases the cloudy to clear column ratio at thicknesses
less than 2 km, but exhibits the same ratio for thicknesses 2 km or
greater. This again implies that the cloud temperature is the
dominant factor in determining the upwelling radiance and thick-
nesses greater than 2 km. Table 4.2b represents a calculation with
the middle cloud temperature decreased by 5 degrees from Table 4.1b

TABLE 4.2 Ratios for 11 HIRS Channel by Introducing Low Clouds
(Part a) and Changing Cloud Temperature (Part b)

Part a (Thick Low Clouds)

Channel	Thickness (km)			
	.5	1.	2.	3.
4	.990	.979	.974	.972
5	.921	.900	.889	.879
6	.866	.847	.835	.835
7	.819	.804	.796	.796
8	.715	.708	.708	.708
9	.646	.637	.637	.637
10	.969	.968	.968	.968
11	.501	.465	.453	.453
12	.556	.506	.448	.448
13	.738	.668	.634	.634
14	.916	.863	.863	.863

Part b (Cloud Temperature 265°A)

Channel	Thickness (265°A)			
	.5	1.	2.	3.
4	.983	.975	.971	.969
5	.894	.878	.869	.862
6	.828	.812	.804	.804
7	.774	.760	.754	.754
8	.662	.647	.646	.646
9	.586	.566	.565	.565
10	.906	.899	.899	.899
11	.439	.387	.377	.377
12	.491	.435	.419	.419
13	.673	.612	.589	.589
14	.877	.838	.838	.838

and no low clouds present. This table retains the same tendencies as shown in Tables 4.2a and 4.1b. The range of the ratios in each channel is decreased when compared to values presented in Table 4.1b. This decrease in range is caused by the decrease in energy due to the Planckian cloud temperature.

Inner comparisons of the channels in Tables 4.1 and 4.2 give a good indication on the effects of clouds on upwelling radiances for different wavenumber regions of the infrared spectrum in conjunction with the peak of the channel's weighting function. The physical factors that influence the ratio for a given cloud type, cloud thickness and channel can be determined from Table 4.1. In the present model, the cloud top is constant at 250 mb. Using a 2 km cirrus as an example, the interaction of these two physical factors (the weighting function and the channel wavenumber) are examined. The channels that are in the 15 μm CO_2 band show a decreasing ratio as the weighting functions peak deeper in the atmosphere. The same decrease is noted in 4.3 μm CO_2 channels but by a greater degree. This fact would indicate a greater impact of clouds on shorter wave lengths. The data shows that this effect when comparing channel 7 (peak at 900 mb) and channel 12 (peak at 850 mb) where the long wave channel has a ratio double that of the short wave channel.

This same tendency can be noted for a case of middle cloud only as in Table 4.1b. Recalling that the middle cloud is based at 700 mb and builds upward. It should be noted that channels

with weighting functions that peak above the base of thin middle
cloud (4, 5, 10, 14) are not affected by the middle cloud as much
as lower peaking channels. Thus, in order to interpret the results
of these theoretical calculations, the effects of the cloud temper-
ature, the peak of the weighting function, and the wavenumber of
the channel must be considered.

4.2 Cloud Type Determination

To utilize the theoretical results in a real atmosphere, the
first step to inferring the cloud scene in the satellite field-of-
view is to determine the vertical location of the cloud. This in
effect will give a measure of the cloud type. The foregoing discus-
sions on ratios would indicate the presence of cirrus or middle
cloud alone can be determined from the analysis of these theoretical
results. As noted earlier, the presence of middle cloud under a
thin cirrus cloud cannot be distinguished from a thick cirrus cloud.

The inability to distinguish multilayer clouds from the
current analysis does not hinder the use of this technique to infer
cloud thickness. As an example, in the classical cold front, one
would expect that by the time a cirrus cloud reaches a thickness
of 3 km that middle cloud will be present under this moderately
thick cirrus layer. Likewise, with the model indicating a thick
middle cloud layer (2 km) lower clouds are probably present. With
this in mind, no attempt was made in this analysis to distinguish
more than one layer of cloud, although based on thickness calcula-
tions and comparison with satellite pictures, the probability

that multilayer clouds exist in the satellite field of view is very high.

For the purpose of determining the cloud type from the theoretical data, the channels were rearranged in order of decreasing ratios for a moderately thick cirrus. The rearrangement of the channels from Table 4.1 is shown in Figure 4.1. Analysis of this figure shows the effects of wavenumber and weighting function peak. The long wave channels 4-7 all have greater ratios than the short wave channels 11-14 with similar weighting function peaks which would indicate that the cloud mass has more impact on shorter wavelengths. The location of channel 14 between channels 5 and 6 would indicate that there is an overlap between the two CO_2 bands depending on the weighting function peak. The locations of channels 10 and 9 are according to weighting function peaks with channel 10 having a higher ratio and a higher weighting function peak than channel 9. The location of their ratios within the CO_2 channel ratios in the figure is due to the model atmosphere humidity profile. By increasing the water vapor amount, there would be an increase in attenuation and thus a lower ratio. Conversely, a decrease in the water vapor would decrease the attenuation and increase the ratio.

The radiance ratios and channel numbers shown in Figure 4.1 were each fitted with a linear equation by means of regression analysis. Part a is for cirrus clouds and Part b is for middle clouds. Each straight line is labeled with the thickness it
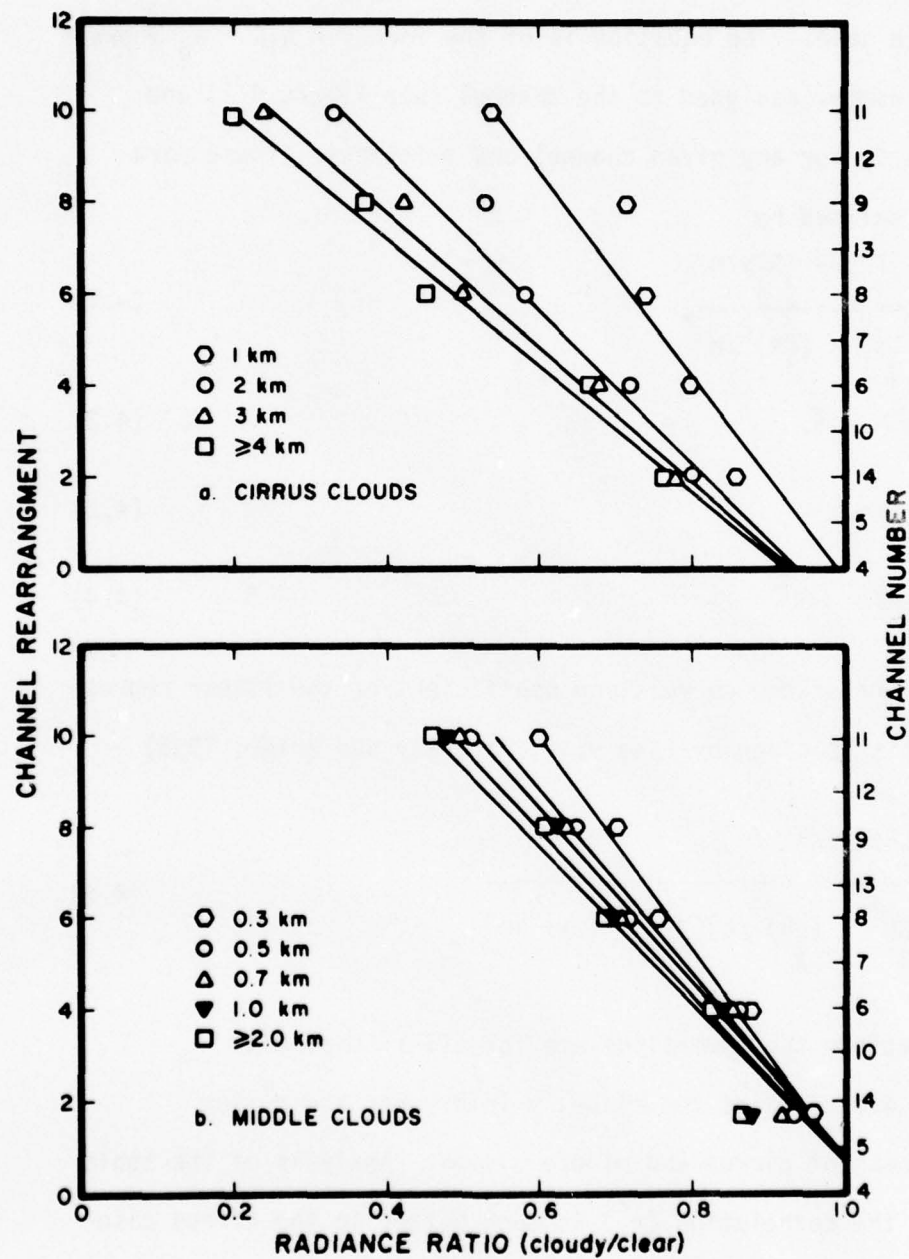
Figure 4.1 The best straight line fit for four cirrus cloud
thicknesses (Part a) and for six middle cloud
thicknesses (Part b).

represents. The data displayed in Figure 4.1 was fit by a straight line in each case. The equation is of the form $y = a_1 R + a_0$ where y equals the number assigned to the channel (see Figure 4.1) and R is the ratio for any given channel and thickness. These parameters are defined by

$$a_1 = \frac{\sum_j Ry - \sum_j R \sum_j y/n}{\sum_j R^2 - (\sum_j R)^2/n}, \tag{4.1}$$

$$a_0 = \overline{y} - a_1 \overline{R}, \tag{4.2}$$

$$\overline{y} = \sum_j y/n, \tag{4.3}$$

$$\overline{x} = \sum_j R/n \tag{4.4}$$

and the square of the correlation coefficient of the linear regression analysis is given by (see e.g., Panofsky and Brier, 1968)

$$r^2 = \frac{[\sum_j Ry - \sum_j R \sum_j y/n]^2}{[\sum_j R^2 - (\sum_j R)^2/n][\sum_j y^2 - (\sum_j y)^2/n]} \tag{4.5}$$

In the equations the summations are for all 11 channels.

Table 4.3 contains the slope, y-intercept, and r^2 for each thickness of cirrus and middle clouds. Analysis of the table shows that the correlation (r^2) is much better in the cirrus case (0.96) when compared to the middle cloud case (0.90). The decrease in correlation in the middle clouds and the 1 km cirrus cases can be explained by the placement of the ratio of channel 10. The

original arrangement was done for a thick cirrus case where the
effects of the cirrus cloud mass on channel 10 were present. In
the middle cloud and 1 km cirrus cases there is no effect of the
cloud mass on channel 10. Therefore, the location of channel 10
in the fitting process decreases the correlation for the 1 km
cirrus and the middle cloud cases. The linear fit developed here
will be used when parameterizing actual HIRS data in Chapter 6.
Another important thing to note in this analysis is that the
magnitude of the slope is greater than the magnitude of the y-
intercept for all cirrus thicknesses and the reverse is true for
middle clouds. This fact will be used in subsequent analysis to
distinguish between middle and cirrus clouds.

TABLE 4.3 Slope, y-intercept, and Correlation Coefficient
           Squared for Several Cloud Thickness for Cirrus
           (Part a) and Middle (Part b) Clouds.

Part a (Cirrus Clouds)

| | Thickness (km) | | | |
	1.	2.	3.	4.
slope	-21.75	-16.82	-14.79	-13.94
y-intercept	21.69	15.70	13.68	12.84
r^2	.872	.968	.977	.977

Part b (Middle Clouds)

| | Thickness (km) | | | | | |
	.3	.5	.7	1.	2.	3.
slope	-22.78	-19.80	-18.80	-18.10	-17.50	-17.50
y-intercept	23.56	20.70	19.70	18.80	18.10	18.10
r^2	.904	.925	.925	.913	.906	.906

Table 4.2 was also fit with a straight line after rearranging the channels. In both cases the magnitude of the slope was less than the magnitude of the y-intercept which is consistent with earlier middle cloud calculations. Furthermore, both the slopes and y-intercepts of Table 4.2 have smaller magnitudes than those in Table 4.1. This decrease in slope and y-intercept is directly caused by the middle cloud temperature. Since the theoretical calculations indicate that the middle clouds become opaque at a thickness of 2 km, the cloud temperature effects are still present in the ratioing. In the atmosphere middle clouds generally build from the base up. In the model the base of the middle cloud was held constant to be consistent. Therefore, a colder cloud temperature than that used in the model would in effect show an increase in cloud thickness. When this is applied to real data and the slope and y-intercept have smaller magnitudes than the ones in the theoretical program it must be assumed that the cloud is thicker than those that could be handled by the model. In this way the parameterizations for only one cloud temperature can be used since the presence of a colder cloud temperature would indicate a higher cloud top and therefore a thicker cloud.

4.3 Ice and Water Content Determination for the Model Atmosphere

A measure of liquid water and ice content distribution over the planet is important to many areas of meteorology. These include the initialization of numerical models to increase long term forcast accuracy and in models that study global circulation. The

inference of compositions for ice clouds has been accomplished as noted in Chapter 1. To measure the liquid water content in the atmosphere, radiometers that are sensitive to the microwave portion of the spectrum are on the Nimbus series of satellites. Grody (1976) used data from the Nimbus V Microwave Spectrometer (NEMS) to relate integrated water vapor and liquid water to brightness temperatures in the channel in the 22.235 GHz water vapor line. In his regression analysis it was shown that a good measure of atmospheric water content was possible over low emmissivity sea surfaces. Staelin et al. (1975) used the NEMS data to drive the abundance of atmospheric liquid water by monitoring the channel at 53.65 GHz. It was shown that a minimum in brightness temperature corresponded to a maximum in atmospheric liquid water content. Further work by Staelin et al. (1976) on the NEMS data used the two channels at 22.235 and 31.4 GHz to map vapor and liquid water over oceans. A high degree of accuracy was obtained when compared to radiosonde parameterizations. This vapor and liquid water content distribution of the atmosphere can also be retrieved from the Nimbus VI Scanning Microwave Radiometer (SCAMS) data since the SCAMS instrument monitors the same channels as the NEMS. Smith and Woolf (1976) also proposed a method to recover temperature and humidity profiles, cloud cover, and integrated liquid water content by combining SCAMS and HIRS data. The following analysis describes a technique to infer cloud ice and water content from the HIRS channels.

From the theoretical calculations each cloud thickness is representative of a cloud mass since only one drop size distribution was used for water clouds and only one particle concentration was used for ice clouds. In the case of the water clouds a liquid water content of 0.15 gm m^{-3} was assumed and for ice clouds a content of 0.0283 gm m^{-3} was used. Table 4.4 gives the cloud mass in gm m^{-2} for a series of middle and high cloud thickness. The remainder of this dissertation will represent cloud thickness as cloud mass.

TABLE 4.4 The Relationship Between Cloud Thickness and Cloud Mass for a Series of Middle and High Clouds.

Cirrus Clouds		Middle Clouds	
Thickness(km)	Ice Content(gm m^{-2})	Thickness(km)	Water Content (gm m^{-2} x 10^2)
1.0	28.3	0.3	0.45
2.0	56.6	0.5	0.75
3.0	84.9	0.7	1.05
4.0	113.2	1.0	1.50
		2.0	3.00

The recovery of liquid water and ice content from the fitted ratios is possible by knowing the theoretical mass of the cloud for which the ratios are being calculated within certain limits. In the cirrus cloud case, it was found that for a cloud mass of less than 28.3 gm m^{-2} the correlation coefficient decreased significantly below the 95 percent level and the ratios could no longer be fit with a straight line. This was also true for middle clouds with a

mass of less than 45 gm m^{-2}. Thick middle clouds (greater than 390 gm m^{-2}) had the same ratios as the 300 gm m^{-2} (2 km thickness) cloud. This would indicate that the cloud mass is a black body and all the energy from below is absorbed by the cloud layer and reradiated. The 113.2 gm m^{-2} (4 km thick) cirrus still seems to be somewhat transparent, but this cloud mass was near the maximum that could be handled by the theoretical model.

To recover ice or water content from the parameterizations of the theoretical radiance ratios, the slopes and y-intercepts for the two cloud types could be fit by a least squares logarithmic function that is given for the slope by

$$a_1 = c_1 + c_2 \ln \Delta z \tag{4.6}$$

and for the y-intercept by

$$a_0 = c_3 + c_4 \ln \Delta z, \tag{4.7}$$

where Δz is the thickness of the ice or water cloud. c_1, c_2, c_3, and c_4 are constants to be determined for each set of slopes and y-intercepts. For the slope, a_1

$$c_1 = \frac{\sum_i (a_1 \ln \Delta z) - \sum_i \ln \Delta z \sum_i a_1 / n}{\sum_i (\ln \Delta z)^2 - (\sum_i \ln \Delta z)^2 / n}, \tag{4.8}$$

$$c_2 = \frac{1}{n}(\sum_i a_1 - c_1 \sum_i \ln \Delta z). \tag{4.9}$$

These equations are derived by substitution of the natural logarithm of the thickness for R and a_1 for y in Eq. (4.1) and (4.2). The

square of the correlation coefficient is given by

$$r^2 = \frac{[\sum_i a_1 \ln\Delta z - \sum_i \ln\Delta z \sum_i a_1/n]^2}{[\sum_i (\ln\Delta z)^2 - (\sum \ln\Delta z)^2/n][\sum_i a_1^2 - (\sum_i a_1)^2/n]}, \qquad (4.10)$$

which is again a direct substitution into Eq. (4.5). For the y-intercept c_3 and c_4 along with r^2 can be calculated by substituting a_0 for a_1 in Eq. (4.8)-(4.10). In the case of middle clouds the summation is over six cloud thicknesses and over four cloud thicknesses for cirrus clouds.

Using the data from Table 4.3, the slopes and y-intercepts were fitted for each cloud type. The resulting fits are shown in Figure 4.2 for middle clouds and Figure 4.3 for cirrus cloud. For middle clouds c_1 and c_2 are equal to -18.53 and 3.007, respectively, with the correlation coefficient of 0.984 while c_3 and c_4 equal 19.19 and -4.089 with a correlation coefficient of 0.960. For the cirrus case the values of c_1, c_2, c_3, and c_4 are -21.40, 5.75, 21.19, and -6.526, respectively. The constants c_1 and c_2 had a correlation coefficient of 0.988 and c_3 and c_4 had a correlation of 0.983.

From the straight line fit and the logrithmic substitution for a_1 and a_2 it can be shown that the thickness of any middle or high cloud is given by

$$\Delta z = e^{[(y-Rc_1 - c_3)/(c_2 R + c_4)]}, \qquad (4.11)$$

where R is the ratio for any channel. The cloud mass is then derived by multiplying the cloud thickness expressed in km by 28.3 gm m^{-2} km^{-1}
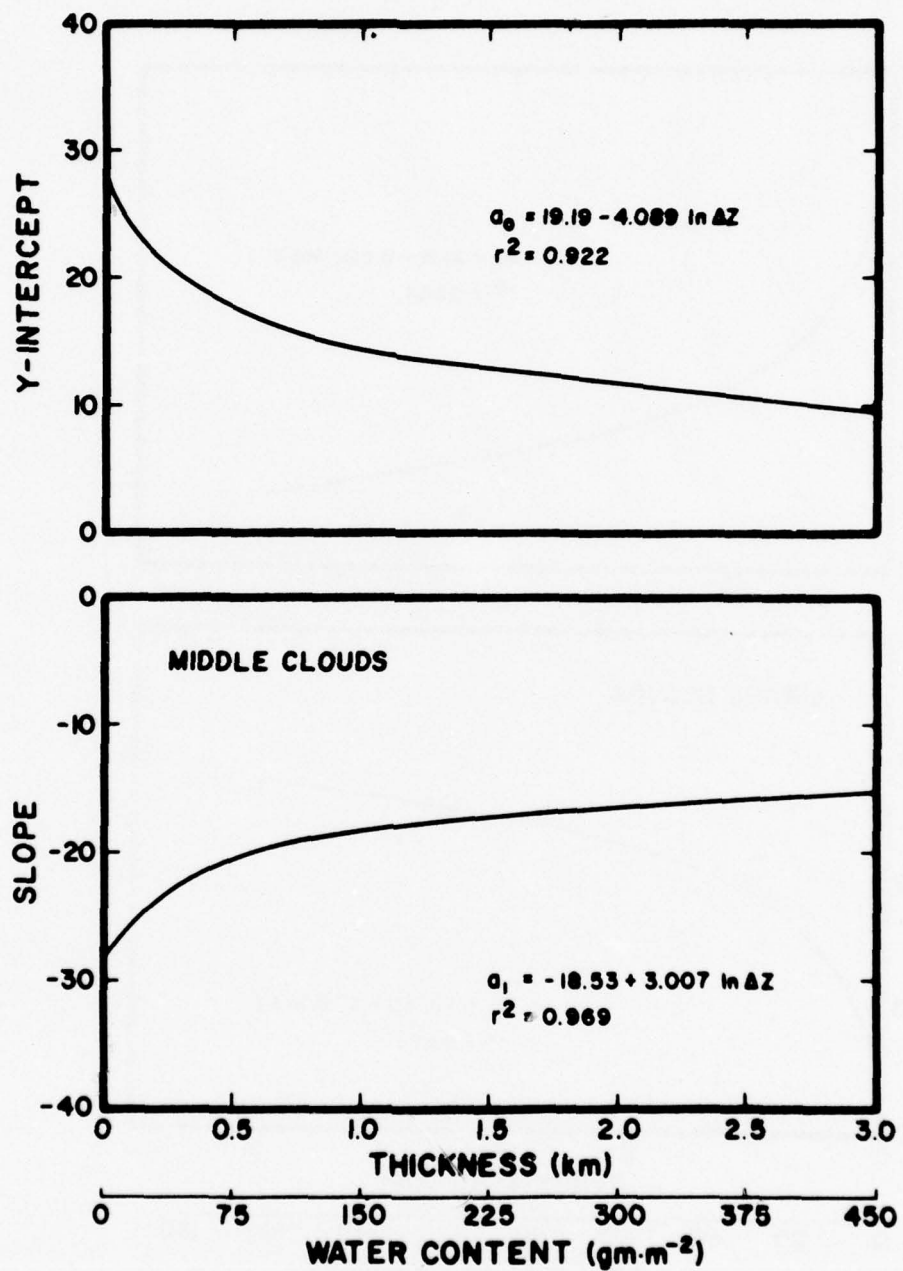
Figure 4.2   Best fit of y-intercept (top) and slope (bottom)
for six middle cloud thicknesses.
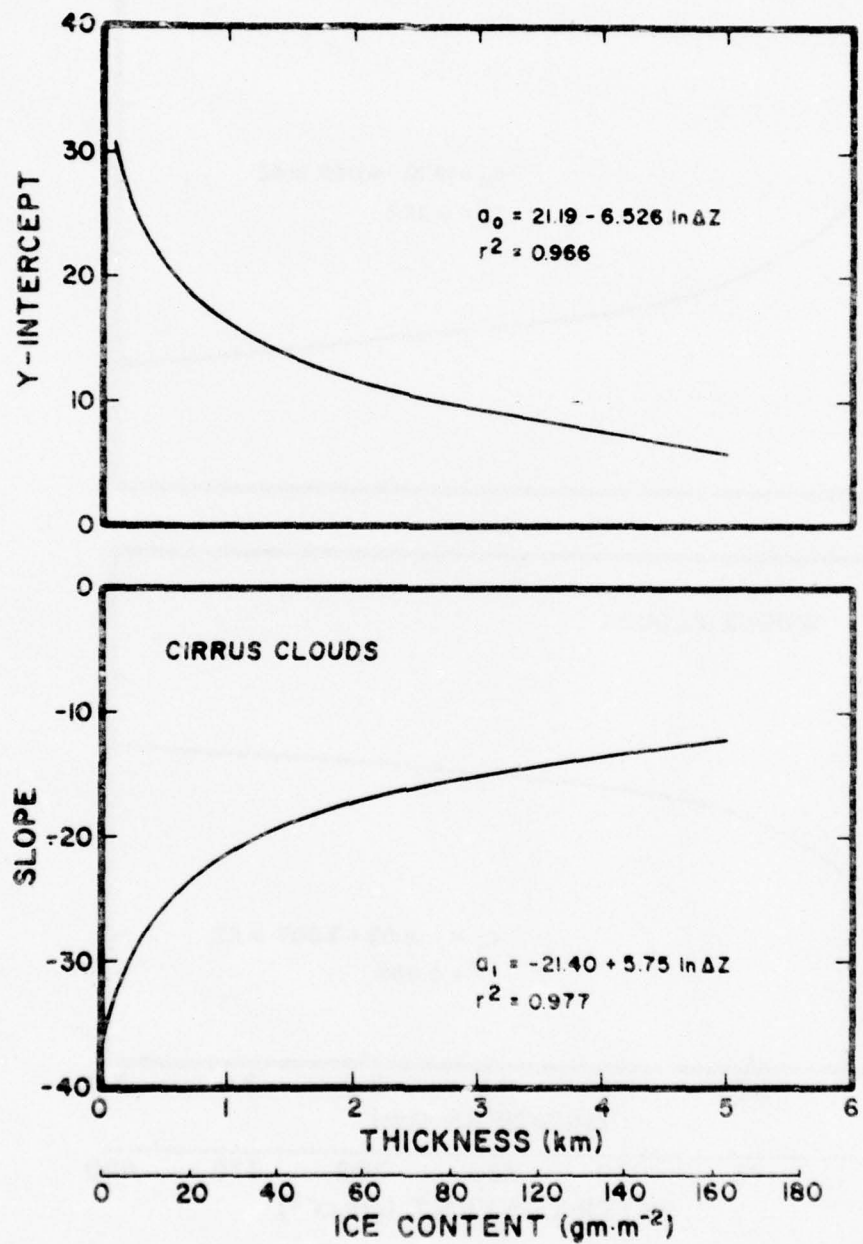
Figure 4.3 Best fit of y-intercept (top) and slope (bottom)
for four cirrus cloud thicknesses.

for cirrus cloud and 1.5×10^2 gm m^{-2} km^{-1} for middle clouds.
These results are used in subsequent chapters to infer cloud ice
and water content in both overcast and partly cloudy fields-of-view
from actual HIRS data.

CHAPTER 5

DATA DESCRIPTION

The method to determine cloud type and ice or water content developed in the previous chapter was applied to a selected set of Nimbus VI data. The results of this application was compared to the Air Force Three Dimensional Nephanalysis (3DNEPH) and satellite cloud pictures since these were the only source, of consistent cloud information on a routine basis. In this chapter, the HIRS data used in this analysis and the 3DNEPH data base are described.

5.1 High Resolution Infrared Sounder Data

The data that is routinely processed at NOAA/NESS is available on nine-track, 1600 bpi tapes. The data is packed in such a way that six or seven orbits are available on each tape. These tapes contain located and calibrated radiance values for all 17 channels. The tapes contain one scan line for each logical record and are packed according to Table 5.1 which is reproduced from the Nimbus VI User's Guide.

The Nimbus VI User's Guide gives a detailed explanation of the calibration procedure used on the radiance measurements in each channel of which part is presented here. The calibration of each channel is derived from the onboard target temperature. For a given monochromatic filter, the target radiance is the Planck

TABLE 5.1 HIRS Calibrated, Located Radiance Tape Format

Word	Format	Description
1	I	Time (GMT in Seconds)
2	I	Julian Day (1-366)
3	I	Year (74, 75 or 76)
4-45	I	Days (Data Quality)
46-759	SPEC	IR Calibrated Channel Data (17x42)
760-801	F2	Latitude (+ is North)
802-843	F2	Longitude (+ is East)
844-885	F2	Zenith Angle (+ is North of Trackline
886-900	--	Zero Fill

I   Integer quantities right adjusted in 32 bit fields.

F2   Floating point quantities multiplied by a scaling factor of
       100 and rounded (i.e., -145.824 would appear as -14582).

F4   Floating point quantities multiplied by a scaling factor of
       10000 and rounded (i.e., 10.98756 would appear as 109876).

SPEC This is a special format and is a combination of the I, F2,
       and F4 formats. The 17 IR channels will be repeated for each
       of the 42 earth samples. The long wave channels (1-10) will
       be in F2 format. The short wave channels (11-16) will be in
       F4 format. The visible channel (17) will be in the I format.

Negative qualities are two's complement.

function at the temperature of the source. From the real filter

profile, it is possible to calculate an effective target tempera-

ture such that this Planck function gives the true radiance for a

channel. The effective temperature may be expressed as a poly-

nomial of the temperature of the source. This polynomial is given

by

$$\text{Radiance} = B(\nu_{oK}, T_{eK}) \atop R \qquad\qquad (5.1)$$

where $T_{eK} = \sum\limits_{i=1}^{2} b_{ik} T^{i-1}$,

and T^{i-1}, the effective target temperature, is obtained from the temperature of a cold and warm source and b_{ik} are predetermined coefficients given in Table 5.2.

TABLE 5.2   Coefficients b_{ik} for Effective Target Temperature

Channel (k)	ν_{ok}	b_{1k}	b_{2k}
1	669.19	0.002	1.00001
2	679.38	-0.029	1.00010
3	690.45	-0.022	1.00009
4	701.91	0.008	1.00004
5	716.83	-0.048	1.00016
6	732.55	-0.039	1.00014
7	749.18	-0.005	1.00007
8	899.99	0.013	1.00019
9	1223.22	-0.180	1.00056
10	1508.29	-0.775	0.99939
11	2191.02	-0.020	1.00003
12	2211.97	-0.020	1.00005
13	2244.21	-0.020	1.00002
14	2274.63	-0.074	0.99993
15	2357.66	-0.021	1.00004
16	261.00	-2.194	1.00316
17	N/A	N/A	N/A

This recalibration procedure is accomplished every 20 scan lines. By knowning the attitude and altitude of the satellite and the angle of the scanner, each derived radiance value can then be earth located. These radiances and their location as well as data time and scan angles are included on the data tapes.

As noted earlier, the resolution of the HIRS data decreases with increasing scan angle. This decrease in resolution of a scan

spot is from approximately 23 km at nadir to 31 km at a scan angle of 36.9°. Figure 5.1 shows the typical scan geometry for the HIRS and the SCAMS instruments. The Scanning Microwave Spectrometer (SCAMS) is another instrument on Nimbus VI. This decrease in resolution will not affect the calculations since only data points near nadir were considered in this analysis.

The data set used in this analysis was for 20-30 August 1975, a time when all channels of the HIRS instrument were operating properly. Further, it was required to have data over North America since the comparison was being made with the 3DNEPH which depends heavily upon good surface observations. We therefore requested data from 20°-55° N and 80°-150° W which includes both land and ocean areas. To further complicate the data selection, examination of satellite photographs indicated a general lack of middle and high clouds over this region except areas north of 40° N for this time period. As a result, all of the data cases used in the analysis are along the storm track north of 40° N.

A total of 26 passes were provided in the data set of which five were analyzed for cloud information at the two scan angles closest to nadir. To check consistency of the data from channel to channel within a pass, the five passes used in the analysis were displayed by using an overprinting technique to simulate grey shading on the line printer. The pass for 24 August 1975 is included here as Figure 5.2.1-5.2.11. Each of the 11 displays is for a given channel. The legend includes channel number, date, time of the pass and the number of scan lines included. Next, the overprint
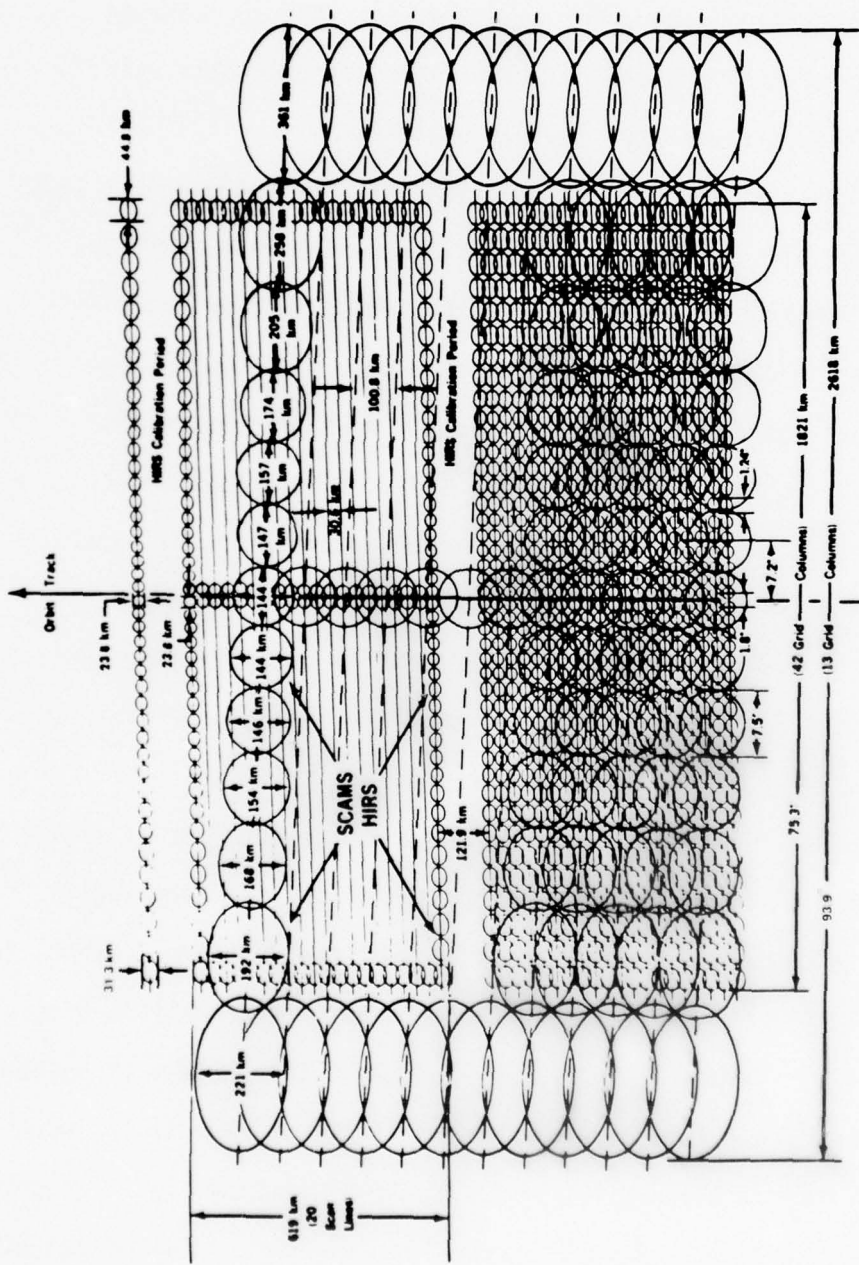
Figure 5.1 Scan grid pattern for HIRS and SCAMS.

characters used are numbered and then the range of radiance values
for each number are indicated. The column of numbers on the right
side of the display is the mean scan angle for that spot position.

Each of the 11 figures were scaled over the maximum and minimum
response of the channel over the contoured area. Each channel was
then divided into equal intervals and displayed by the 16 over-
print patterns shown at the top of the figures. The scale was then
inverted in such a way that darker areas correspond to lower upwell-
ing radiances at the satellite. Figures 5.2.1-5.2.4 are overprints
for HIRS channels 4-7. The weighting function in successive channels
peak deeper in to the atmosphere. Less energy is available in
cloudy areas so that darker areas correspond to colder surfaces
and clouds. It should be noted that the channels that peak deep-
est in the atmosphere have the greatest cloud definition in both
the water vapor and CO_2 channels. Comparison of Figure 5.2.4 with
the infrared mosaic in Figure 5.3 shows good agreement with the
cloud patterns north of 40° N. In this area the least amount of
energy reaching the satellite is from an area north of 50° N between
95°-100° W which can be verified from the infrared moasic. The
same patterns can be seen in Figures 5.2.5-5.2.7 with the best
definition in the window channel (Figure 5.2.5) and the water
vapor channel that peaks deep in the atmosphere (Figure 5.2.6).
The very warm area shown in Figure 5.2.5 corresponds well with the
cloud free area over the central United States where very warm
surface temperatures are present. Figures 5.2.8-5.2.11 are for the
CO_2 channels in the 4.3. μm band. Figure 5.2.8 peaks lowest in the

CHANNEL 4 AUGUST 24, 1975 AT 16.00Z   WITH 111 SCANS

```
 12 14 13 14  11 10   9  8   7   6   5   4   3   2   1
< 50.00=15 50.00-38.00=14 38.00-40.00=13 40.00-42.00=12 42.00-44.00=11 44.00-46.00=10 46.00-48.00= 9 48.00-50.00= 8
  50.00-52.00= 7 52.00-54.00= 6 54.00-56.00= 5 56.00-60.00= 4 60.00-62.00= 3 62.00-64.00= 2 64.00= 1 > 64.00= 0
```

115°
110°
105°
100°

100°
95°
90°

20° 25° 30° 35° 40° 45° 50°

-44.770
-42.411
-40.088
-37.797
-35.531
-33.288
-31.066
-28.863
-26.673
-24.495
-22.333
-20.181
-18.034
-15.900
-13.770
-11.647
-9.530
-7.420
-5.320
-3.234
-1.260
1.270
3.288
5.330
7.430
9.540
11.657
13.780
15.910
18.044
20.191
22.343
24.506
26.683
28.873
31.076
33.298
35.541
37.807
40.098
42.421
44.780

Figure 5.2.1 Overprint for channel 4 on August 24, 1975.

BEST AVAILABLE COPY
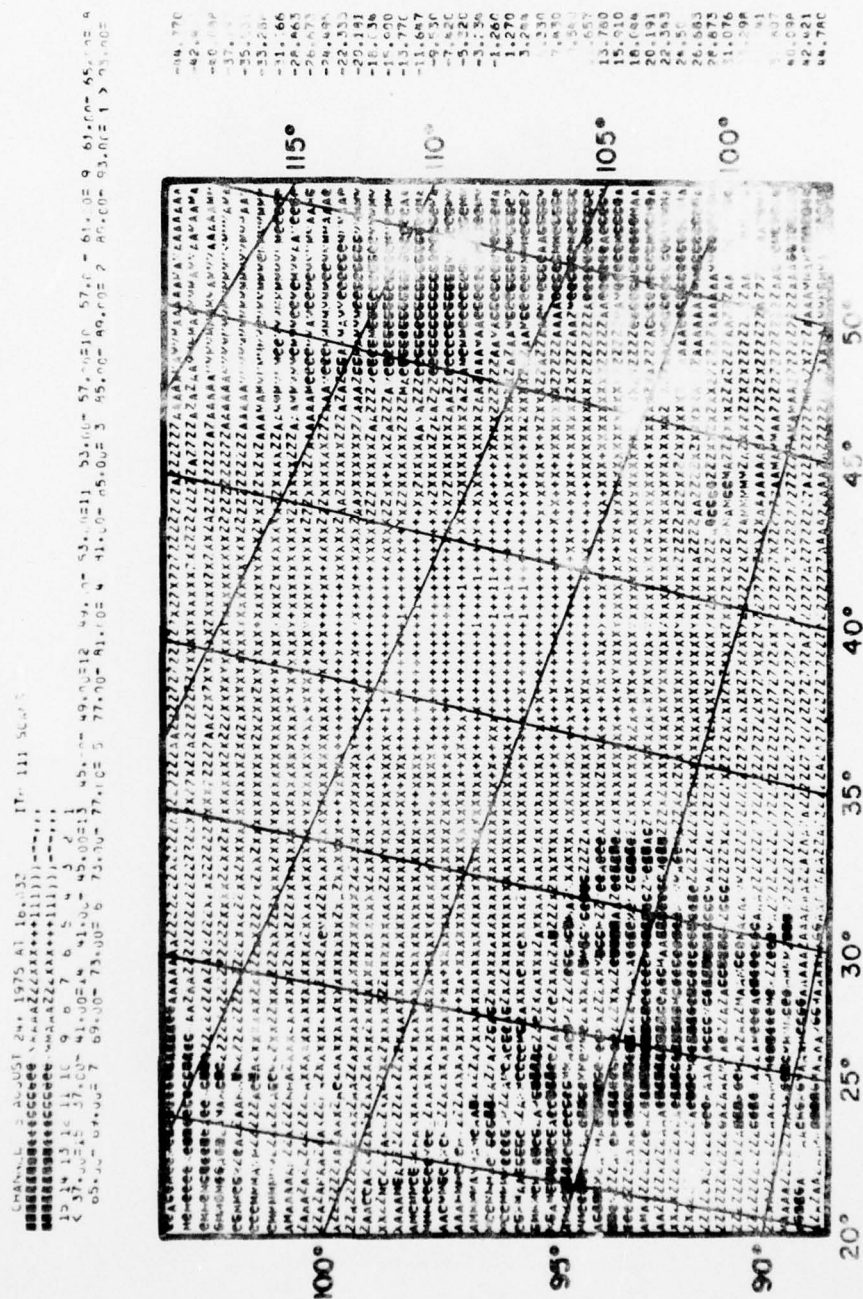
Figure 5.2.2 Overprint for channel 5 on August 24, 1975.

BEST AVAILABLE COPY

CHANNEL 6 AUGUST 24, 1975 AT 18.03Z   WITH 111 SCANS

15 14 13 12 11 10 9 8 7 6 5 4 3 2 1 0
< 47.00=15 47.00- 51.00=14 51.00- 55.00=13 55.00- 59.00=12 59.00- 63.00=11 63.00- 67.00=10 67.00- 71.00= 9 71.00- 75.00= A
  75.00- 79.00= 7 79.00- 83.00= 6 83.00- 87.00= 5 87.00- 91.00= 4 91.00- 95.00= 3 95.00- 99.00= 2 99.00-103.00= 1 >103.00= 0

-44.770
-42.411
-40.088
-37.797
-35.531
-33.288
-31.066
-28.863
-26.673
-24.495
-22.333
-20.181
-18.034
-15.900
-13.770
-11.647
-9.530
-7.420
-5.320
-3.234
-1.260
1.270
3.244
5.330
7.430
9.540
11.657
13.780
15.910
18.044
20.191
22.343
24.506
26.683
28.373
31.076
33.298
35.541
37.807
40.09A
42.421
44.780
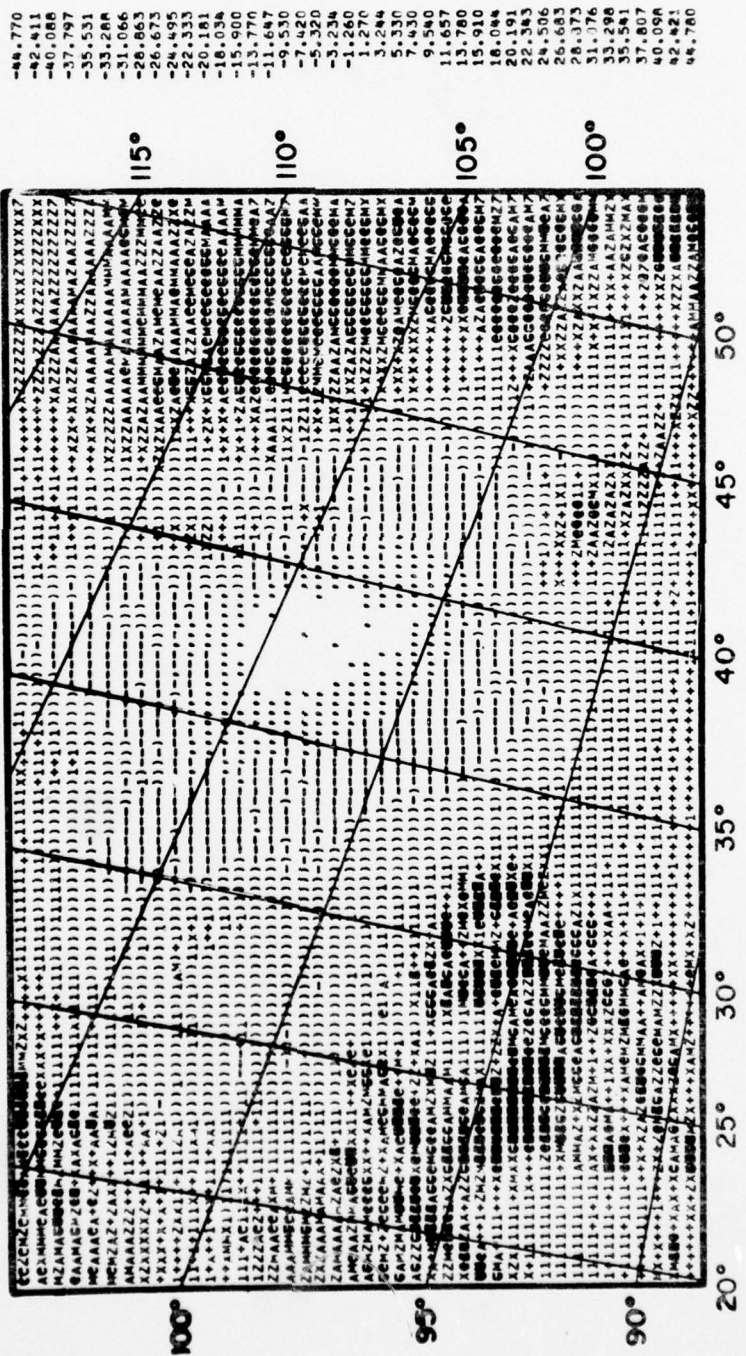
Figure 5.2.3 Overprint for channel 6 on August 24, 1975.
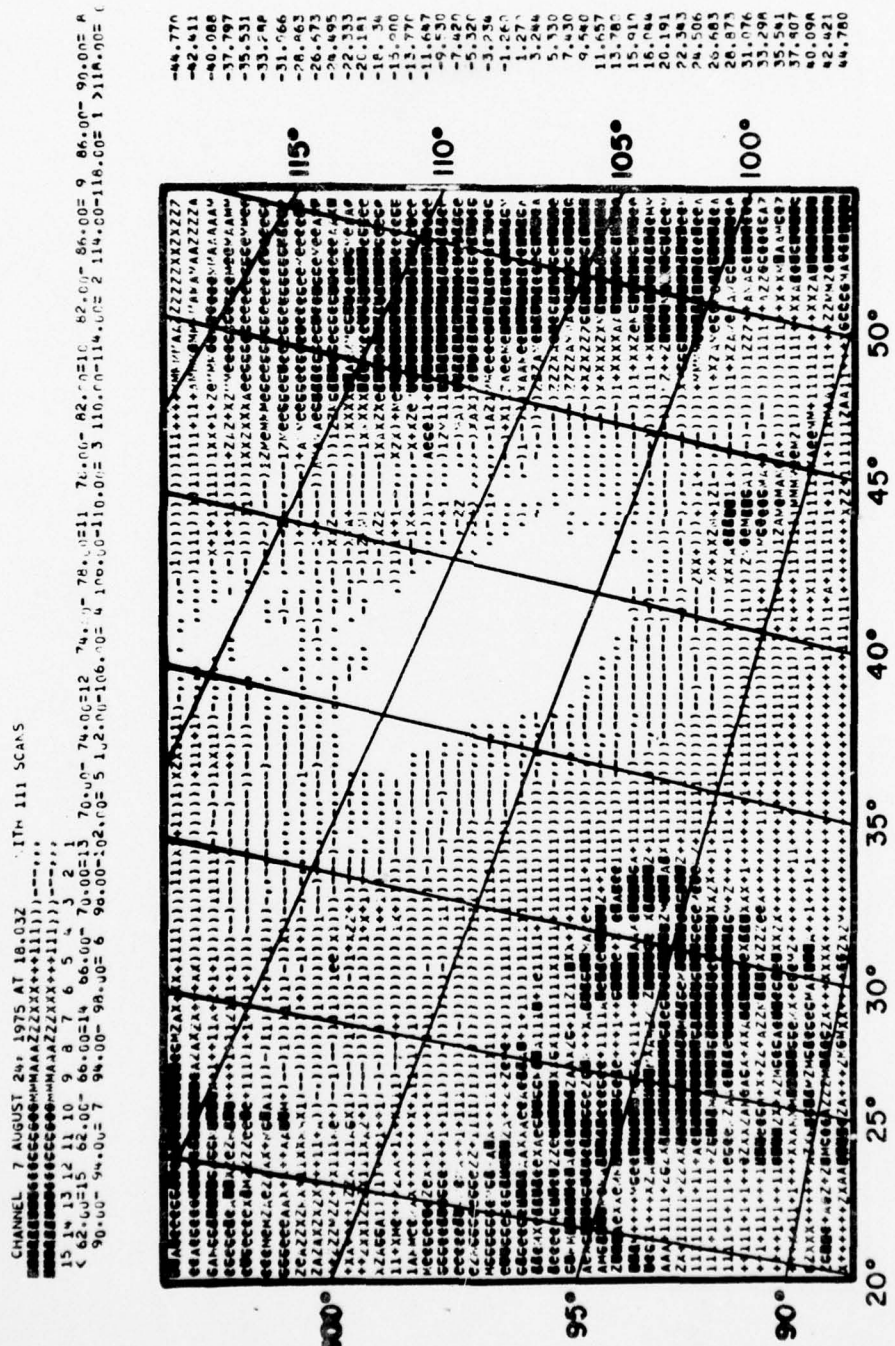
Figure 5.2.4 Overprint for channel 7 on August 24, 1975.

76
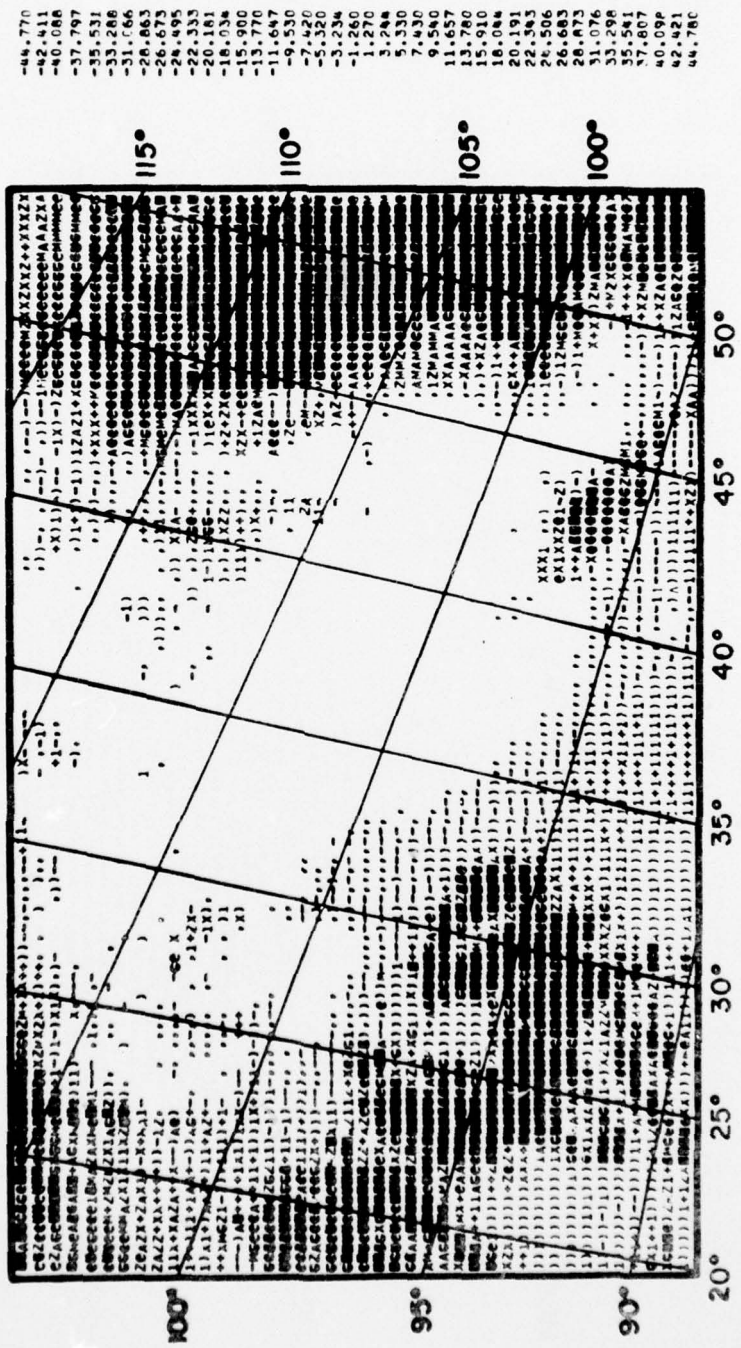
Figure 5.2.5 Overprint for channel 8 on August 24, 1975.

BEST AVAILABLE COPY
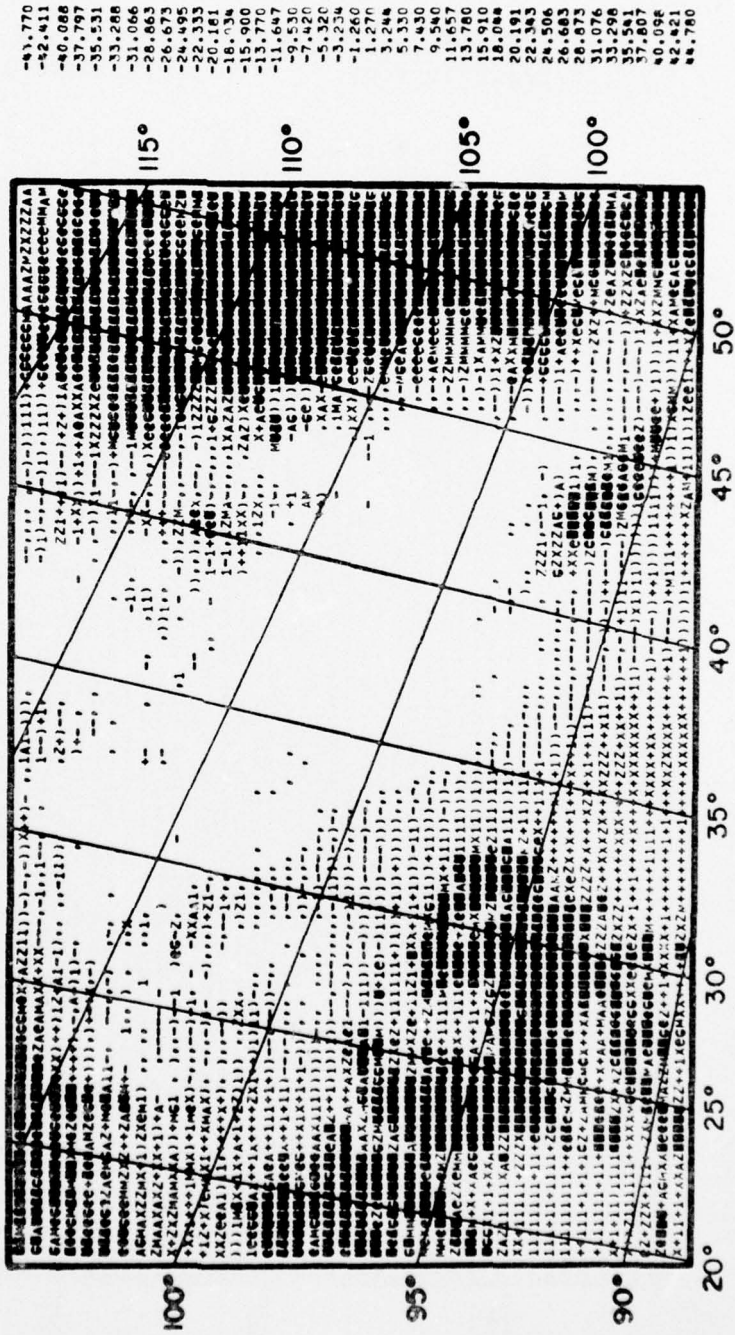
Figure 5.2.6 Overprint for channel 9 on August 24, 1975.

78
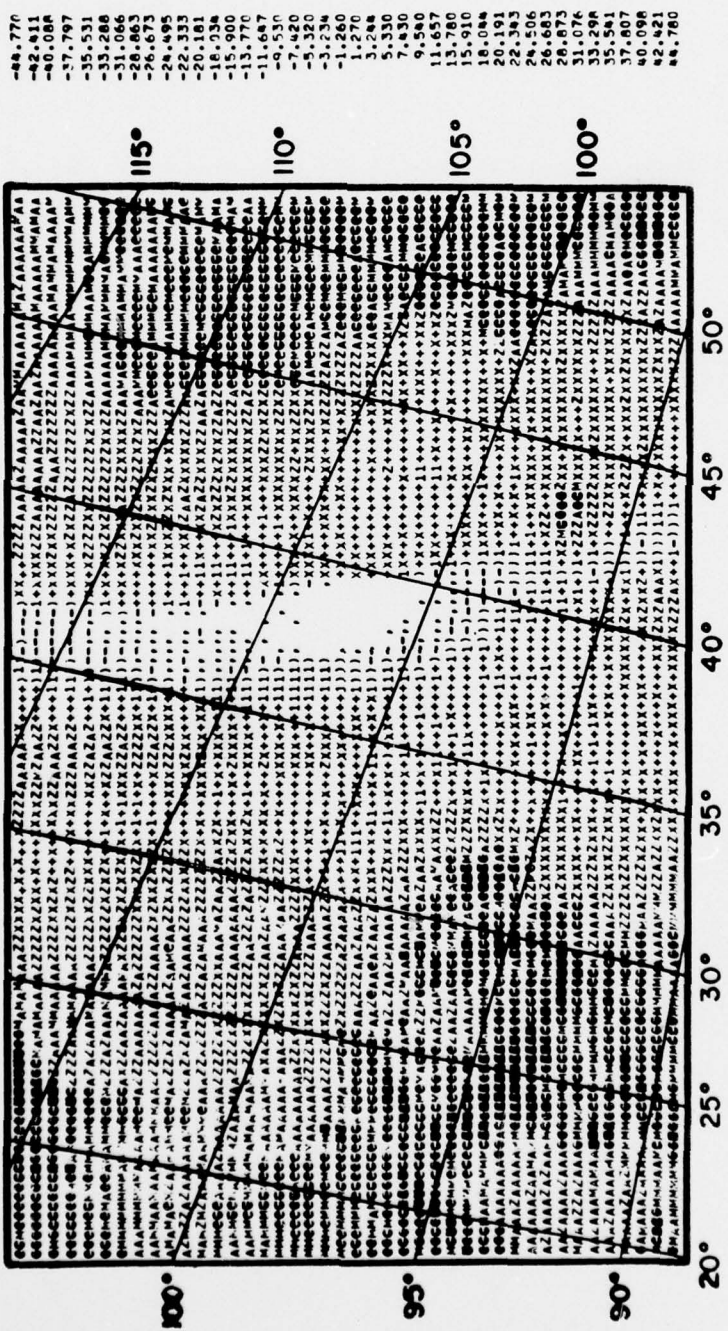
Figure 5.2.7 Overprint for channel 10 on August 24, 1975.
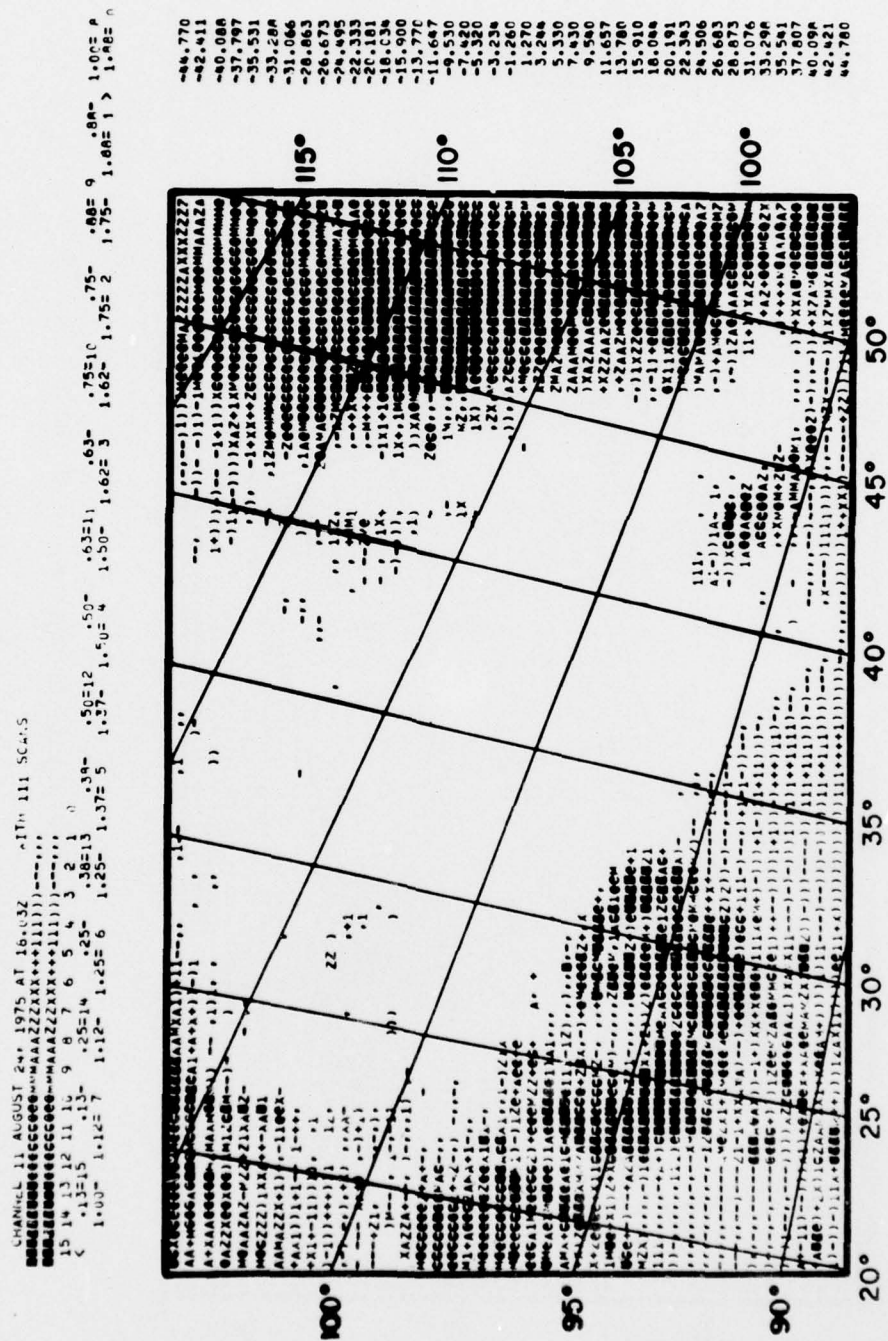
Figure 5.2.8 Overprint for channel 11 on August 24, 1975.

80
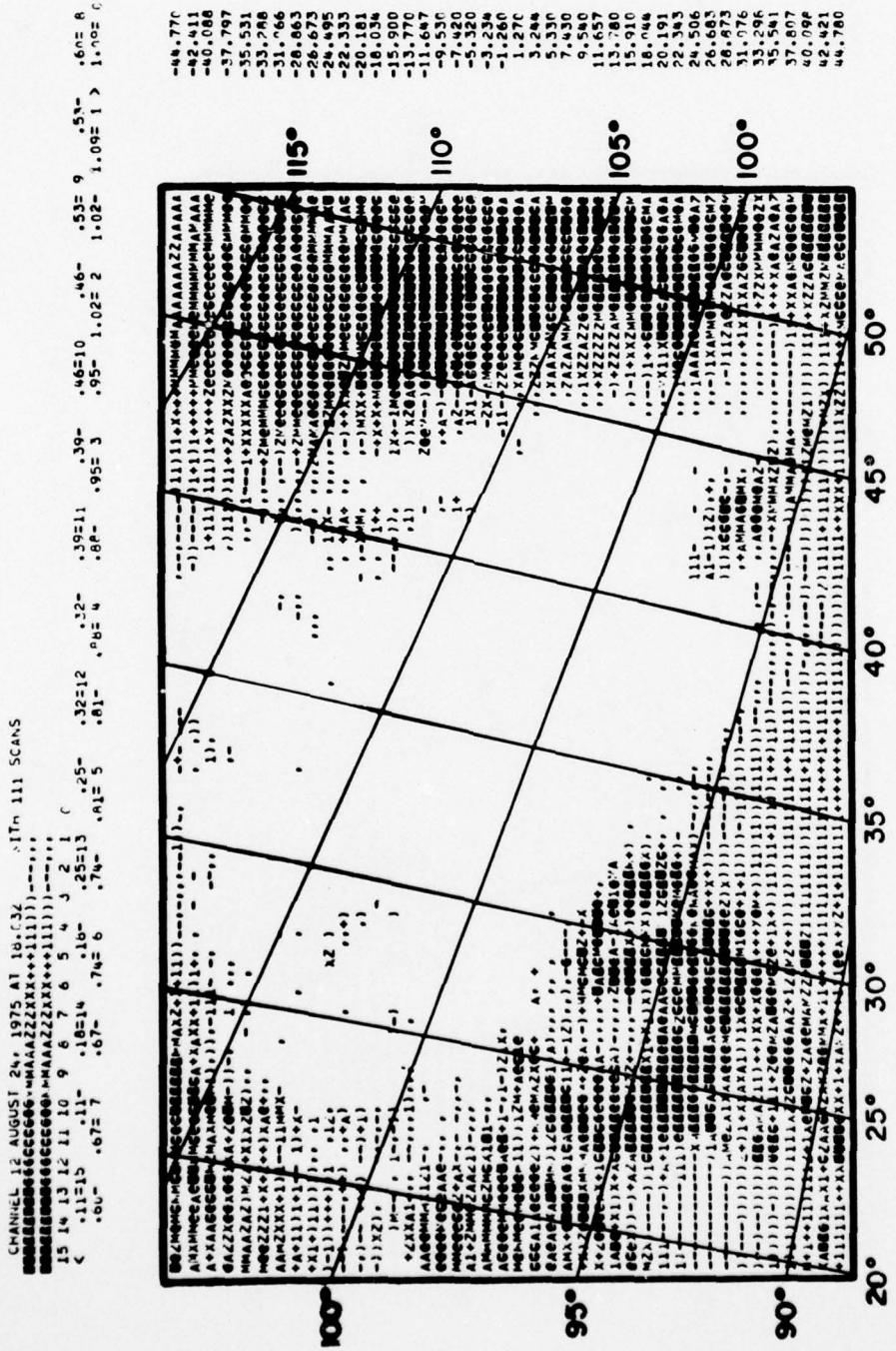
Figure 5.2.9 Overprint for channel 12 on August 24, 1975.

81
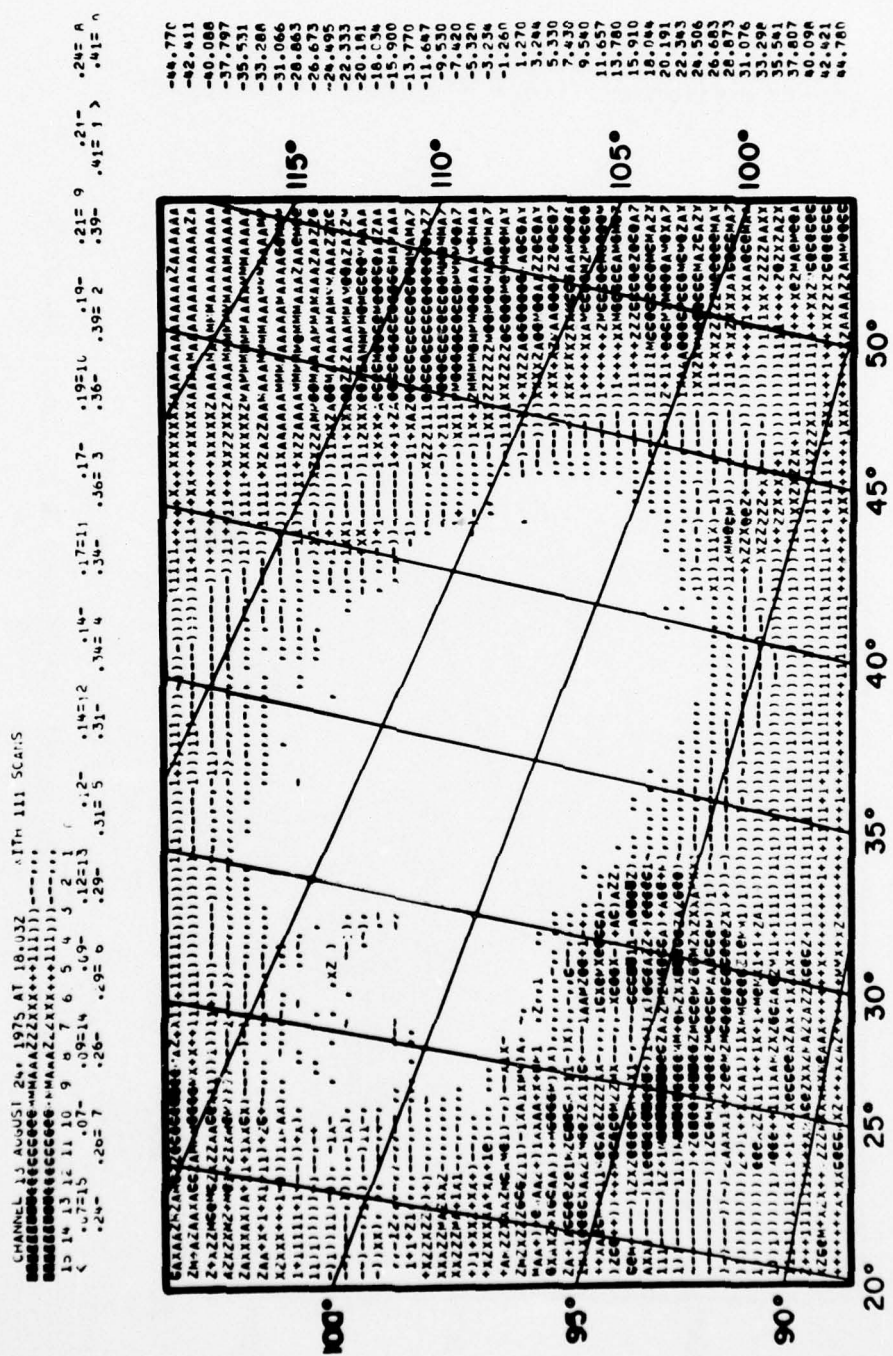
Figure 5.2.10 Overprint for channel 13 on August 24, 1975.

82
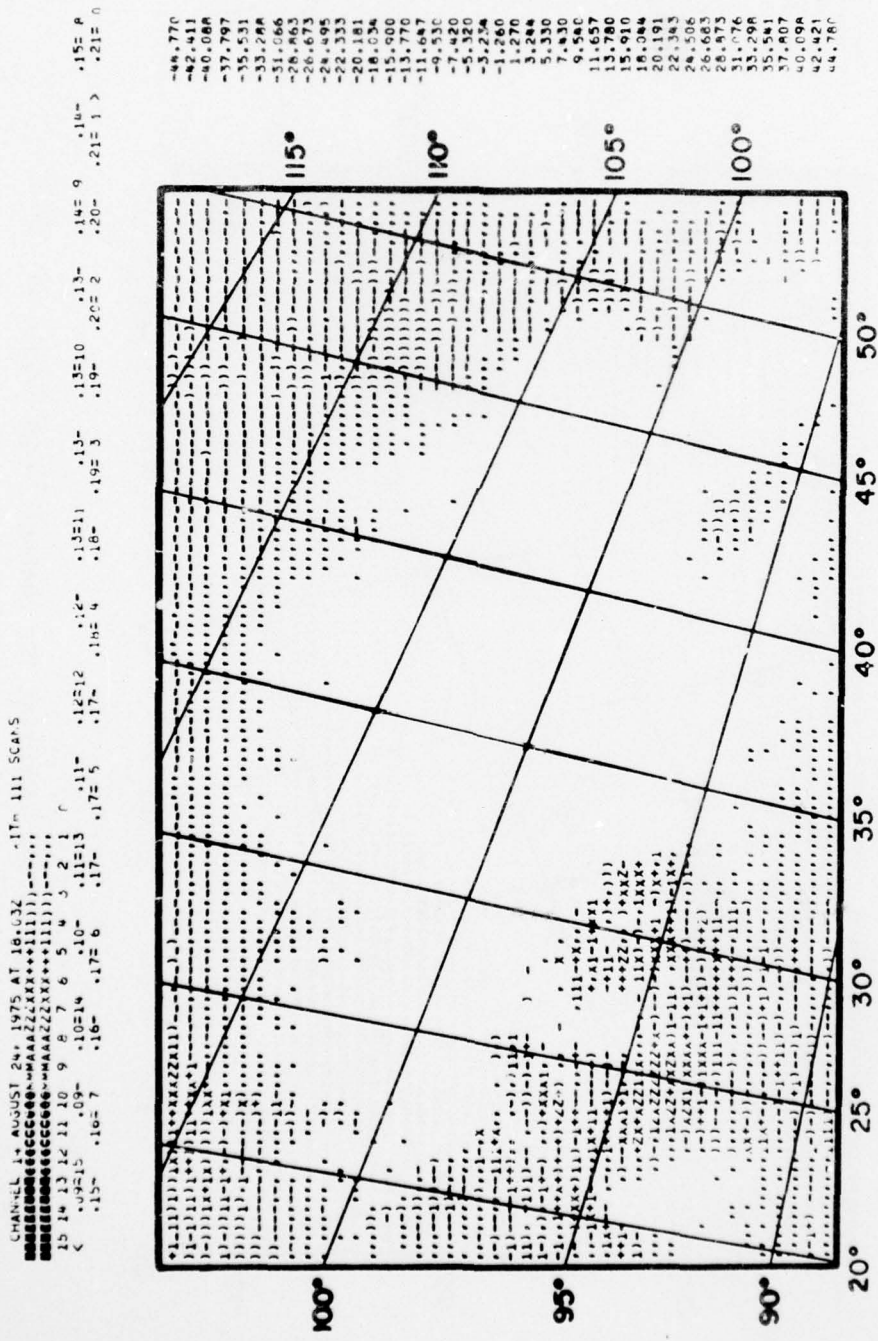
Figure 5.2.11 Overprint for channel 14 on August 24, 1975.
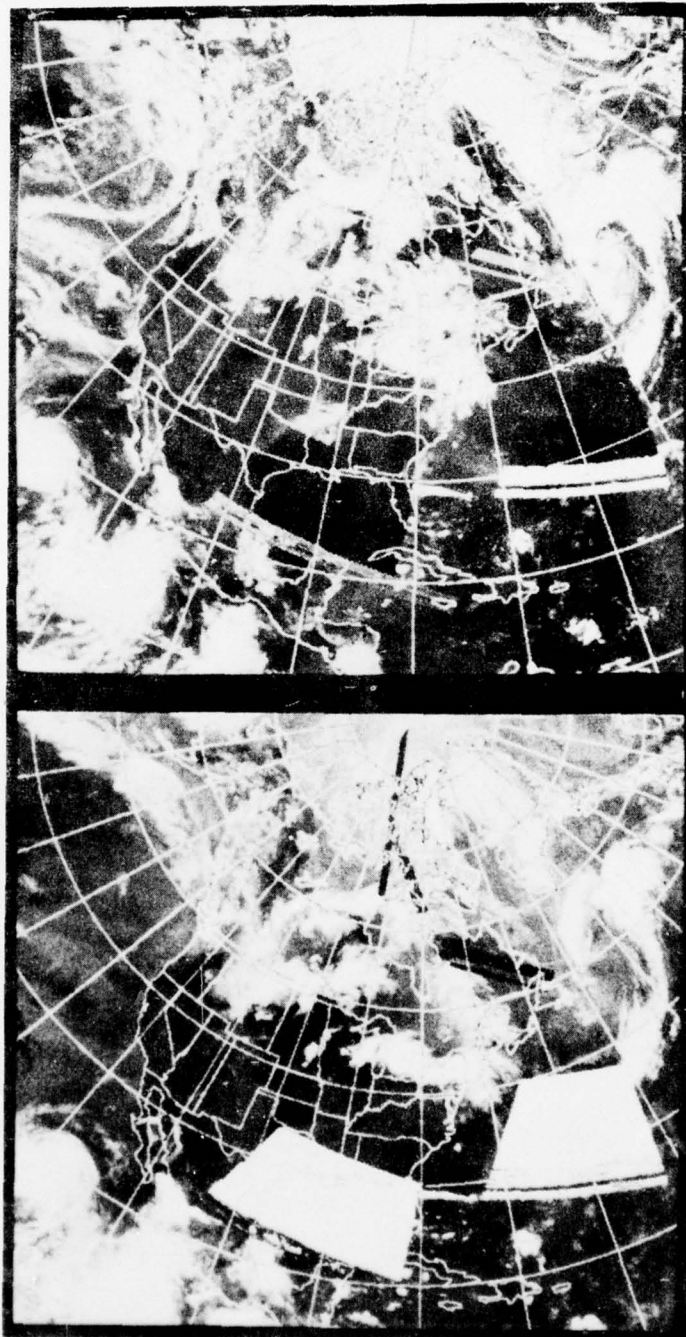
Figure 5.3   NOAA 4 mosaic for August 24, 1975 with
the visible channel on the top and the
infrared channel on the bottom.

atmosphere and 5.2.11 peaks highest for channels analyzed in this band. Comparison of the channels in the two CO_2 bands show a great amount of similarity as would be expected. The lower upwelling radiances indicated in all figures over the southern portion of the overprints corresponds to clouds over Mexico and the Gulf of Mexico. These clouds were indicated by surface observations although data was unavailable over part of the area on the satellite pictures. All the passes used in subsequent analyses were overprinted to verify the HIRS data by comparing the overprints with surface analysis and satellite pictures.

5.2 The Three-Dimensional Nephanalysis

The Three-Dimensional Nephanalysis (3DNEPH) program was developed at the Air Force Global Weather Central (AFGWC) to incorporate the tremendous quantity of satellite sensed cloud data and conventionally sensed meteorological parameters into a three-dimensional cloud model of the atmosphere. Maximum efficiency could be achieved through the use of the computer facilities at the AFGWC in handling this vast amount of data to ouput a high-resolution, operational product.

Basic to the design of the 3DNEPH is the assumption that satellite information is available for its data base in a timely manner. However, in the event that satellite data is not available, the 3DNEPH has the capability of extrapolating past analysis until such time as satellite data does become available.

The 3DNEPH program is built as a series of input processors. These processors include the surface data processor, radiosonde

observation (RAOB) processor, aircraft data processor, manual data processor, decision tree processor, satellite video data processor, satellite infrared data processor, final processor, forecast processor, verification processor, and display processor. Because of the modular nature of the 3DNEPH program, processors can be added to or deleted from the system with a minimum of programming problems. Descriptions and functions of each of the processors can be found in the AFGWC Technical Memorandum 71-2 by Coburn (1971).

The horizontal resolution of the 3DNEPH program is limited by the resolution, and mapping and gridding accuracy of the input satellite data. The hemispheric grid chosen for the 3DNEPH which was compatible with the accuracy of its input satellite data was a 512 x 512 array centered at the north (south) pole of a polar stereographic map and having a distance between grid points of 40 km at 60° latitude. This 512 x 512 grid was further subdivided into 64 squares (boxes), so that the finest mesh was 4096 grid points over each hemisphere. Once again, each grid point contains information representative of a 40 km square centered at the grid point when at 60° latitude. The vertical resolution of the 3DNEPH program divides the atmosphere into 15 layers (see Table 5.3). The first six layers are terrain following layers and the last nine layers are categorized in feet above mean sea level (MSL).

In addition to the information given for cloud amounts in the layers, seven additional pieces of data are given at each point that pertain to the point. These data denote information about the cloud types, maximum tops and minimum bases, the current weather,

TABLE 5.3 Bases and Tops of the 15 Layers of the 3DNEPH

Layer	Base of Layer (feet)	Top of Layer (feet)
1	SFC	150 AGL (Above Ground Level)
2	151	300 AGL
3	301	600 AGL
4	601	1000 AGL
5	1001	2000 AGL
6	2001	3500 AGL
7	3501	5000 MSL (Mean Sea Level)
8	5001	6500 MSL
9	6501	10000 MSL
10	10001	14000 MSL
11	14001	18000 MSL
12	18001	22000 MSL
13	22001	26000 MSL
14	26001	35000 MSL
15	35001	55000 MSL

and the total cloud cover. The type of information contained in each entry is presented below.

a. _Type of LOW Cloud_. Stratus, stratocumulus, cumulus, cumulonimbus, and combinations of these types are used (15 types). A zero indicates the parameter is not present or its existence is unknown.

b. _Type of MIDDLE Cloud_. Nimbostratus, altocumulus, altostratus, and combinations of these types are used. There is a total of seven types. An entry of zero means the same as indicated for the LOW clouds.

c. _Type of HIGH Cloud_. Cirrus, cirrostratus, and cirrocumulus, and combinations of these are used. There is a total of seven HIGH cloud entries. A zero entry means the same as for the middle and low clouds.

d. <u>Present Weather</u>. The present weather parameter is coded as a past weather code, range 0-9 (WMO Present Weather code divided by integer 10 with truncation).

e. <u>Maximum Cloud Tops</u>. The maximum-cloud-top parameter is coded using WMO Table 1677.

f. <u>Minimum Cloud Base</u>. The minimum cloud base is coded using the same table as used for the maximum cloud tops (WMO Code 1677).

g. <u>Total Cloud Cover</u>. Percent of cloud cover at the point is coded directly to the nearest whole percent (0-100).

The parameters for a point are related to the vertical layers by the definition of low, middle, and high clouds which are a function of terrain. Table 5.4 shows the relationship between low, middle, and high clouds as a function of terrain. For example with a terrain of 3500 feet, layers 1-9 are low clouds, 10-12 are middle clouds, and 13-15 are high clouds. An exception to this rule is, of course, convective low clouds (cumulus and cumulonimbus combinations). The top of these convective clouds will be governed by the maximum cloud top entry.

TABLE 5.4   Relationship of Low, Middle, and High Clouds to
the 15 Layers when Terrain is Present.

Terrain (ft)	Low Cloud Layers	Middle Cloud Layers	High Cloud Layers
$\leq$ 1750	1- 8	9-12	13-15
> 1750 $\leq$ 5500	1- 9	10-12	13-15
> 5500 $\leq$ 9500	1-10	11-13	14-15
> 9500 $\leq$ 13500	1-11	12-13	14-15
>13500 $\leq$ 17500	1-12	13-14	15
> 17500	1-13	14	15

The use of the 3DNEPH as a source of comparison to the techniques developed here has many shortcomings. The 3DNEPH was used as a comparison since no other known source containing the routine analysis of cloud parameters 3DNEPH is available. These problems include timeliness, layer resolution, dependence on subjective observations, and the horizontal spreading of the data.

The timeliness of data is very crucial in this analysis. The 3DNEPH is produced every three hours. If there is no new data for an update, the previous analysis or a cloud forecast is used for the new analysis. The ever-changing cloud scene at a point makes the timeliness of the 3DNEPH and the HIRS data very important. This problem is minimized since we are considering overcast cases in which the cloud scene at a point will probably not change significantly over a short period of time.

A second problem area is the layer resolution of the 3DNEPH. In the middle cloud layers this can be as much as one layer thickness, up to 4,000 ft. In the high cloud layers this can be up to 20,000 ft. If a thin layer of cloud is reported to be in one of the layers, the model must automatically fill the entire layer with clouds. As noted earlier, an error of 4,000 ft (1.2 km) is one-half the thickness of middle cloud that can be detected by the theoretical model. In the case of cirrus clouds, a 20,000 ft error is equivalent to 6.1 km, a greater thickness than the model can handle. This large error can be somewhat off-set when the maximum cloud top parameter is considered. At middle and high cloud top levels, the coding for this parameter is accurate to 5,000 ft or

1.5 km. For lower middle cloud tops, this parameter is accurate to 1,000 ft or 0.3 km.

The use of subjective weather observations plays an important role in the accuracy of the 3DNEPH cloud thickness determination. If the observation is overcast clouds and there is no current satellite data, the cloud top cannot be determined and persistence prevails, and the cloud thickness is over or underestimated. Another case would be when satellite data is available but no surface observation is present (over oceans), the satellite can determine the cloud top height only and no information about the cloud depth can be determined.

The need to take surface observations and spread them horizontally is another area in which the comparison would not match. The 3DNEPH grid point represents a 40 km box at 60° N. If there is no current satellite data and the observation network is not at a 40 km resolution, some influence of the surface observation is spread to adjacent points in the 3DNEPH. This can be seen by examining an area of 3DNEPH data where the cloud thickness will be constant over a large area.

Steps taken to minimize these problem areas will be discussed in the next chapter under data selection.

CHAPTER 6

DATA SELECTION AND COMPARISON

This chapter will describe how the HIRS data used in the comparison with the 3DNEPH was chosen. The next section will include a synoptic discussion and maps and satellite data for the days used in the analysis. Section three of the chapter will contain the comparisons and a discussion of their validity. The last section of the chapter will present the possibility of mapping the ice and water content of cirrus and middle clouds on more than a local basis utilizing the technique developed here.

6.1 Data Selection

The basic criteria for the selection of the HIRS data to be compared with the 3DNEPH must consider the use of data where the 3DNEPH is most reliable. This criteria dictated that data be chosen where the 3DNEPH had good surface data as well as satellite data. Additionally, the areas of interest must be in the presence of synoptic scale weather so that continuous cloud decks would be insured. The use of HIRS data points at or near nadir would insure the least amount of error in applying the real data to the theoretical calculations, since the fitting of the theoretical upwelling radiances to different scan angles would be most accurate at nadir.

Based on the foregoing criteria five passes on five consecu-
tive days were chosen for this comparison. These days included
August 21 through August 25, 1975. The pass on each day that
included Western North America and is closest to a 3DNEPH analysis
time is used. Since Nimbus VI has an approximate equator crossing
at 1000 local time on its ascending pass this would correspond to
1800Z (GMT) analysis time for the 3DNEPH. The area of the 3DNPEH
that covers this area in box number 44 which has the following
latitudes and longitudes for the upper left, upper right, lower
left and lower right, respectively, 52°N 125°W, 62°N 80°W, 31°N
106°W, and 36°N 80°W.

Inspection of satellite pictures on these five days show that
all the clouds are north of 40°W and a majority of them are north of
45°N. For this reason all the points used in the comparison are at
these latitudes.

To apply the theoretical results to the real HIRS data a method
had to be developed to reduce the cloudy radiances to ratios. The
theoretical data would be compatable since the atmosphere used in
the calculations were mid-latitude summer and the real data is also
for mid-latitude summer. To obtain a clear column radiance that is
representative of a localized area the HIRS data was examined in
conjunction with the satellite pictures. The point chosen for the
clear column radiance was then used to obtain the cloudy ratios for
that day. The point chosen had the same scan angle as the cloudy
radiances. This choosing was done for all five days to obtain ratios
for the cloudy cases. This clear column radiance location was done

manually, but could have been automated by comparing the real data with the clear column radiances calculated for the model atmosphere. In this way a point could be chosen where the radiances match the theoretical clear column radiances and thus minimize the difference between the theory and the actual data.

The colocation of the HIRS data with the 3DNEPH was accomplished using the latitude and longitude from the HIRS data. These quantities were then converted to 3DNEPH grid location. Since this location is never an exact 3DNEPH point, the 3DNPEH point used for the comparison was that point closest to the calculated grid location.

6.2 Synoptic Discussion

The synoptic discussion for each day will include a surface analysis for 1200Z, a 500 mb analysis for 1200Z and NOAA 4 satellite data. The NOAA 4 satellite data for each day are the mapped, normalized and gridded mosaics from the Very High Resolution Radiometer (VHRR). A two picture set includes the broad band visible channel from .5 - .7 μm and the broad band window channel from 10.5 - 12.5 μm. In addition there is a general synoptic discussion for each day. The figures for each day are arranged with the surface and 500 mb analysis on one page and the visible and infrared satellite pictures following. All satellite data is for 1000 local which is equivalent to 1800Z over the western United States. These include Figures 6.1-6.10.

<u>August 21, 1975 1200Z</u>

The 500 mb analysis shows a closed low at 63°N-57°W with trough line extending south-southwestward. A deep low pressure trough is located over central California supported by an open long wave trough centered over southern Alaska. The trough line extends from this low down the west coast of Canada across the western United States into the central California trough. The eastern United States is dominated by high pressure south of 40°N.

On the surface analysis a low centered over Lake Superior has a warm front extending into eastern Wisconsin and across southern Lake Michigan. A stationary front from this low extends across Minnesota westward across Nebraska, Colorado and Utah. Rain and drizzle is occurring east and north of the low. A low pressure area in northern Idaho has a cold front extending southwestward through Oregon into the Pacific. Shower activity is indicated in much of the western United States with drizzle being reported on the northwest coast.

The satellite pictures for this day show the rain area associated with the Lake Superior low and the general showery conditions in the western United States. Shower activity is also present along the cold frontal system in Idaho and Oregon. Extensive low clouds are present in the eastern Pacific. The HIRS pass for this day had a subsatellite track along a line from 19.°N and 103.6°W to 50°N and 114°W. The pass had a time of 1845Z. The satellite pictures indicate most cloud along this line are north of 30°N. The shower-like activity is indicated in both the IR and visual pictures.

94
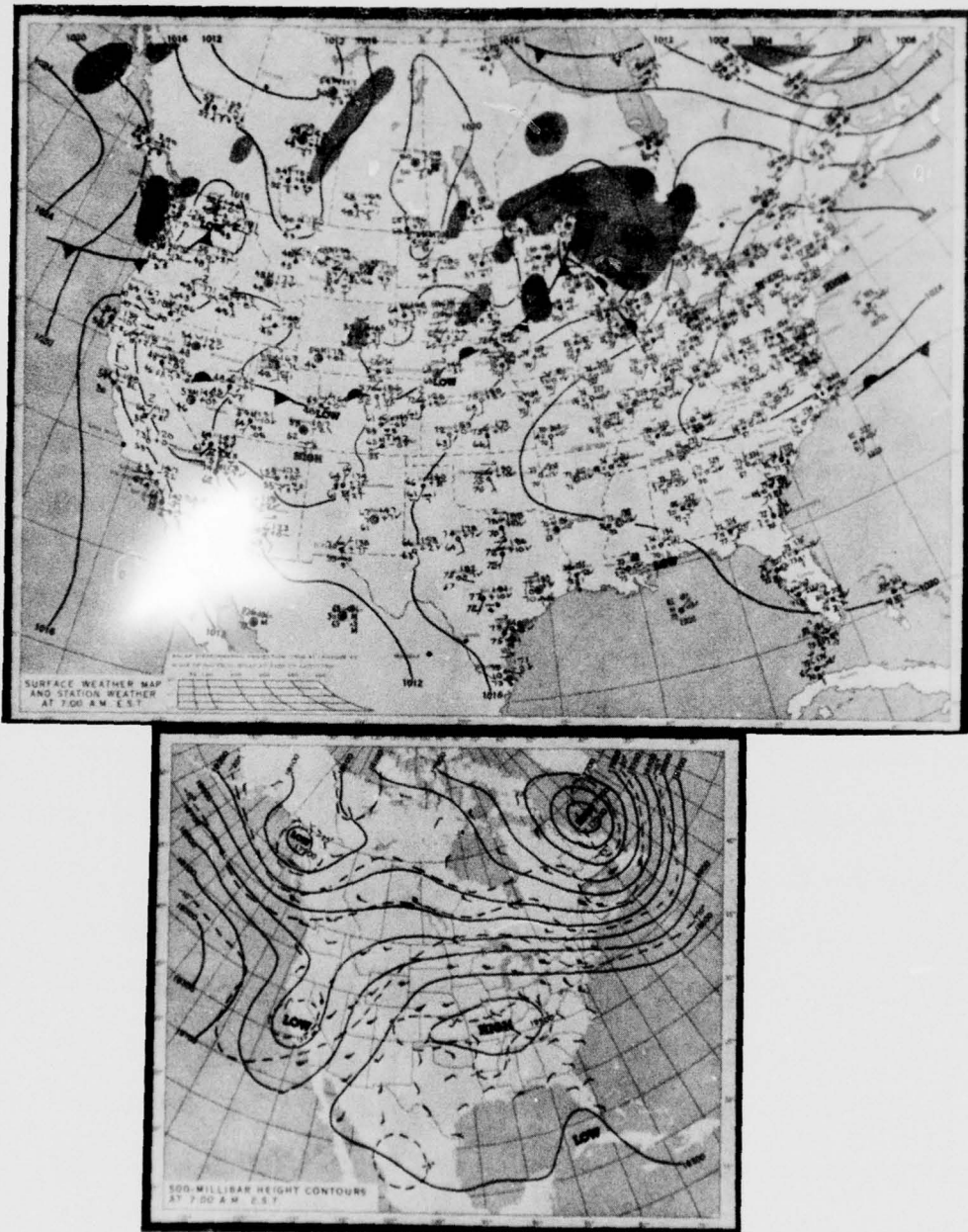
Figure 6.1   Surface (top) and 500 mb (bottom) analysis for
August 21, 1975 at 1200Z.
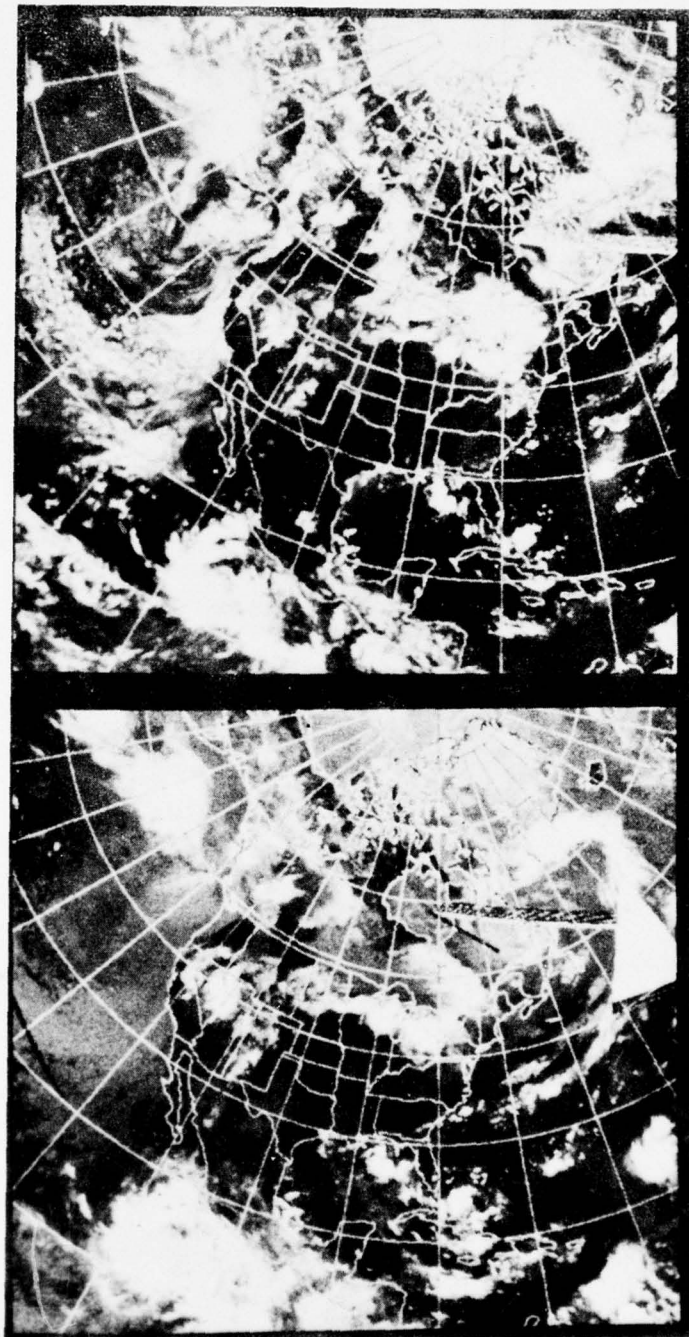
Figure 6.2 NOAA 4 mosaic for August 21, 1975 with the
            visible channel on the top and the infrared
            channel on the bottom.

August 22, 1975   1200Z

The 500 mb analysis shows the low at 63°N, 57°W has weakened and moved eastward. The low over southern Alaska has progressed eastward to 55°N, 125°W. The low in central California has continued to fill.   The trough line in the western United States is now located along a line through western Washington and Oregon, through western Nevada, central California and out into the Pacific.   The upper level high in the southeastern United States has moved southward and eastward.

The surface map shows the low that was over Lake Superior on August 21 has moved over Maine. The frontal system associated with this low pressure extends across southern Canada, southern Lake Michigan and across Iowa and Nebraska. Showers are indicated all along this frontal system. The cold front that was located in Idaho has moved northeastward into eastern Alberta with the frontal system extending through Montana and southern Idaho. A warm front is located in eastern Montana.   Shower activity is present along this frontal system. There has been a decrease in shower activity over the southwestern United States.

The satellite pictures reflect the frontal positions quite well, with all of the activity in the western United States north of 45°N. In addition to the frontal systems noted, a new system has appeared in the Gulf of Alaska. The subtrack for the HIRS pass is along a line from 18.7°N, 91.6°W to 52°N, 104°W. The pass had a time of 1745Z. Examination of the IR satellite picture indicates a good combination of middle and high clouds north of 43°N on the satellite subtrack.

Figure 6.3 Surface (top) and 500 mb (bottom) analysis for
August 22, 1975 at 1200Z.
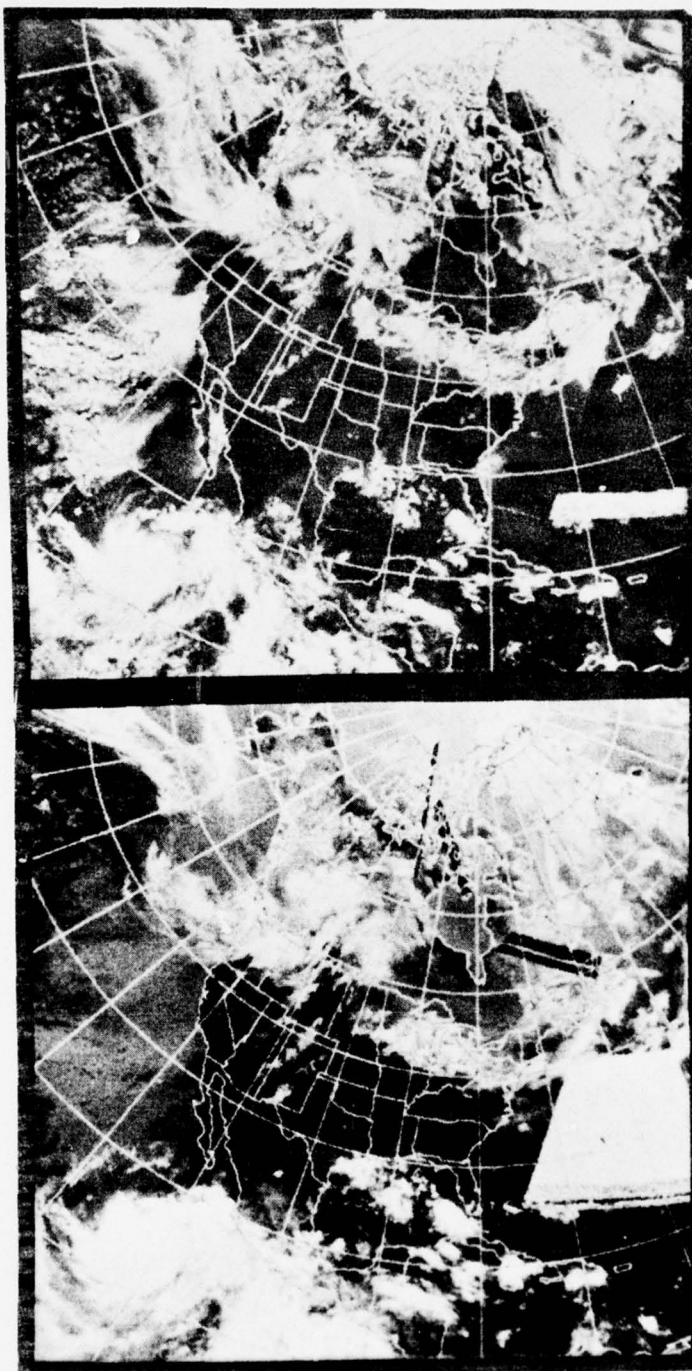
Figure 6.4   NOAA 4 mosaic for August 22, 1975 with the
visible channel on the top and the infrared
channel on the bottom.

August 23, 1975   1200Z

The 500 mb analysis shows the continued filling of the low
at 69°W. The trough in western North America has continued north
and eastward. This low now has two closed centers, one at 58N
and 100W and the other at 50°N and 125°W. There is a weak trough
from the more northerly low center extending southeastward from
its center into central Saskatchewan. The more southerly center
has the troughline just off the western coast. The high center
in the southeastern United States has moved slightly southeast
and is now centered over Alabama and Georgia.

The surface analysis still carries the stationary front across
the eastern part of the country from Virginia to southern Lake
Michigan. The low in eastern Alberta has moved a little north
and deepened. The occluded front from this system is approaching
100°W in Canada and then becomes stationary along a line through
North Dakota, southern Montana and southern Idaho. A new surface
low supported by the upper closed low off the west coast is now
into extreme western Washington.

There is a good support for this analysis when analyzing the
satellite pictures. The pictures show a good cloud shield with
the system along 100°W and showers northern along the front through
Virginia. The IR picture indicates cirrus clouds along all of
these frontal areas. The HIRS pass for this day has a subsatel-
lite track along a line from 18.6N, 107.3°W to 52.2°N, 119.0°W. The
satellite picture indicates a good cirrus shield over Washington
and Oregon under the satellite pass. The pass had a time of 1845Z.
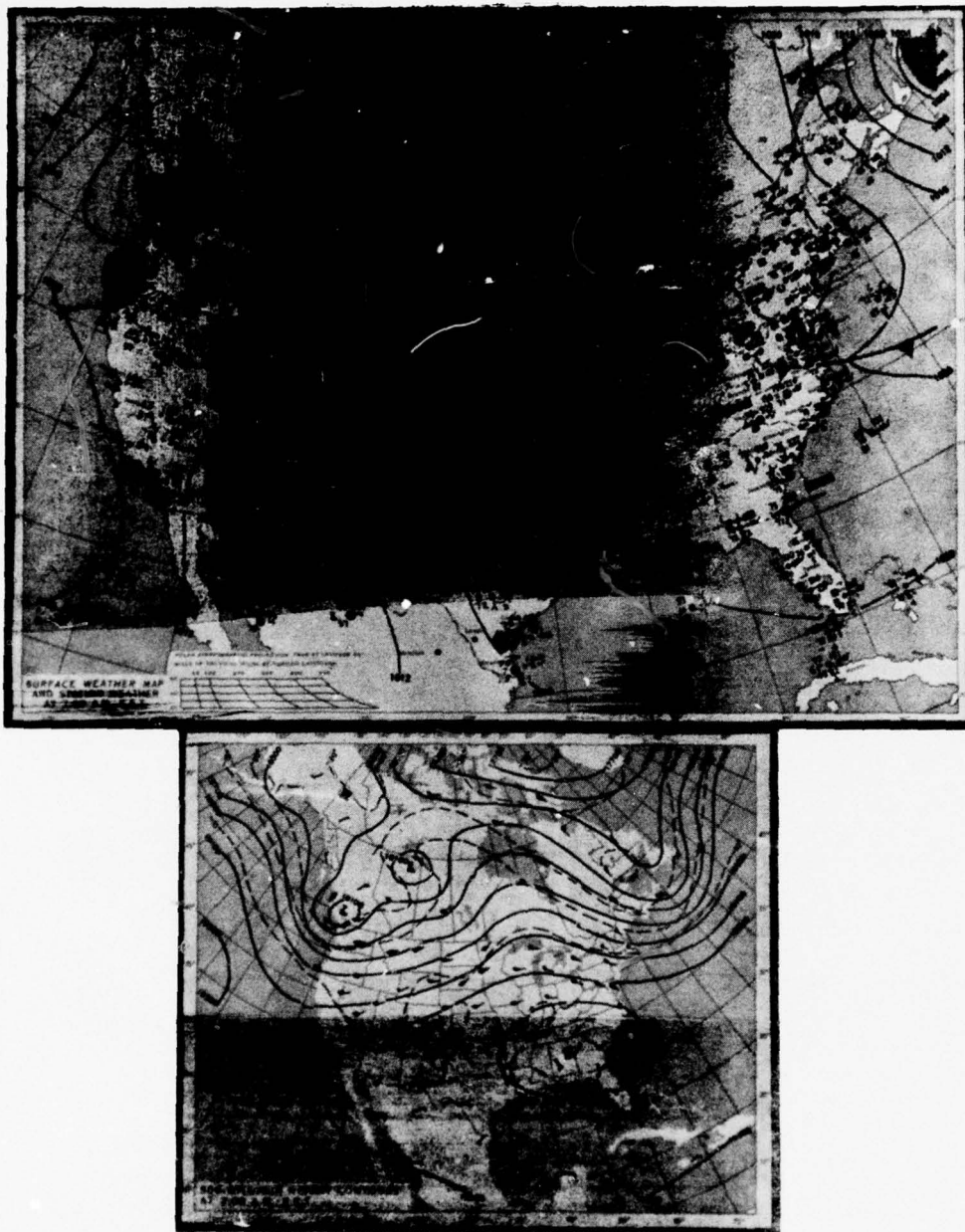
Figure 6.5 Surface (top) and 500 mb (bottom) analysis for
August 23, 1975 at 1200Z.

101
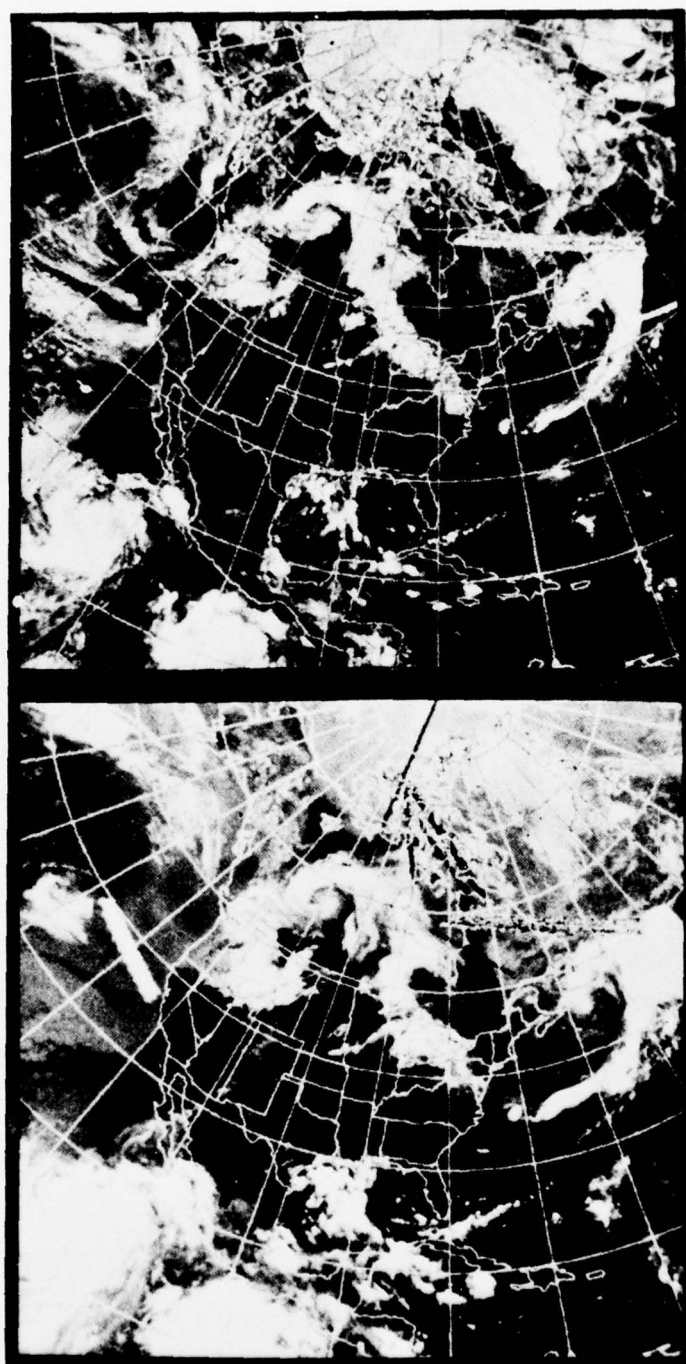
Figure 6.6 NOAA 4 mosaic for August 23, 1975 with the
visible channel on the top and the infrared
channel on the bottom.

24 August 1975 1200Z

The upper level trough over western North America has moved over northern Saskatchewan with the troughline extending through western Montana into northern Nevada. The high pressure area over the southeastern United States has moved eastward off the Georgia-South Carolina coast. High pressure is now dominating the Pacific Northwest. The surface map shows a complex frontal system. The occluded front in Canada has now moved to 85°W with a warm front extending across the Great Lakes area into Pennsylvania and New Jersey. The analysis indicates a strong squall line across Wisconsin southwestward into Iowa. The sationary front extends across northern Minnesota to the Dakotas and into Wyoming with a cyclone developing on the front in North Dakota.

The satellite pictures show general cloudiness along the northern United States border and and over the Great Lakes and eastward. This is in good agreement with the 1200Z analysis. The HIRS pass for this day has a subtrack along a line from 18.6°N, 96.2°W to 52°N 108.3°W. The pass is over the rain area indicated on the surface map in eastern Montana and southern Canada.

August 25, 1975 1200Z

The last day of the analysis shows that the 500 mb trough over central Canada has become closed and moved eastward with the troughline now extending southward through western Minnesota into Nebraska. The high over the southeast United States has weakened with the movement of the trough. High pressure remains strong in the eastern Pacific.
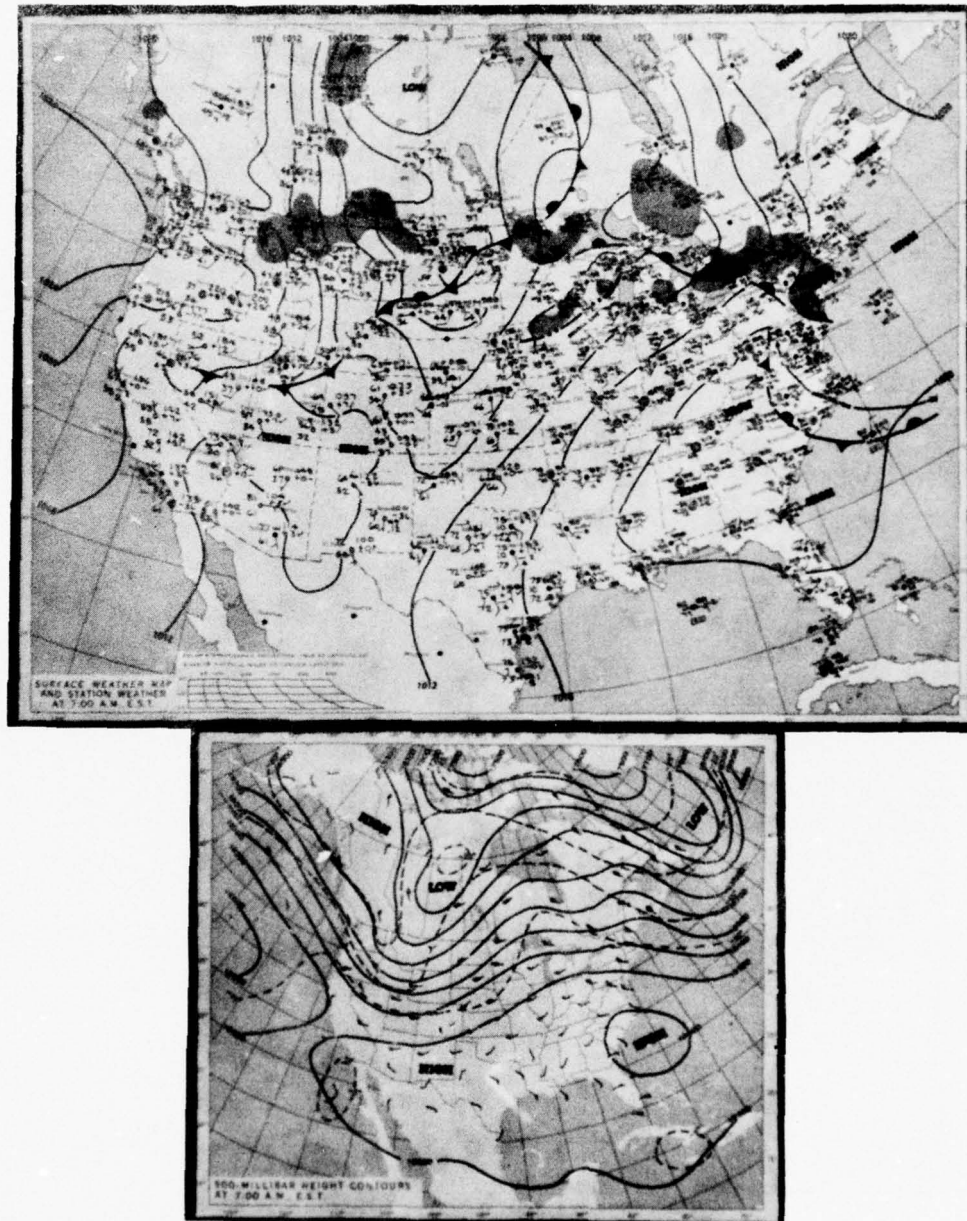
Figure 6.7 Surface (top) and 500 mb (bottom) analysis for
August 24, 1975 at 1200Z.
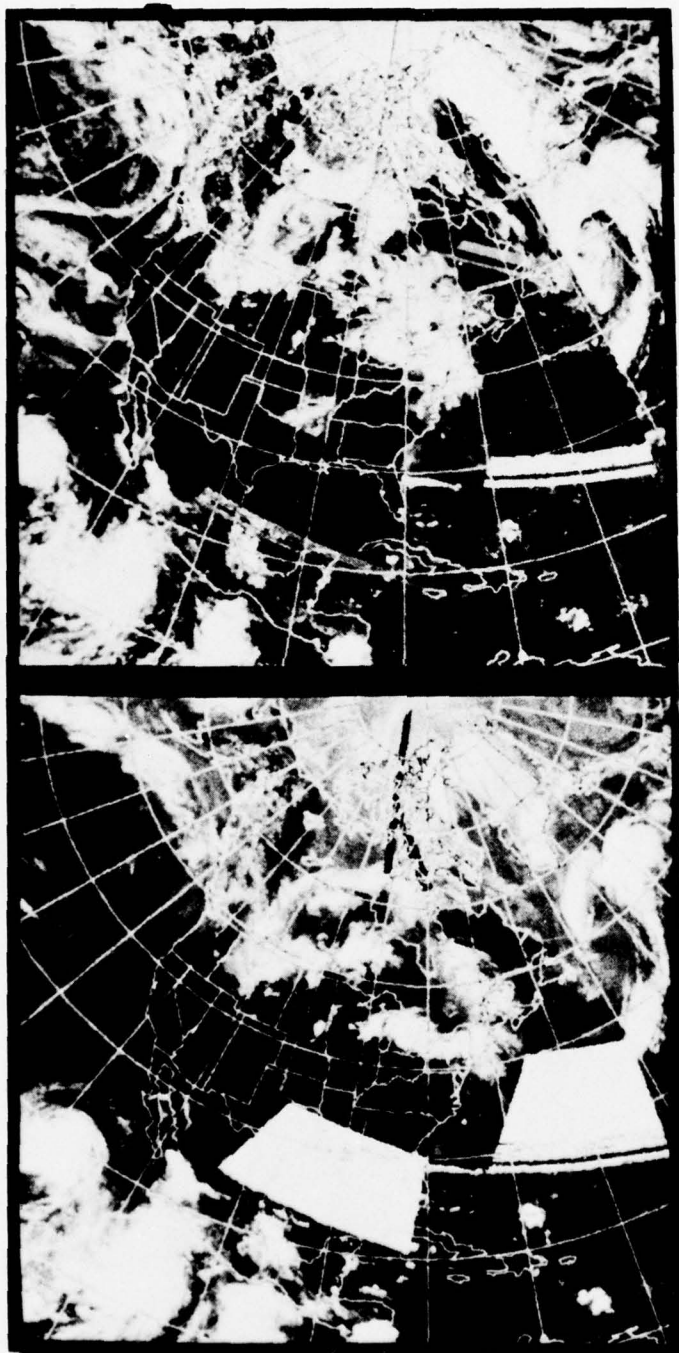
Figure 6.8 NOAA 4 mosaic for August 24, 1975 with the
visible channel on the top and the infrared
channel on the bottom.

A strong surface low that formed over North Dakota on the previous day has intensified and a low is located south of Hudson Bay with a cold front extending through Lake Superior, southward into Kansas and then westward into Colorado. The stationary front across the northern Great Lakes and Pennsylvania has moved northward across New York. Some shower activity is also indicated in mountains of western Montana and southern Canada.

The surface map and 500 mb analysis indicate heavy shower activity along the frontal system in Illinois, Iowa and Missouri as well as east and north of the surface low pressure center. Shower activity is also indicated in Montana and southern Canada. The satellite pictures reinforce the surface and 500 mb analyses with cloud cover in these areas. The HIRS pass had a subtrack extending from 19°N, 85.6°W to 52°N and 98.7°W. This would pass over the strong activity in the midwest as well as lower clouds north of Lake Superior and the cirrus clouds further north.

6.3 Data Comparisons

Two sources of data that are generated routinely are used for comparison with the calculated HIRS cloud parameters from the empirical-theoretical parameterizations. These two sources include the 3DNEPH for cloud mass comparisons and the satellite mosaics for the cloud type comparisons.

6.3.1 Cloud Type

All of the HIRS data applied to the theoretically based empirical relationships are from the cloudy areas, north of 40°N,

BEST AVAILABLE COPY
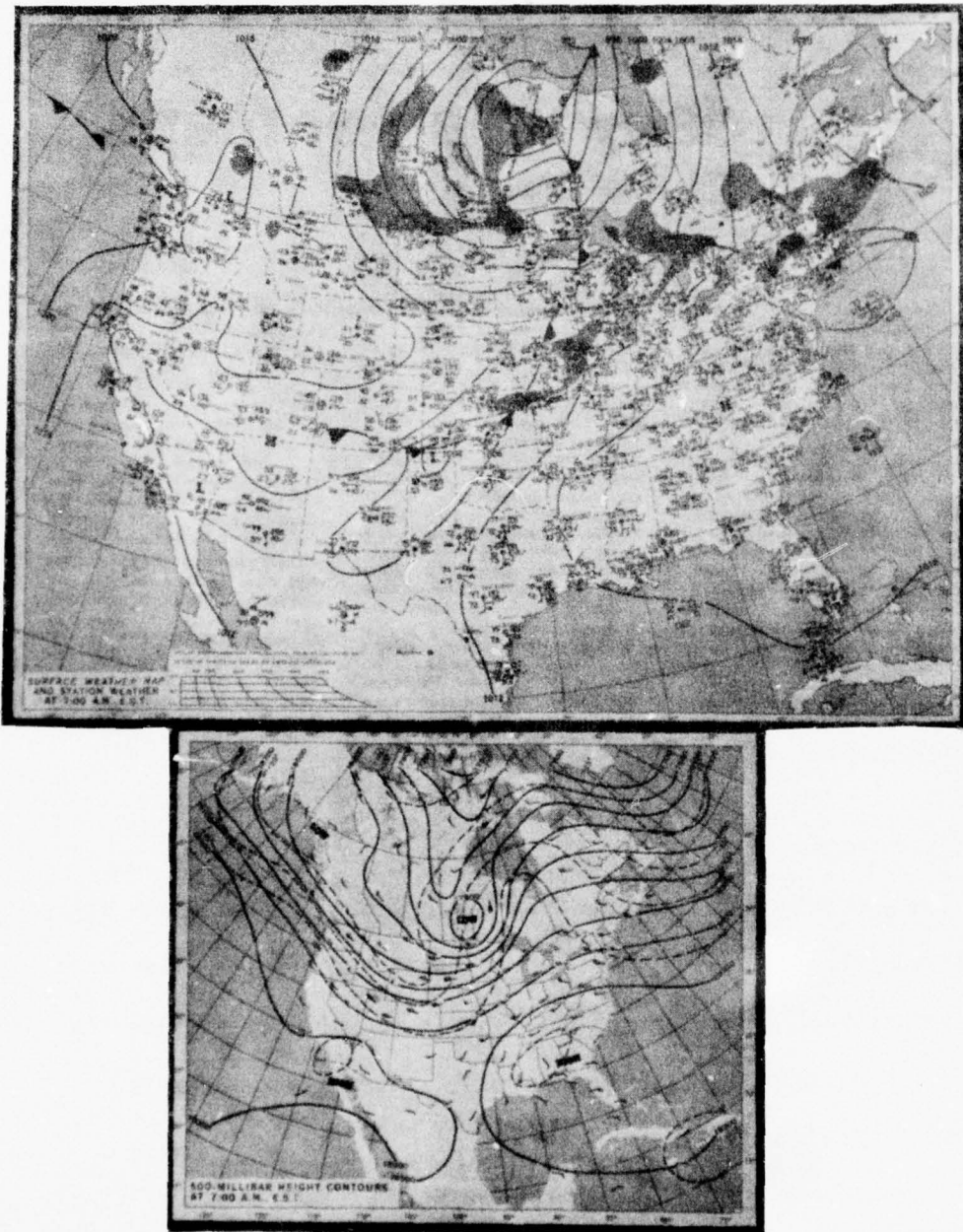
Figure 6.9   Surface (top) and 500 mb (bottom) analysis for
August 25, 1975 at 1200Z.
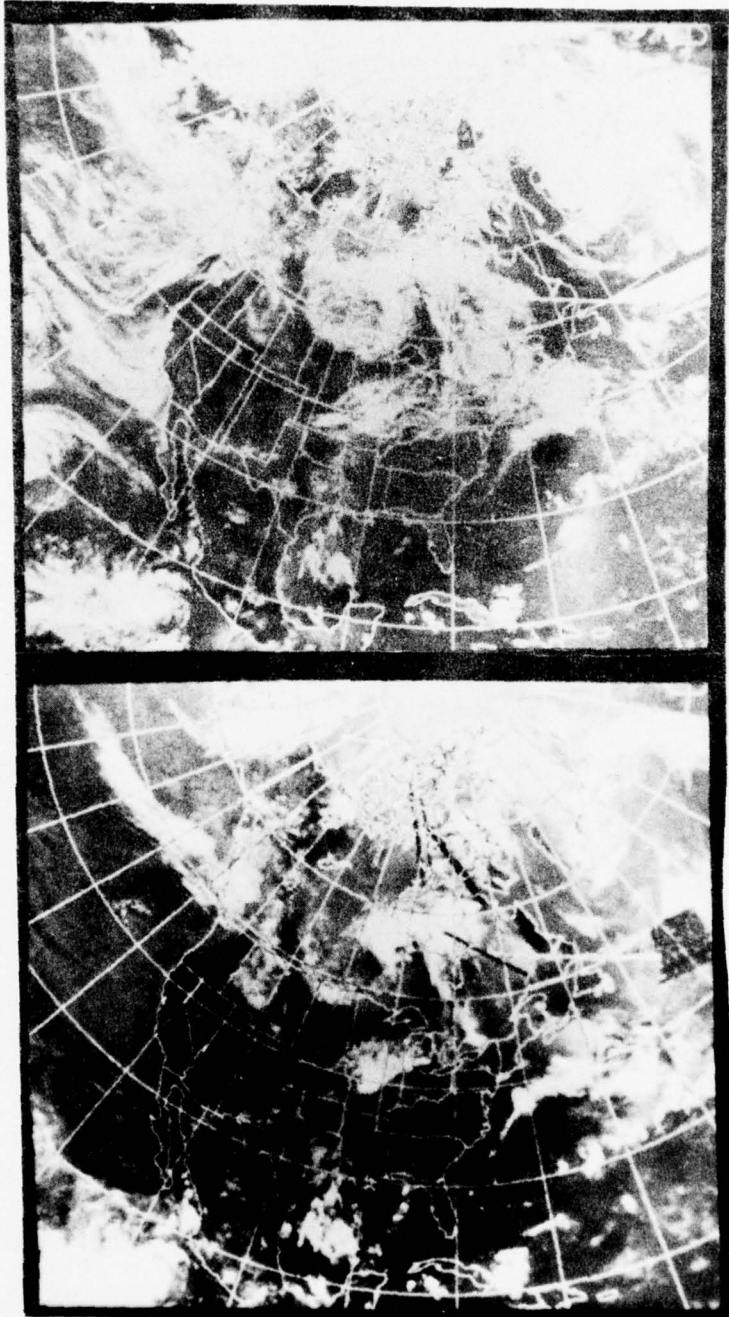
Figure 6.10 NOAA 4 mosaic for August 25, 1975 with the visible channel on the top and the infrared channel on the bottom.

discussed in the previous section. The slope and y-intercept of each case was calculated. The cases with the magnitude of the slope greater than the magnitude of the y-intercept were assumed to be cirrus clouds. The cases with the magnitude of the y-intercept greater than the magnitude of the slope were assumed to be middle or lower clouds. These cases were then examined in conjunction with the IR pictures of the previous section. In all cases, the empirically derived relationships that were based on the theoretical model indicated the proper cloud type.

The model indicated the presence of middle clouds in the vicinity of 52°N, 115°W to 43°N, 100°W on August 21. Examination of the IR picture in Figure 6.2 verifies the presence of lower clouds in this area. For August 22, the model indicated a mixture of cirrus and lower clouds from 52°N, 104°W to 49°N, 102°W and then extensive lower clouds to 43°N, 99°W. This same pattern can be noted by examining Figures 6.4. In the vicinity of 50°N the IR picture shows an area of some cirrus clouds and some warmer lower clouds. South of 49°N there is only lower clouds in the IR picture of Figure 6.4. It also indicates little cloud south of 43°N. One of the clear points in this area was used for the clear column radiance in the ratioing for this day. The IR picture for August 23 (Figure 6.6) shows extensive cirrus on the subtrack of the satellite from 53°N, 120°W to 42°N, 115°W. The model shows all cirrus clouds in this area except for the indication of some middle clouds near 53°N. Further examination of Figure 6.6 reveals some breaks in the cirrus cloud in this area. On August 24, cirrus

was again indicated from 52°N, 109°W to 48°N, 106°W and middle
clouds were present south the 47°N. Examination of the satel-
lite picture for that day (Figure 6.8) verifies this analysis.
The clear column radiance for this day was taken from an area just
south of 47°N along the subtrack of the satellite. The model ana-
lyzed middle clouds from 53°N, 97.5°W to 47°N, 94.5°W and cirrus
clouds from 44°N, 93°W to 39°N, 91.7°W for August 25. This again
is represented well on the IR picture of Figure 6.10. The clear
column radiance for this day was from near 38°N and 91°W. The
ice and liquid water content for this pass along with the pass for
August 22 are mapped in a subsequent section.

6.3.2   Cloud Mass

To determine the cloud mass the data described in the previous
section was divided into middle and high clouds. The 3DNEPH points
that correspond to these data cases were then selected from Box
44 of the 3DNEPH at 1800Z for the five days analyzed. In all cases
the 3DNEPH indicated lower clouds below the cirrus or middle cloud.
This indicates one of the basic problems discussed earlier about
the 3DNEPH, that with only surface analysis the cloud top is over
estimated and with only satellite data the cloud base is lower than
it should be, so that the error can be greater than the thickness
of the cloud. It is virtually impossible to correct this problem
without instrumentation that can see through clouds. In addition,
the spreading of an observation to many 3DNEPH points tends to
smooth the data out so that cloud thicknesses are constant over
large areas. To minimize these problems, the 3DNEPH cloud

thickness data were used as either cirrus or middle cloud. As noted earlier, this would not affect the ice and water content calculation significantly because middle cloud in the presence of thin cirrus has the same appearance as moderately thick cirrus. The effect of lower clouds on middle cloud ratios remained virtually unchanged when comparing the slopes and y-intercepts derived from the empirical-theoretical approach.

The 3DNEPH thicknesses were parameterized by assuming the base of the cloud corresponding to the theoretical base of the cloud. This was 3.1 km for middle cloud and 6.7 km for cirrus clouds. The cloud thickness in the middle cloud case was then obtained by adding the terrain to the middle cloud base and subtracting this from the layer top or the maximum cloud top parameter. This was then multiplied by 1.5×10^2 gm m^{-2} km^{-1} to obtain the liquid water content. The cirrus cloud thickness was obtained by subtracting 6.7 km from the height of the top of the layer top containing clouds or the maximum top parameter whichever was smaller. This result was then multiplied by 28.3 gm m^{-2} km^{-1} to obtain the ice content. In this way, it should minimize as much as possible the thickness grouping in the 3DNEPH.

Figure 6.11 is a graph comparing the model ice and liquid water contents with the 3DNEPH derived ice and water contents. Part a of the graph is for middle cloud cases and part b is for cirrus cloud cases. In both parts, both the 3DNEPH and the theoretical-empirical relationships indicated middle or cirrus clouds. The ordinate is for the 3DNEPH and is labeled in both thickness and

equivalent ice or liquid water content based on the ice and liquid water contents used in the theoretical calculations. The abscissa is for the empirical-theoretical calculations and is also labeled in thickness and equivalent liquid water content for a part a and equivalent ice content for part b.

Comparison of the 3DNEPH derived water contents in Figure 6.11a with the empirically derived theoretical water contents are some-what variable. The linear relationship desired is not present although some correlation can be noted. The data points in the comparison primarily occur at four 3DNEPH thicknesses while the model derived water contents covering a wide range. This grouping is present since the 3DNEPH has only four middle cloud layers in the 3DNEPH data base. The further parameterizations done to the 3DNEPH in this analysis made it possible to increase the number of water contents that could be obtained from the 3DNEPH. The error range of the comparisons for part a of Figure 6.11 is up to 2.25 x 10^2 gm m^{-2}. Analysis of Figure 6.11b also indicates the grouping of the 3DNEPH data at basically three ice content values although the range from the empirical-theoretical calculations very over a wide range for a given 3DNEPH value. The error range in Figure 6.11b is up to 84.9 gm m^{-2}. Although the desired linear result is not present for the comparisons in Figure 6.11, some agreement between the two independent methods of computing cloud ice or liquid water content is indicated.

The above comparisons point out the simple fact that new methods for determining cloud structures from satellite data cannot be
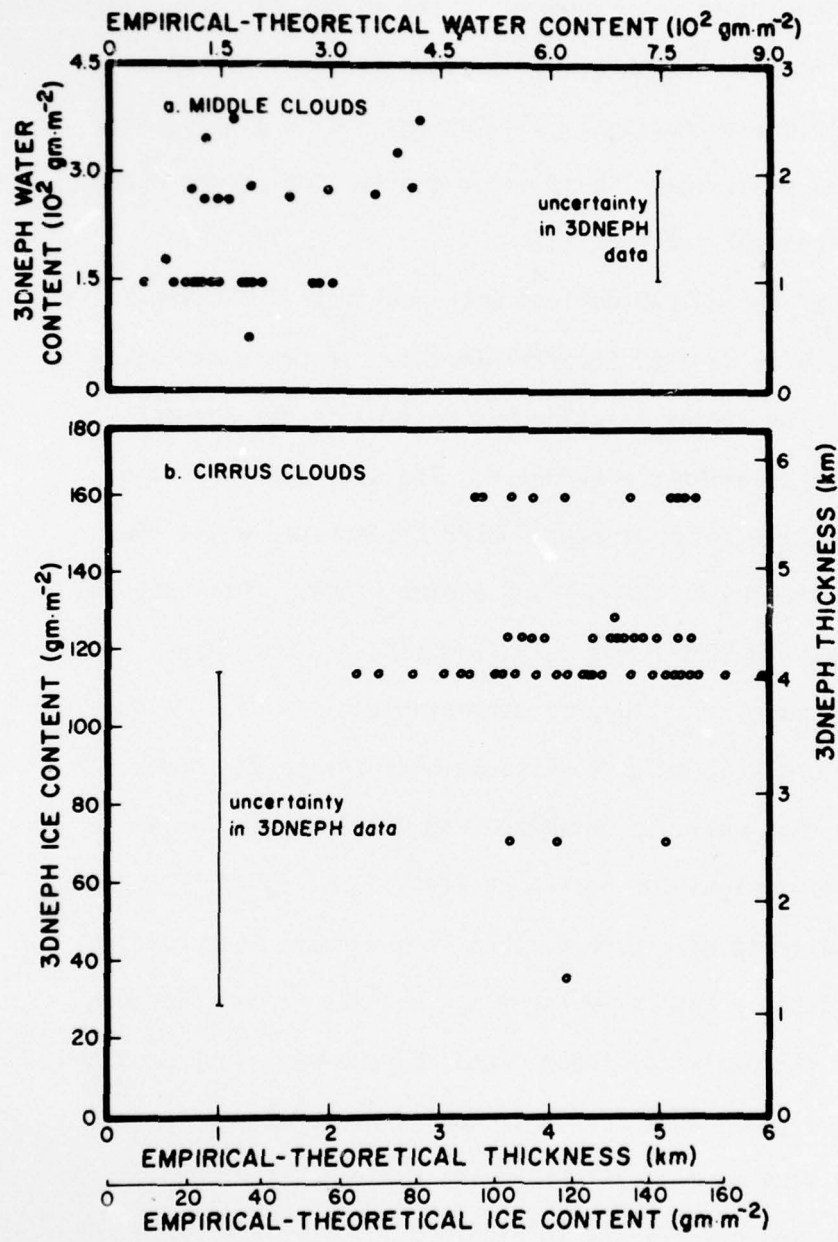
Figure 6.11 Comparison of 3DNEPH middle cloud water content with empirical-theoretical middle cloud water content from HIRS in part a and comparison of 3DNEPH cirrus cloud ice content with empirical-theoretical cirrus ice content from HIRS in part b.

properly verified with the current data bases that are available. The cloud typing derived in this analysis can be compared with simultaneous cloud photographs and these comparisons appear to be good in light of discussions in the previous section. The verification of ice and liquid water content will require well planned and controlled measurements of cloud structures within the satellite field-of-view. With this type of verification, it will be possible to reformulate parameterizations of theoretical calculations to improve the accuracy of these estimates of cloud compositions. Until this can be accomplished, the use of theoretical-empirical relationships should prove to be more accurate than purely statistical methods.

6.4 Cloud Moisture Mapping

The use of the parameterizations described in previous chapters and applied to HIRS data in this chapter can be used to map ice and water content of middle and cirrus clouds. To perform this mapping on a global scale over long periods of time would be the desired result. However, to accomplish this on a routine basis would require the availability of global satellite data and a large block of dedicated computer time. In this section, portions of two orbits over central North America are mapped to illustrate the concept.

The maps used for these projections is polar stereographic and it is therefore possible to compare rather easily to NOAA 4 satellite pictures displayed in Section 3 of this chapter. In each of the cases the clear column radiance at satellite nadir was used to

perform the ratioing over ten scan spots on each side of the nadir.
Beyond these scan angles a clear column radiance representative
of a large scan angle should be used to perform the rationing to
derive the amount of liquid water or ice content.

As noted earlier the slope and y-intercept of the linear fit
determines whether middle or high cloud are present. If the magni-
tude of the slope is greater than the y-intercept cirrus cloud is
assumed. Further criteria established to perform the mapping were
to eliminate data points where the magnitude of the slope is greater
than 25, or the correlation coefficient was less than 0.70. These
criteria were used after comparing many cases of actual data with
theoretical calculations. Cases that do not meet the above criteria
are low cloud which were not addressed in this analysis or partly
cloudy atmosphere, which will be discussed in the next chapter.

In both passes analyzed, the latitudes and longitudes of the
data points that met the above criteria were plotted on the polar
projection and then analyzed. The two figures containing the
analysis Figure 6.12 and 6.13 are for August 22 and August 25,
respectively. In both cases the cirrus and middle cloud are mapped
on the same figure. The isolines are labeled with vertical ice or
liquid water content based on the constants derived from parameter-
izations of the theoretical calculations. As an example the line
labeled 150 is equivalent to a middle cloud thickness of 1 km
from the theoretical calculations. The solid lines are isolines of
middle cloud, dashed lines are for cirrus cloud and the darker
lines are separation of middle and high cloud analysis.

The analysis for August 22 shows two areas of overcast conditions under the satellite. The northern area is over southern Canada and extreme northern Montana and North Dakota is characterized by both middle and high clouds. Since the data is cutoff to the north, east and west the analysis shows sharp break points in these directions. Analysis of the NOAA 4 indicates that these cloud areas analyzed for this pass no cirrus cloud is present, although the analysis shows middle cloud less than 1 km thick both south of the northern area and north of the southern area of clouds. This is also true south of the southern cloud area for one scan line.

Analysis of the figure for August 25 shows a similar set of two distinct cloud areas. The southern area is the cirrus on top of an active area of thunderstorms and the sharp southern edge of this cloud mass corresponds very well to the NOAA 4 picture. The northern cloud mass is dominated by middle cloud with some cirrus on the southwest side. This again agrees well with the NOAA 4 satellite picture. On the southern edge of the northerly cloud mass the middle cloud thicknesses fall off very rapidly both by examination of the picture and from mapping.

With proper verification, the use of this technique on a global scale is feasible. Proper verification as noted in the previous section would require the use of cloud physics measurements in the satellite field-of-view. These types of measurements would be required in a variety of atmospheric conditions. Global mapping requires the solution of the problem of determining ice and water
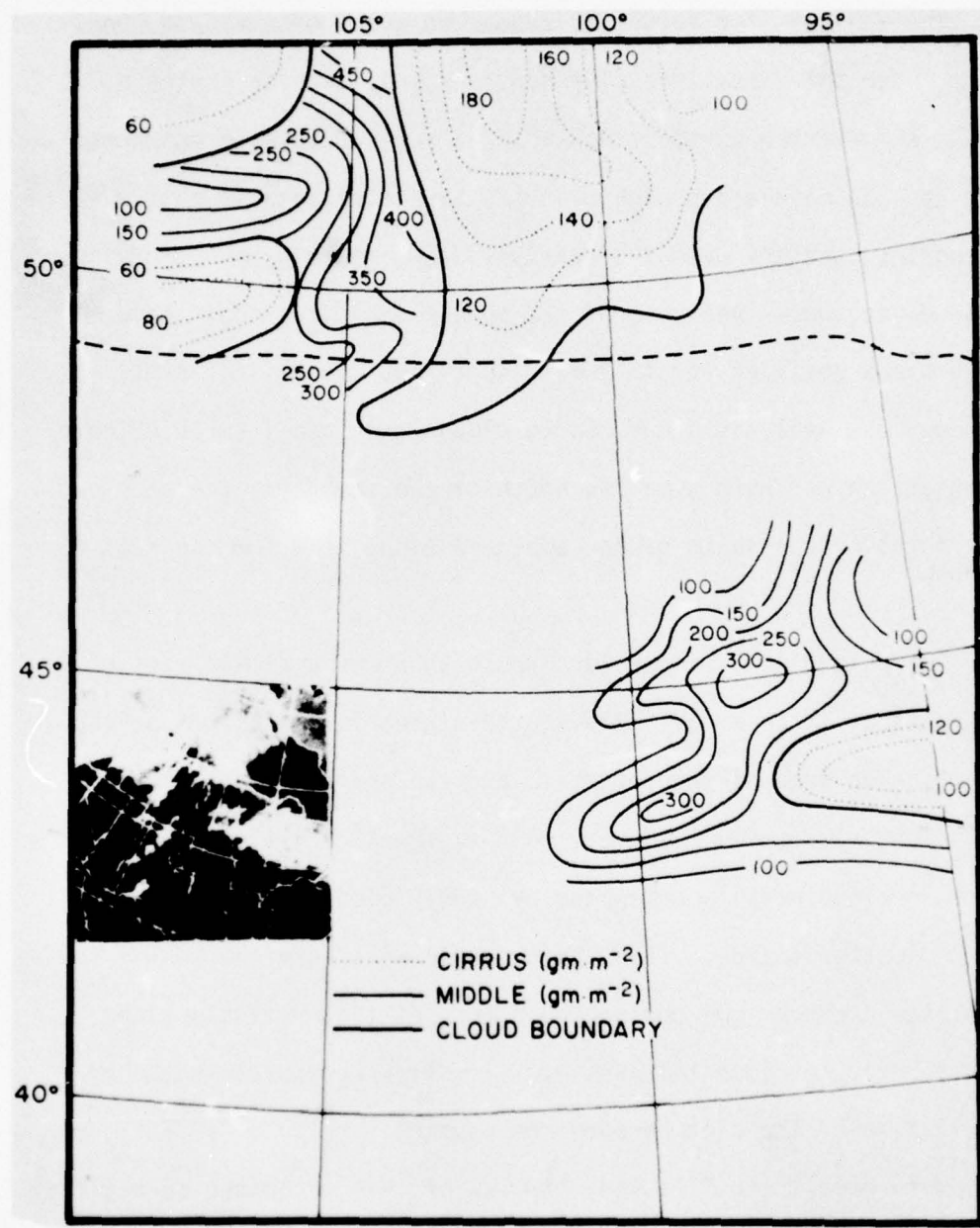
Figure 6.12   Cloud ice and water content based on empirical-
theoretical calculations for August 22, 1975.
Dotted lines are for cirrus clouds (gm m^{-2}) and
solid lines are for middle clouds (gm m^{-2}).   The
heavy line is the cloud boundries.
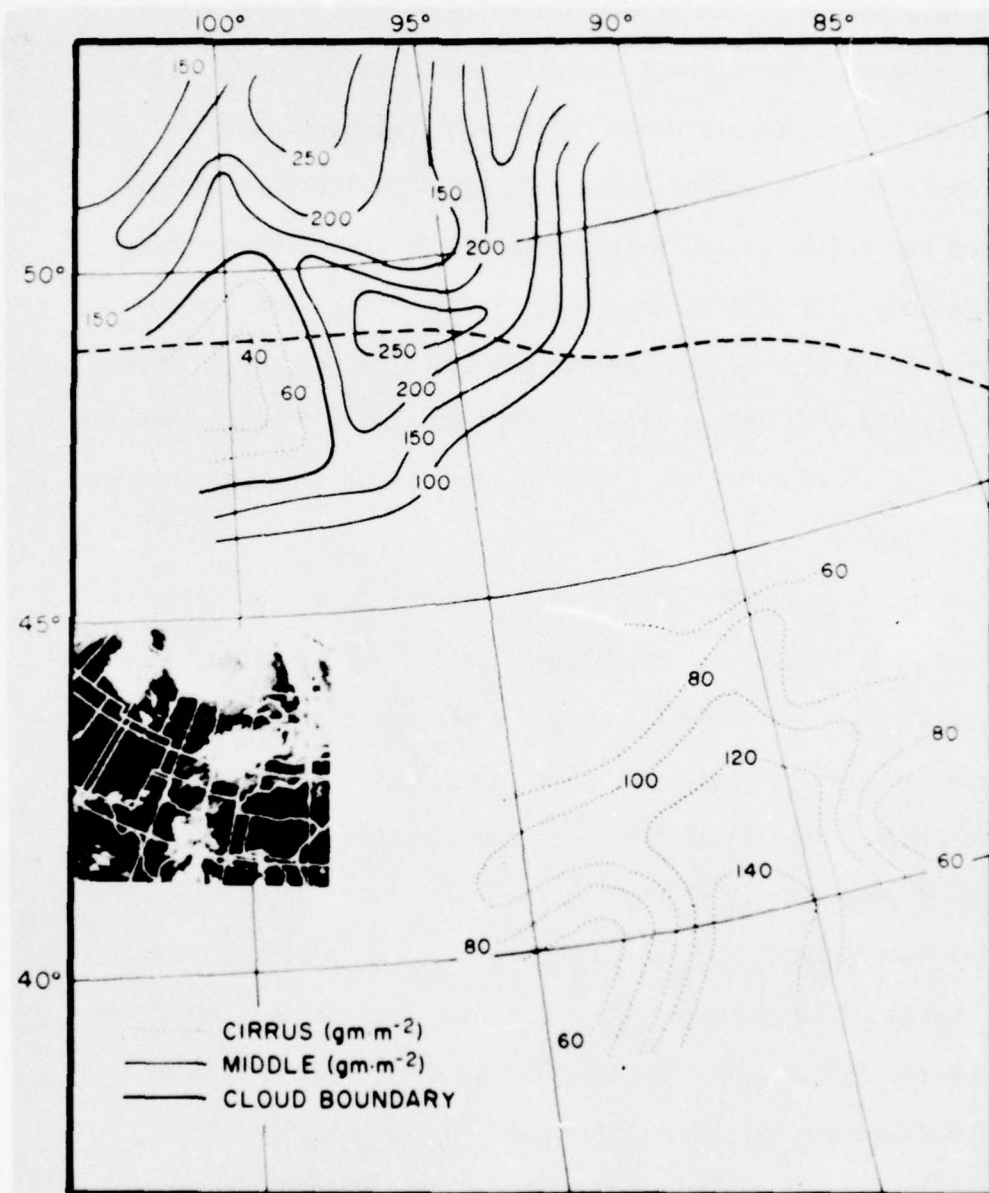
Figure 6.13 Cloud ice and water content based on empirical-theoretical calculations for August 25, 1975. Dotted lines are for cirrus clouds (gm m^{-2}) and solid lines are for middle clouds (gm m^{-2}). The heavy line is the cloud boundries.

content in a partly cloudy atmosphere which will be discussed in
the next chapter. The current analysis lends itself to real time
analysis since the computer time requirement has been minimized
by the empirical parameterizations. In addition the ratioing has
decreased the effect of the real atmosphere on the cloud moisture
determination. The effects of middle clouds with colder tempera-
tures than those used in the theoretical calculations are accounted
for by assuming that colder clouds represent clouds thicker than the
model can handle since middle clouds usually build from the base up
in the atmosphere.

The technique developed here when compared to microwave tech-
niques has both advantages and disadvantages. Two advantages are the
higher resolution of the HIRS instrument when compared to the SCAMS
instrument and the detection of cirrus clouds that are transparent
in the microwave portion of the spectrum. Another advantage of this
technique is that it can be applied over both land and oceans, while
microwave interpretation of clouds is restricted to oceans because
of the change of land emmissivity. Disadvantages of this technique
when compared to microwave includes the opacity of water clouds in
the infrared portion of the spectrum and the sensitivity of the
technique to the water cloud temperature. By combining infrared
and microwave measurements along with the proper cloud physics
verification data, operationally significant recovery of cloud para-
meters from satellite data is feasible.

CHAPTER 7

THE PARTLY CLOUDY ATMOSPHERE

The foregoing analysis considered only the overcast case of middle and cirrus clouds. The use of this technique on a global scale requires the determination of the equivalent liquid water and/or ice content of the partly cloudy atmosphere and possibly the cloud cover in the field of view. The ice or water content can be recovered through determining the cloud cover and then applying the overcast parameterizations, the equivalent ice content in a partly cloudy atmosphere can be recovered directly from the overcast parameterizations. The first section of this chapter will discuss the problems associated with the partly cloudy field of view. The second section will describe difficulty in recovering cloud cover from the empirical parameterizations and the final section will describe a simple method to determine equivalent ice or water content from a partly cloudy atmosphere.

7.1 Problems in the Partly Cloudy Atmosphere

The verification of the method proposed for a cloudy atmosphere described in the previous chapter used the 3DNEPH which gave very marginal results. In the same way even to a greater extent the verification of cloud cover from a partly cloudy atmosphere is more difficult. Current products available for determining cloud amount are the 3DNEPH analysis and the empirical derivation of cloud cover

from broadband radiometers. The major problem with these sources
is the timeliness of the analysis. Since the cloud amount in a
given field of view is always changing a simultaneous measurement
in the field of view would be required. This would require simultan-
eous sampling of the HIRS field of view by another instrument that
has a resolution that is much finer than the HIRS so that infor-
mation about the distribution of clouds in the horizontal can be
determined. This is necessary since the radiance measurements in
the HIRS field-of-view are integrated, which would result in an
infinite number of cloud heights or coverages from the same set of
radiance measurements. A second area that will give improper
representation of cloud cover is the accuracy of the radiance
measurements both in theoretical calculations and actual HIRS data.
This is true for all channels.

The basic equation for recovering cloud amount from a given
channel is expressed by

$$I^{PC}_{(\nu)} = \eta \, I^{C}_{(\nu)} + (1-\eta)I^{NC}_{(\nu)} \tag{7.1}$$

where $I^{PC}_{(\nu)}$ is the partly cloudy radiance, $I^{C}_{(\nu)}$ is the cloudy radiance,
$I^{NC}_{(\nu)}$ is the clear column radiance and η is the cloud cover. The
cloud cover (η) can be expressed as

$$\eta = (I^{PC}_{(\nu)}) - I^{NC}_{(\nu)}/(I^{C}_{(\nu)} - I^{NC}_{(\nu)}) \tag{7.2}$$

where the only known parameter is the partly cloudy radiance and
the other two radiances must be assumed for come from a "prior"
parameterization such as an assumed temperature profile. Because

the cloud cover information is expressed in terms of the ratio of
the radiance differences, it should be noted that a small error
in any of the radiances will produce a significant change in the
cloud amount calculation to the point that the results are meaning-
less. Analysis of these small differences in the radiances used
in this equation and the resulting error will be analyzed in the
next section. These large errors in cloud cover are very sensi-
tive to small errors in the radiance values even in idealized theo-
retical parameterizations.

7.2 Cloudy Parameterizations in a Partly Cloudy Atmosphere

The partly cloudy equation Eq. (7.1) shown in the previous
section can be converted to ratios and is given by

$$R_{(\nu)}^{PC} = 1 - \eta + \eta \, R_{(\nu)}^{C} \qquad (7.3)$$

where $R_{(\nu)}^{C}$ is the cloudy radiance and $R_{(\nu)}^{PC}$ is the partly cloudy
radiance from the theoretical calculations divided by the theo-
retical clear column radiances. Based on Eq. (7.1) and the
theoretical results of the cloudy atmosphere ice or liquid water
content, cloudy cover can be recovered in principle. Recalling
that $R_{(\nu)}^{C}$ was fit with a straight line of the form $y = a_1 x + a_0$
from which the cloud type was determined from the relationship
of a_1 and a_0. These two constants were further fit with an equa-
tion of the form $a_1 = c_1 + c_2 \ln(\Delta z)$ and $a_0 = c_3 + c_4 \ln(\Delta z)$
where Δz is the thickness of the cloud and c_1, c_2, c_3, and c_4 were
determined over a range of a_1 and a_0 for which thicknesses are known.

For any two adjacent channels on the HIRS instrument

$$R^{PC}_{(\nu_1)} = 1 - \eta + \eta \, R^{C}_{(\nu_1)} \tag{7.4}$$

$$R^{PC}_{(\nu_2)} = 1 - \eta + \eta \, R^{C}_{(\nu_2)} \tag{7.5}$$

where the subscripts are any two adjacent channels. Substituting the straight line and logrithmic fits, Eq. (7.4) and (7.5) become

$$R^{PC}_{(\nu_1)} = 1-\eta+\eta[(y_1-c_3-c_4\ln(\Delta z))/(c_1+c_2\ln(\Delta z))] \tag{7.6}$$

$$R^{PC}_{(\nu_2)} = 1-\eta+\eta[(y_2-c_3-c_4\ln(\Delta z))/(c_1+c_2\ln(\Delta z))] \tag{7.7}$$

where y_1 and y_2 are the ordinate from the straight line fit and $c_3=21.19$ and 19.19, $c_4=-6.53$ and -4.089, $c_1=-21.40$ and -18.53, and $c_2=-5.75$ and 3.007 for cirrus and middle clouds, respectively. The above results can be solved for the cloud cover (η) and the equivalent ice or liquid water thickness (Δz) by solving Eq. (7.6) in term of Eq. (7.7) in such a way that

$$\eta = [R^{PC}_{(\nu_1)}-1]/[\frac{y_1-c_3-c_4\ln(\Delta z)}{c_1+c_2\ln(\Delta z)}] \tag{7.8}$$

$$\Delta z = e^{\left[\frac{y_1(1-R^{PC}_{(\nu_2)}) - y_2(1-R^{PC}_{(\nu_1)})}{(R^{PC}_{(\nu_1)} - R^{PC}_{(\nu_2)})c_6} - \frac{c_5}{c_6}\right]} \tag{7.9}$$

where $c_5=c_3+c_1$ and $c_6=c_4+c_1$.

To examine the error in this analysis a 2 km cirrus cloud of 0.5 coverage will be used as an example. Using successive channel in both the 15 μm band and the 4.3 μm band a total of six estimates of ice content and cloud cover can be calculated. The channel ratios

used were 4-5, 5-6, 6-7, 14-13, 13-12, and 12-11. The results of
the calculations for the 6 estimates are given in Table 7.1. As
can be seen from these results the method will not consistantly
give a reasonable measure of eouivalent ice content or cloud cover
from the theoretical parameterizations. This would be equally
true when considering actual data.

TABLE 7.1   Calculation of Thickness (Δz) and Cloud
Cover (η) for a Series of Adjacent Channels
for a Theoretical Cirrus Cloud 2 km Thick
and 0.5 Cloud Cover.

	4-5	5-6	6-7	14-13	13-12	12-11
y_1	0	1	4	2	7	9
y_2	1	4	5	7	9	10
$R_1^{PC}(\nu)$	.978	.905	.858	.899	.772	.684
$R_2^{PC}(\nu)$	.905	.858	.822	.772	.684	.664
Δz	1.125	520.9	.710	.974	.073	4879.9
η	.51	-.227	.84	.99	1.67	-.547

To examine the sensitivity of the ratios in this analysis an
ideal case of a 2 km cirrus cloud that had 0.5 cloud cover was
assumed. The idealized ratios for channels 11 and 12 were used
assuming that they perfectly fit the curves in Figure 4.2. These
perfect ratios for channels 11 and 12 were 0.720 and 0.6914 giving
a result of 2 km thickness and 0.5 cloud cover. By changing one of
the ratios by 0.01, the thickness calculations now becomes 0.05 km

and the cloud cover is 1.46. Thus it can be seen that small changes in the ratios has an extra large impact on the resultant thickness and cloud cover calculations. In the next section a method to recover equivalent ice or liquid water content from a partly cloudy atmosphere will be demonstrated. It appears that cloud cover information may not be so important in light of the calculations in the next section.

7.3 Equivalent Ice and Water Content in Partly Cloudy Atmospheres

Ice or water content in partly cloudy atmospheres can be recovered from the overcast theory if the partly cloudy radiance ratios use the cloudy parameterizations. This can be seen when examining Table 4.3 and Figures 4.2 and 4.3. Figures 4.2 and 4.3 are the best fit of the slope and the y-intercept for cirrus and middle clouds. Returning to the equation for the partly cloudy atmosphere, denoted in Eq. (7.3) and substituting for a series of cloud amount theoretically produced partly cloudy ratios are calculated. Table 7.2 is for various cloud covers for a 2 km thick cirrus (Part a) and a 1 km thick middle cloud (Part b). It should be noted that the slope and the y-intercept both begin to increase in magnitude as the amount of cloud cover decreases. It should also be noted that the distinction between cloud type (middle and cirrus cloud) is retained for all cloud covers. This would indicate that cloud type could be distinquished even in the presence of a partly cloudy atmosphere. When comparing Table 4.3 with Table 7.2 an overlap between the partly cloudy ratios and overcast ratios exists. This implies that it is impossible to tell the

TABLE 7.2 Ratios, y-intercept, Slope and the Square of the
Correlation Coefficient for a Series of Cloud
Covers. Part a is for Cirrus Clouds. Part b
is for Middle Clouds.

Part a (Cirrus Clouds (2 km)

| Ordinate | Cloud Cover (Tenths) | | | | |
	0.9	0.7	0.5	0.3	0.1
0	.961	.970	.978	.987	.995
1	.830	.868	.905	.943	.981
2	.810	.859	.899	.939	.980
3	.799	.844	.888	.933	.978
4	.744	.801	.858	.915	.972
5	.680	.750	.822	.893	.964
6	.625	.708	.792	.875	.958
7	.590	.681	.772	.863	.954
8	.576	.670	.765	.859	.953
9	.431	.558	.684	.810	.937
10	.394	.529	.664	.798	.933
y-intercept	17.66	23.00	32.69	55.00	168.32
slope	-18.7	-24.04	-33.75	-56.08	-169.41
r^2	.968	.968	.968	.967	.969

Part b (Middle Cloud (1 km))

| Ordinate | Cloud Cover (Tenths) | | | | |
	0.9	0.7	0.5	0.3	0.1
0	.981	.985	.990	.994	.998
1	.910	.930	.950	.970	.990
2	.877	.904	.931	.959	.986
3	.971	.978	.984	.990	.997
4	.862	.893	.924	.954	.985
5	.824	.863	.902	.941	.980
6	.737	.796	.854	.912	.970
7	.701	.768	.834	.900	.967
8	.673	.746	.818	.891	.964
9	.559	.657	.755	.853	.951
10	.519	.626	.733	.840	.947
y-intercept	20.74	26.49	36.81	61.04	182.23
slope	-20.10	-25.80	-36.16	-60.41	-181.61
r^2	.912	.912	.912	.914	.914

the difference between a partly cloudy thick cloud and an over-
cast thinner cloud. To illustrate this concept a 2 km cirrus with
0.7 cloud cover has the same ratios as a cirrus cloud that is 0.7
km thick and completely overcast. Because of the close values for
the slope and y-intercept for different middle cloud thicknesses
the overlap noted in the cirrus clouds is not as great. Therefore
it can be seen that the partly cloudy upwelling ratios follow
closely the cloudy ratios and therefore the cloudy parameterizations
can be used to infer equivalent ice or water content in partly
cloudy atmospheres.

The use of the cloudy parameterizations in the partly cloudy
atmosphere is demonstrated using the pass of the western United
States for August 21, 1975 (Figure 7.1). The infrared satellite
picture shows a good area of middle cloud under the satellite
between 45°N to 52°N. The picture indicates that this is possi-
bly a broken area although it is very difficult to tell. The
3DNEPH for this time indicates a broken layer of middle cloud
ranging from 15 percent coverage to 75 percent coverage. The
analysis of this area with the cloudy parameterizations indicate
that the slope and y-intercept range of the upper range of cloud
covers from Table 7.2. Table 7.3 includes the latitude, longitude,
slope, y-intercept, thickness and equivalent water content along
the satellite subtrack from 45°N to 52°N. The liquid water content
is derived by multiplying the thickness by 150 gm m^{-2} km^{-1}.

The mapping of ice and water content that was displayed in
Chapter 6 did not address the partly cloudy case, although some
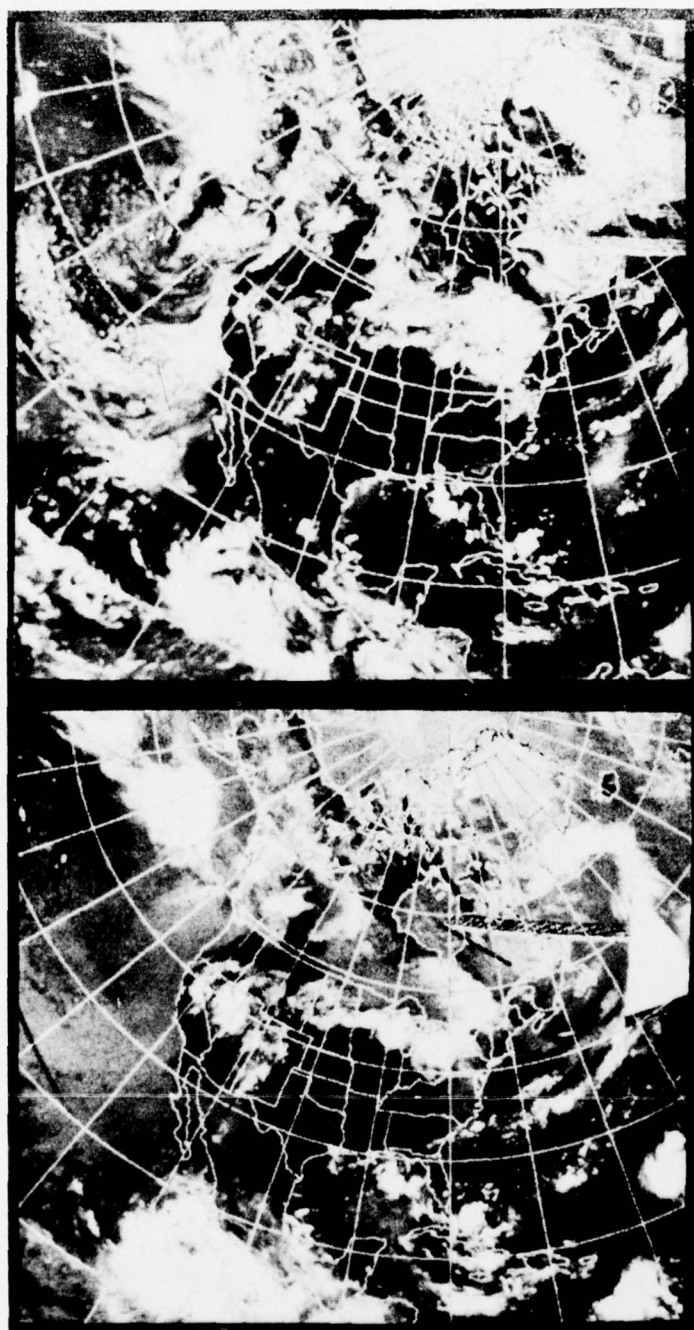
Figure 7.1   NOAA 4 mosaic for August 21, 1975 with the
             visible channel on the top and the infrared
             channel on the bottom.

TABLE 7.3 Liquid Water Content of Partly Cloudy Conditions
Along the Satellite Subtrack for August 21, 1975
from 46.1°N to 52.7°N.

Latitude	Longitude	Slope	y-intercept	Thickness (km)	Water Content (gm m^{-2})
52.71	115.90	-21.89	23.53	.500	75.00
52.40	115.09	-23.71	25.16	.383	57.45
52.19	114.90	-26.38	27.63	.287	43.05
51.93	114.75	-25.43	27.08	.270	40.50
51.66	114.61	-27.37	28.42	.274	41.10
51.40	114.46	28.79	30.26	.153	22.95
51.14	114.32	-30.38	31.69	.154	23.10
50.88	114.18	-31.32	32.48	.133	19.95
50.62	114.04	-29.38	30.12	.186	27.90
50.35	113.90	-29.27	30.56	.161	24.15
49.30	113.36	-25.72	28.26	.154	23.10
49.04	113.24	-28.17	30.15	.164	24.60
48.77	113.10	-28.80	31.94	.051	7.65
48.51	112.98	-28.77	32.32	.036	5.40
48.25	112.85	-27.17	30.28	.066	9.90
47.98	112.72	-28.94	32.02	.065	9.75
47.72	112.59	-27.23	29.54	.132	19.80
47.45	112.47	-30.79	33.40	.084	12.60
47.19	112.35	-28.66	31.09	.100	15.00
46.93	112.22	-22.03	23.70	.430	64.50
46.66	112.10	-13.16	14.16	3.023	453.45
46.40	111.98	-14.41	14.92	2.765	414.75
46.13	111.86	-15.62	16.44	1.917	287.55

of the points on the leading and trailing edges of these overcast cloud masses are partly cloudy fields-of-view. On the basis of previous analysis the requirement for the knowledge of cloud cover no longer exists and ice and water content of single cloud layers can be produced on a global scale with the techniques developed throughout this analysis.

CHAPTER 8

CONCLUSIONS, APPLICATION AND LIMITATIONS,

AND RECOMMENDATIONS

8.1 Conclusions

A theoretical model that calculates transfer of spectral

infrared radiation based on the discrete-ordinate method was

developed to include cirrus and middle clouds and absorbing

gases. This analysis used one model atmosphere and one middle

and high cloud type for all calculations. The top of the cirrus

cloud and the base of the middle cloud were held constant to

minimize computer time. The layers in the transfer computations

were assumed to have constant temperatures so that the effects

of the change in cloud thickness on the upwelling radiance could

be studied. Various thicknesses and combinations of middle and

cirrus clouds were used in the analysis. This model was then

applied to the HIRS channels of the Nimbus VI satellite. Avail-

able transmittances for each of the channels used were employed

and modified to generate upper and lower boundary conditions and

gaseous absorption in and between the cloud layers.

The model was further modified to calculate upwelling radi-

ances over a range of satellite scan angles for these cloud com-

binations. Comparison of these results show that the thick

cirrus dominates the transfer process. In addition, the thick

middle cloud had greater upwelling radiance at all angles when compared to the thin middle cloud in the 15 μm CO_2 band and in the 4.3 μm CO_2 band for channels that have weighting functions above the thin middle cloud top. This reversal of expected results is caused by the attenuation of the upwelling radiance by gases above the cloud. The results also show that the window channels and water vapor channels to not have this effect in the model atmosphere used.

In the case of multilayered clouds the differences between the four multicloud combinations are reduced when compared to the single cases. In the case of thick cirrus, changes in the middle cloud thickness do not effect the upwelling radiance. This effect again shows the dominance of thick cirrus in the transfer process. For thin cirrus clouds changing the middle cloud thickness does show a small effect on the final upwelling radiance. The thick middle cloud has greater upwelling radiances than the thin cloud in all channels that show this effect in the single layer middle cloud case. The short wave CO_2 channels show a slight better contrast in the thin cirrus case of multilayered clouds than the long wave CO_2 channels. The window and water vapor channels show a greater contrast than the short wave CO_2 channels.

The theoretical calculations of upwelling radiance were divided by their clear column radiances to give a ratio for each channel. These ratios were then fitted with a straight line for each theoretical cloud thickness for both cirrus and middle clouds. It was found that cases where the slope was greater than the magnitude of

the y-intercept derived from transfer calculations corresponded
to cirrus clouds. The reverse of the slope and y-intercept
relation corresponded to middle clouds or lower clouds. The
resulting slopes and y-intercepts for different cloud thicknesses
for the two cloud types were then fitted with a logarithmic func-
tion. This made it possible to infer ice content in the case
of middle clouds for a given thickness based on the theoretical
calculations.

These theoretical parameterizations were then applied to five
days of HIRS data. The resulting cloud ice and liquid water con-
tents were then compared to the 3DNEPH to indicate whether this
technique could be applied in an operational mode. It was found
that the comparisons with the 3DNEPH were not satisfactory. This
can be traced to the 3DNEPH and the methods used to determine cloud
thicknesses as well as approximations in the theoretical calcula-
tions and the parameterization of these calculations. Two days of
ice and water content for actual HIRS data were then mapped. These
results were good when comparing the resulting maps with the cor-
responding NOAA IV infrared and visible satellite pictures.

The impact of a partly cloudy atmosphere on ratios of HIRS
channels showed that due to errors in the parameterizations of the
overcast theory and the extreme sensitivity of the ratios in the
partly cloudy equation that it was difficult to recover reliable
ice or water content and cloud cover from the partly cloudy equa-
tion. The overlapping in the parameterization when partly cloudy
atmospheres were considered indicated that it was not possible to

tell the difference between a partly cloudy thick cloud and an overcast thinner cloud. However, it has been demonstrated that is was possible to recover an equivalent water content when using the empirical relationships developed in the completely cloudy atmosphere in a partly cloudy atmosphere. To this end an area of partly cloudy water clouds were examined to indicate the use of the overcast theory in the partly cloudy atmosphere. This result in conjunction with the overcast mapping of ice and water content would make the use of this technique possibly on a global scale with the improvement that the parameterizations are purely based on theoretical-empirical considerations.

8.2 Application and Limitations

To apply this technique on a global scale on a routine basis would require several additional sets of input as well as a dedicated block of computer time. This block of computer time required has been minimized since the technique substitutes parameterizations of climatological atmospheres for the real atmosphere. These parameterizations should be accurate within the band of the climatological area. It would be required to compute parameterizations of theoretical atmospheres over a range of atmospheres found around the globe. As a start the tropical, mid-latitude summer and winter, and the artic summer and winter atmospheres could be used to generate theoretical results for different drop size distributions (cloud types) and representative cloud temperatures for each model atmosphere. With this set of empirical constants derived from the parameterizations of the theoretical results, the proper set of

constants could be determined from point location and cloud
type.

This type of technique is ideally suited to enhance the cloud
parameterizations in the 3DNEPH. As noted earlier the 3DNEPH is
a modular program that processes all kinds of meteorological data.
The only satellite data that is currently used is broad band visi-
ble and infrared channels of a NOAA 4 type scanning radiometer.
The addition of this technique would use satellite data that is
not in current use for cloud detection and it would give valu-
able input into the final results. Since the 3DNEPH is a routinely
produced product, much of the software required to implement this
procedure is already in existence and the operational development
could be carried out independently of 3DNEPH production. As noted
earlier the resolution of the HIRS and the 3DNEPH are similar so
that in an operation implementation the 3DNEPH could be used to
further verify the technique.

8.3 Recommendations

Further studies seem warrantable for the determination of cloud
parameters from satellites. Although an objective way of deriving
cloud type information and cloud ice or water content has been il-
lustrated in this analysis, a more reliable method of verification
must be found. However, verification of satellite sensing tech-
niques requires carefully designed field experiments in which highly
reliable cloud parameters could be obtained under the satellite
pass. With sufficient cases from which cloud parameters may be

derived locally, intercomparisons with satellite derived values may be carried out to establish the statistical significance of this technique to parameterize satellite measurements.

To fully utilize the present state of the art in satellite sensing, combination of the technique developed here along with measurements in other regions of the spectrum would compliment each other in describing the cloud composition in the field of view. Two instruments are currently operational that can be combined with this technique. The NOAA 4 broad band type radiometer and a instrument like the Scanning Microwave Spectrometer (SCAMS) on Nimbus VI are two instruments that have been tested and should be capable of routine operations. We describe below some of the features of these instruments that would supplement the technique developed for the HIRS instrument in this analysis.

The recovery of cloud cover from the partly cloudy atmosphere proved unsuccessful because of the extreme sensitivity of the equation to small changes in the radiance measurements. The availability of cloud cover derived from the finer resolution of a broad band radiometer could be used to convert the partly cloudy radiances to cloudy radiances and then to cloudy ratios that would give a better estimate of the ice or water content than simply applying the partly cloudy ratios to the overcast parameterizations. This information of cloud cover could come from a instrument such as the Temperature Humidity Infrared Radiometer (THIRS) that is on Nimbus VI. At nadir the THIRS has a resolution of a box 8 x 8 km while the HIRS has a resolution in the form of a circle 23.8 km in

diameter. Thus a 3 x 3 array of the THIRS could be used to com-
pute the cloud cover in the HIRS field of view. Since the THIRS
channel is at 11.5 µm, the problems associated with the trans-
parency of cirrus clouds must be considered. The need for pick-
ing a point near the cloudy area that will serve as the clear
column radiance is required. The broad band radiometer could also
be used to pick this point during the calculations of cloud cover.
This would completely automate the selection of the clear column
radiance used in the ratioing and there would be no need to select
this point from satellite pictures.

The use of microwave data would have the advantages and dis-
advantages noted in Chapter 6. It would eliminate the problems
associated with opaque clouds noted throughout this analysis al-
though it would be only over oceans and at a much larger resolution.
As was noted in Chapter 4, investigators have successfully mapped
cloud liquid water content over oceans. To fully utilize the
microwave data to infer cloud parameters in conjunction with the
infrared data, improvements in the microwave theory would be the
first step. This could be accomplished by replacing the govern
ring equations in the model described in Chapter 2 with a set of
equations for microwave region of the spectrum. The output
from this model could then be parameterized into empirical func-
tions. The results would enhance the determination of water content
in middle clouds which become opaque in the infrared region. The
SCAMS parameterizations would also be very useful in multilayered
cloud scenes. Since microwave is virtually transparent to ice

clouds, the presence of middle clouds under a thick ice cloud would be determined. With these three instruments scanning at the same time and over the same areas along with improved resolution in the SCAMS type instrument, the global determination of three dimensional ice and water content produced routinely is feasible. This type of data base would have a great impact on climatology studies and it would enhance the input into global circulation models.

REFERENCES

Arvett, E. H. and D. G. Hummer, 1965: Non-coherent scattering. II. Line formation with a frequency independent source function. Mon. Not. Roy Astron. Soc., 130, pp. 295-331.

Bunting, J. R. and J. H. Conover, 1976: Estimates from satellites of total ice and water content of clouds. Preprint, International Conf. Cloud Phys., Boulder, Colorado, Amer. Meteor. Soc., pp. 407-412.

Chahine, M. T., 1970: Inverse problems in radiative transfer: Determination of atmospheric parameters. J. Atmos. Sci., 27, pp. 960-967.

Chahine, M. T., 1974: Remote sounding of cloudy atmospheres, J. Atmos. Sci., 31, pp. 233-243. I. The single cloud layer.

Chandrasekhar, S., 1950: Radiative Transfer. New York, Dover Publ., pp. 393.

Coburn, A. R., 1971: Improved three-dimensional nephanalysis model. Air Force Global Weather Center Tech. Memo., AFGWCTM 71-2, pp. 72.

Conrath, B. J., 1969: On the estimation of relative humidity profile from medium resolution infrared spectra obtained from a satellite. J. Geophys. Res., 74, pp. 3347-3361.

Feddes, R. G. and R. D. Smith, 1974: A synoptic scale model for simulating condensed atmospheric moisture. USAFETAC TN74-4, United States Air Force Environmental Technical Applications Center, Washington, D.C., pp. 31.

Grody, N. C., 1976: Remote Sensing of Atmospheric water content from satellites using microwave radiometry. IEEE Trans. Antennas Propagat., AP-24, pp. 155-162.

Hale, G. M. and M. R. Querry, 1973: Optical constants of water in the 200 nm to 200 μm wavelength region. Appl. Opt., 12, pp. 555-563.

Houghton, J. T. and G. E. Hunt, 1971: The detection of ice clouds from remote measurements of their emission in the far infrared. Quart. J. Roy Meteor. Soc., 96, pp. 1-17.

Kaveney, W. J., R. G. Feddes and K. N. Liou, 1977: Statistical inference of cloud thickness from NOAA IV scanning radio-meter data: Mon. Wea. Rev., 105, pp. 99-107.

Liou, K. N., 1972: Light scattering by ice clouds in the visible and infrared: A theoretical study. J. Atmos. Sci., 29, pp. 524-536.

Liou, K. N., 1973: A numerical experiment on Chandrasekhar's discrete-ordinate method for radiative transfer: Applications to cloudy and hazy atmospheres. J. Atmos. Sci., 30, pp. 1303-1326.

Liou, K. N., 1974: On the radiative properties of cirrus in the window region and their influence on remote sensing of the atmosphere. J. Atmos. Sci., 31, pp. 522-532.

Liou, K. N., 1975: Applications of the discrete-ordinate method for radiative transfer to inhomogeneous aerosol atmospheres. J. Geophys. Res., 80, pp. 3434-3440.

Liou, K. N., 1977: Remote sensing of the thickness and composition of cirrus clouds from satellites. J. Appl. Meteor., 16, pp. 91-99.

Liou, K. N. and T. Sasamori, 1975: On the transfer of solar radiation in aerosol atmospheres. J. Atmos. Sci., 32, pp. 2166-2177.

Liou, K. N., T. L. Stoffel, R. G. Feddes and J. T. Bunting, 1977: Radiative properties of cirrus clouds in NOAA 4 VTPR channels: Some explorations of cloud scenes from satellites. Submitted for publication.

McClatchey, R. A., R. W. Fenn, J. E. Selby, F. E. Volts and J. S. Garing, 1972: Optical properties of the atmosphere. (Third Edition), AFCRL-72-0497.

Miller, D. B. and R. G. Feddes, 1971: Global atlas of relative cloud cover 1967-1970 based on data from operational satellites. National Environmental Satellite Service, Washington, D. C., pp. 237.

Panofsky, H. A. and G. W. Brier, 1968: Some Application of Statistics to Meteorology. University Park, Pa., Pa. St. Univ., pp. 224.

Park, S. U., D. N. Sidkar and V. E. Suomi, 1974: Correlation between cloud thickness and brightness using Nimbus 4 THIR data (11.5 channel) and ATS 3 digital data. J. Appl. Meteor., 13, pp. 402-410.

Prabhakara, C., B. J. Conrath, R. A. Hanel and E. J. Williamson, 1970: Remote sensing of atmospheric ozone using 9.6 μm band. J. Atmos. Sci., 27, pp. 689-697.

Shaaf, J. W. and D. Williams, 1973: Optical constants of ice in the infrared. J. Opt. Soc. Amer., 63, pp. 726-732.

Smith, W. L., 1970: Interative solution of the radiative transfer equation for the temperature and absorbing gas profile of an atmosphere. Appl. Opt., 9, pp. 1993-1999.

Smith, W. L., 1976: Clear column radiance program. (Private communication).

Smith, W. L., P. G. Abel, H. M. Woolf, A. W. McCulloch and B. J. Johnson, 1975: The high resolution infrared radiation sounder (HIRS) experiment. Nimbus VI Users Guide, Goddard Space Flight Center, Greenbelt, Md., pp. 227.

Smith, W. L. and H. M. Woolf, 1976: The use of eigenvectors of statistical covariance matrices for interpreting satellite sounding radiometer observations. J. Atmos. Sci., 33, pp. 1127-1140.

Staelin, D. H., A. L. Cassel, K. F. Kunzi, R. L. Pettyjohn, R. K. L. Poon, P. W. Rosenkranz and J. W. Waters, 1975: Microwave atmospheric temperature soundings: Effects of clouds on Nimbus V satellite data. J. Atmos. Sci., 32, pp. 1970-1976.

Staelin, D. H., K. F. Kunzi, R. L. Pettyjohn, R. K. L. Poon, R. W. Wilcox and J. W. Waters, 1976: Remote sensing of atmospheric water vapor and liquid water with the Nimbus V microwave spectrometer. J. Appl. Meteor., 15, pp. 1204-1214.

Stoffel, T. L., 1976: Radiative properties of cirrus clouds in the infrared: Application to remote sensing. Masters Thesis, University of Utah, Salt Lake City, Utah., pp. 99.

Taylor, F. W., 1976: Remote temperature sounding in the presence of cloud by zenith scanning. Appl. Opt., 13, pp. 1559-1566.